Special role of the first Matsubara frequency for superconductivity near a quantum critical point: Nonlinear gap equation below T_{c} and spectral properties in real frequencies

Yi-Ming Wu, Artem Abanov, Yuxuan Wang, and Andrey V. Chubukov

Phys. Rev. B **99**, 144512 — Published 15 April 2019

DOI: 10.1103/PhysRevB.99.144512

Special role of the first Matsubara frequency for superconductivity near a quantum-critical point – the non-linear gap equation below T_c and spectral properties in real frequencies

Yi-Ming Wu,[1] Artem Abanov,[2] Yuxuan Wang,[3] and Andrey V. Chubukov[1]

[1]*School of Physics and Astronomy and William I. Fine Theoretical Physics Institute, University of Minnesota, Minneapolis, MN 55455, USA*

[2]*Department of Physics, Texas A&M University, College Station, USA*

[3]*Department of Physics, University of Florida, Gainesville, FL 32611, USA*

(Dated: March 18, 2019)

Abstract

Near a quantum-critical point in a metal a strong fermion-fermion interaction, mediated by a soft boson, destroys fermionic coherence and also gives rise to an attraction in one or more pairing channels. The two tendencies compete with each other, and in a class of large N models, where the tendency to incoherence is parametrically stronger, one would naively expect an incoherent (non-Fermi liquid) normal state behavior to persist down to $T = 0$. However, this is not the case for quantum-critical systems, described by Eliashberg theory. In such systems, the part of the fermionic self-energy $\Sigma(\omega_m)$, relevant for spin-singlet pairing, is large for a generic Matsubara frequency $\omega_m = \pi T(2m+1)$, but vanishes for fermions with $\omega_m = \pm\pi T$, while the pairing interaction between fermions with these two frequencies remains strong. It has been shown [Y. Wang *et al* PRL 117, 157001 (2016)] that due to this peculiarity, the onset temperature for the pairing, T_p, is finite even at large N, when the scaling analysis predicts a non-Fermi liquid normal state. We consider the system behavior below T_p and contrast the conventional case, when $\omega_m = \pm\pi T$ are not special, and the case when the pairing is induced by fermions with $\omega_m = \pm\pi T$. We obtain the solution of the non-linear gap equations in Matsubara frequencies and then convert to real frequency axis and obtain the spectral function $A(k, \omega)$ and the density of states $N(\omega)$. In a conventional BCS-type superconductor, $A(k, \omega)$ and $N(\omega)$ are peaked at the gap value $\Delta(T)$, and the peak position shifts to a smaller ω as temperature increases towards T_p, i.e. the gap "closes in". We show that, when the pairing is induced by fermions with $\omega_m = \pm\pi T$, the situation is qualitatively different from the standard BCS result. Namely, the peak in $N(\omega)$ remains at a finite frequency even at $T = T_p - 0$, the gap just "fills in" near this T. The spectral function $A(k, \omega)$ either shows almost the same "gap filling" behavior as the density of states, or its peak position shifts to zero frequency already at a finite Δ ("emergent Fermi arc" behavior), depending on the position of $\mathbf{k}$ on the Fermi surface. As an example, we compare our results with the data for the cuprates and argue that "gap filling" behavior holds in the antinodal region, while the "emergent Fermi arc" behavior holds in the nodal region.

I. INTRODUCTION.

The pairing near a quantum-critical point (QCP) in a metal is a fascinating subject due to highly non-trivial interplay between superconductivity and non-Fermi liquid (NFL) behavior [1–34]. In most cases, the dominant interaction between low-energy fermions near a QCP is mediated by critical fluctuations of the order parameter. In dimensions $D \leq 3$, this interaction gives rise to a singular fermionic self-energy, and a coherent Fermi-liquid behavior gets destroyed below a certain temperature T_{coh}, either on the full Fermi surface[13,15,35,36] or in the hot regions[6–8,13,20,37,38]. The same interaction, however, also mediates fermion-fermion interaction in the particle-particle channel. The electron-mediated interaction is positive (repulsive), but it depends on both momentum and frequency and generally has at least one attractive component ($d-$wave for antiferromagnetic QCP, $p-$wave for a ferromagnetic QCP, s, p, d-wave for a nematic QCP, Ref.[18]) If such a system generates pairing below some finite T_p (i.e., either becomes a true superconductor or develops preformed pairs), the range of NFL behavior shrinks to $T_{coh} > T > T_p$, and even vanishes when $T_p > T_{coh}$[19]. A naked quantum-critical $T = 0$ behavior can only be observed either if the pairing interaction is repulsive in all channels[19], or at attractive component exists, but fermionic incoherence prevents Cooper pairs to develop down to $T = 0$.

In this paper we analyze the pairing within Eliashberg theory, which does not include phase fluctuations and, hence, does not distinguish between a true superconductivity and preformed pairs. We will use the term "superconducting" to describe the state below the onset temperature of the pairing, but label this temperature as T_p to distinguish it from the actual T_c, which can be lower. We analyze superfluid stiffness and the role of phase fluctuations in Ref.[39].

Calculations of the onset temperature for the pairing in all quantum-critical (QC) systems, studied so far, show that it is finite[5,6,19,22,33,34]. This can be interpreted as an evidence that the tendency to pairing is stronger than towards incoherent, NFL behavior. The situation can potentially be reversed if the interaction in the pairing channel is somehow reduced compared to that in the particle-hole channel. This can be achieved by either modifying the momentum dependence of the interaction, mediated by critical fluctuations, to reduce the magnitude of the attractive pairing component, or by extending the model to an $SU(N)$ global symmetry[21] (the original model corresponds to $N = 1$). Under this extension, the

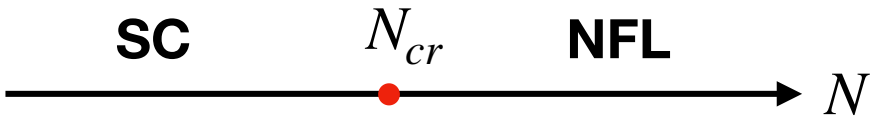

FIG. 1. The $T = 0$ phase diagram of an itinerant QC model with fermion-fermion interaction mediated by a critical boson with dynamical propagator $\chi(\Omega_m) = (g/|\Omega_m|)^\gamma$, where $0 < \gamma < 1$. The original model with $N = 1$ has been extended to $N > 1$ in such a way that the pairing interaction is reduced by $1/N$, while the interaction in the particle-hole channel (the one which gives rise to NFL behavior in the normal state) remains intact. The critical $N_{cr} = N_{cr}(\gamma) > 1$ separates the regions of superconductivity at $N < N_{cr}$ and NFL normal state behavior at $N > N_{cr}$.

pairing interaction is reduced by $1/N$, but the self-energy stays intact[21]. In both cases, the equation for the (frequency dependent) pairing vertex in the attractive channel retains its form, but the overall magnitude of the pairing interaction is reduced. The analysis of a large-N QC model at $T = 0$ shows[21,22] that there exists a critical N_{cr}, separating a superconducting region at $N < N_{cr}$ and a region of a $T = 0$ NFL normal state behavior at $N > N_{cr}$ (see Fig. 1). A conventional reasoning in this situation would be that the $T_p(N)$ terminates at $T = 0$, $N = N_{cr}$, and vanishes for $N > N_{cr}$. However, numerical studies of large-N QC models yield a different result[22] – $T_p(N)$ by-passes $N = N_{cr}$, and remains finite at all N (see Fig. 2).

This unusual behavior was argued in Ref. 22 to be the consequence of the special form of Matsubara fermionic self-energy $\Sigma(\omega_m)$ at the two lowest Matsubara frequencies: $\omega_m = \pi T$ and $\omega_m = -\pi T$. Namely, in Eliashberg theory $\Sigma(k_F, \omega_m)$ is given by the convolution of local fermionic and bosonic propagators and the formula for $\Sigma(k_F, \omega_m)$ contains the sum over internal fermionic Matubara frequencies $\omega_{m'}$ (see Eq. (6) below). For $\omega_m = \pm\pi T$, the sum reduces to the term with $m' = m$ (the self-action term), all other terms in the sum over $\omega_{m'}$ cancel out. The self-action term in $\Sigma(k_F, \omega_m)$ comes from scattering with zero frequency transfer and finite momentum transfer, and mimics the scattering by impurities. The same thermal scattering also contributes to the pairing vertex $\Phi(k_F, \omega_m)$. Both contributions

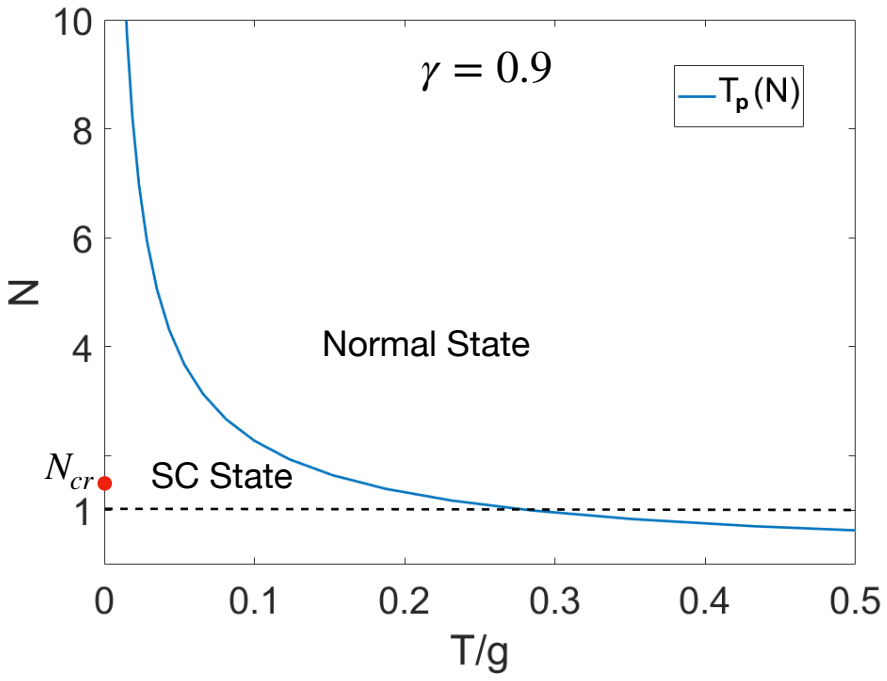

FIG. 2. The onset temperature of the pairing, $T_p(N)$, in the γ model, extended to $N > 1$. We set $\gamma = 0.9$. The line $T_p(N)$ by-passes N_{cr} (the red dot). At large N, $T_p(N) \propto 1/N^{1/\gamma}$.

diverge at a QCP, either on the whole Fermi surface, or at special hot spots. However, for spin-singlet pairing, singular contributions to $\Phi(k_F, \omega_m)$ and $\Sigma(k_F\omega_m)$ cancel out in equation for the gap function $\Delta(k_F, \omega_m) = \Phi(k_F, \omega_m)/(1 + \Sigma(\omega_m)/\omega_m)$, by analogy with the Anderson's theorem[37,40–42]. As the consequence, fermions with $\omega_m = \pm\pi T$ can be viewed for the pairing problem as free particles. Meanwhile, the pairing interaction between fermions with $\omega_m = \pi T$ and $\omega_m = -\pi T$ remains strong. This strong interaction, not countered by the self-energy, gives rise to the emergence of a non-zero $\Delta(k_F, \pm\pi T)$ below a certain $T_p(N)$, which remains finite for all values of N. A finite $\Delta(k_F, \pm\pi T)$ then induces non-zero $\Delta(k_F, \omega_m)$ at other Matsubara frequencies, for which the self-energy is strong even without the self-action term.

In this communication we extend the analysis of superconductivity, induced by first fermionic Matsubara frequencies, to $T < T_p(N)$. We argue that, although $T_p(N)$ by-passes $N = N_{cr}$, there is a crossover in the system behavior at $T_{cross}(N)$. The crossover temperature is numerically smaller than T_p for the physical case $N = 1$, and the line $T_{cross}(N)$ terminates at $T = 0$ at $N = N_{cr}$. In the temperature range $T_{cross}(N) < T < T_p(N)$, superconductivity

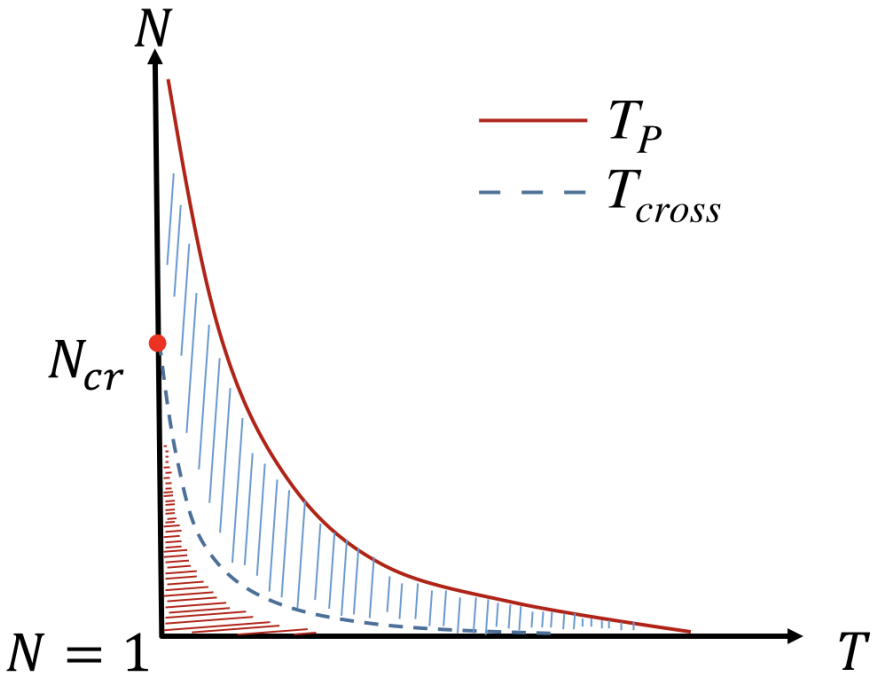

FIG. 3. A schematic phase diagram of our QC model, extended to $N > 1$, for some $\gamma < 1$. The solid line is the onset temperature for superconductivity, $T_p(N)$. The dashed line marks the crossover from the behavior similar to a BCS superconductor at a lower T to the novel behavior at a higher T, in which superconducting order does not provide a substantial feedback effect on the fermionic self-energy, and it largely remains the same as in the normal state. In this region, the spectral function $A(\omega)$ and the DOS $N(\omega)$ are functions of ω/T rather than of $\omega/\Delta(T)$. The critical N_{cr} separates superconducting and normal states at $T = 0$. This phase diagram has been obtained within the Eliashberg theory, which neglects gap fluctuations. The latter likely destroy long-range superconducting order in some T range below $T_p(N)$, leading to pseudogap behavior between the actual T_c and T_p. Our results for $N(\omega)$ and $A(\omega)$ above T_{cross} do not rely on the existence of a long-range superconducting order and should survive in this range.

can be viewed as induced by fermions with $\omega_m = \pm\pi T$; at smaller $T < T_{cross}(N)$ fermions with all ω_m contribute to superconductivity, and the ones with $\omega_m = \pm\pi T$ are no longer special. At $N > N_{cr}, T_{cross} = 0$, and superconductivity induced by fermions with $\omega_m = \pm\pi T$ extends down to $T = 0$. We show the schematic phase diagram in Fig. 3. We emphasize that the system behavior at $T_{cross} < T < T_p$ is qualitatively different from that in a weakly coupled superconductor for any gap symmetry. The conventional superconducting behavior

develops only at temperatures below $T_{cross} < T_p$.

We analyze the evolution of the gap $\Delta(k_F, \omega_m)$ below $T_p(N)$ along the Matsubara axis, and then convert from Matsubara to real frequencies and analyze the behavior of $\Delta(k_F, \omega)$, the spectral function at the Fermi surface $A(k_F, \omega)$, and the density of states (DOS) $N(\omega)$. We argue that the frequency dependence of $A(k_F, \omega)$ and of $N(\omega)$ is qualitatively different for $T < T_{cross}(N)$ and $T_{cross}(N) < T < T_p(N)$. The dependence on k_F is determined by Fermi surface topology, the nature of the pairing boson, and the symmetry of the superconducting state. As our goal is to analyze the universal, model-independent features of the frequency dependencies, present for all pairing symmetries, in the bulk of the paper we will not explicitly specify the dependencies of the pairing vertex, the self-energy, the gap function, and the spectral function on $\mathbf{k}_F$. We will reinstate the dependencies on $\mathbf{k}_F$ when we discuss the specific case of magnetically-mediated $d-$wave superconductor.

A. Summary of the results

Along the Matsubara axis, we find that at large $N > N_{cr}$, the pairing vertex $\Phi(\omega_m)$ is smaller than $\Sigma(\omega_m)$ for all temperatures and all Matsubara frequencies, including $\pm\pi T$. The self-energy $\Sigma(\omega_m)$ with $m \neq 0, -1$ remains essentially the same as in the normal state , i.e., the feedback effect from superconductivity on this self-energy is weak. We show that the pairing gap $\Delta(\omega_m)$ is strongly peaked at $\omega_m = \pm\pi T$. Specifically, $\Delta(\pm\pi T)$ is larger by the factor N than $\Delta(\omega_m \neq \pm\pi T)$. As T decreases below $T_p(N)$, $\Delta(\pi T)$ first increases, and then reaches the maximum and eventually vanishes at $T = 0$. At $N < N_{cr}$, $\Delta(\pi T)$ tends to a finite value at $T = 0$, and the magnitude of $\Delta(0)$ increases as N gets progressively smaller.At $N < N_{cr}$, the temperature dependence of $\Delta(\pi T)$ is still non-monotonic, with the maximum at a finite T. When N gets smaller, the maximum becomes more shallow, and at $N \to 1$, $\Delta(\pi T)$ monotonically increases as T decreases below T_p.

We use the results along the Matsubara axis as an input and obtain the behavior of $\Phi(\omega)$ and $\Sigma(\omega)$ along real frequency axis. Using these $\Phi(\omega)$ and $\Sigma(\omega)$, we obtain the DOS

$$N(\omega) = N_0 \,\mathrm{Re}\left[\frac{1}{\sqrt{1 - \left(\Phi(\omega)/(\omega + \Sigma(\omega))\right)^2}}\right] \tag{1}$$

We show below that the ratio $\Phi(\omega)/(\omega + \Sigma(\omega)$ can be re-expressed exactly as $\Phi^*(\omega)/(\omega + \Sigma^*(\omega))$, where $\Phi^*(\omega)$ and $\Sigma^*(\omega)$ are the solutions of the modified Eliashberg equations, in

which thermal contributions are explicitly taken out.

At the lowest $T < T_{cross}(N)$, $N(\omega)$ displays a conventional BCS-like behavior: it nearly vanishes at $\omega < \Delta(0)$ (more exactly, at $\omega < \omega_0$, where ω_0 is the solution of $\Delta(\omega_0) = \omega_0$), and has a sharp peak at $\omega = \omega_0 \sim \Delta(0)$. As T increases, the position of the maximum in the DOS initially shifts to a lower frequency (because $\Delta(0)$ gets smaller with increasing T), i.e., the gap in the DOS "closes in" with increasing temperature. However, once temperature exceeds $T_{cross}(N)$, this behavior changes qualitatively. We show that at $T_{cross} < T < T_p$, $N(\omega)$ is finite at all frequencies, including $\omega = 0$, and its dependence on ω is determined by the universal scaling function of ω/T. As the consequence, the frequency, at which $N(\omega)$ has a maximum, linearly increases with increasing T. As T approaches T_p from below, DOS "fills in", i.e., $N(\omega)$ approaches N_0, but the position of the maximum in $N(\omega)$ remains at a finite frequency. At $N > N_{cr}$, $T_{cross} = 0$, and the frequency dependence of $N(\omega)$ is determined by the scaling function of ω/T at all T. In this case, $N(\omega = 0)$ remains finite even in the limit $T \to 0$.

We emphasize that these two distinct regimes of the behavior of $N(\omega)$ are present even in the original physical model with $N = 1$. In this respect, the extension to $N > 1$ is just a convenient way to understand the origin of such behavior by extending the width of the regime, in which superconductivity is generated solely by fermions with $\omega = \pm\pi T$. A representative of our results for the DOS is shown in Fig.4

The phenomenon in which $N(\omega = 0)$ remains finite at $T \to 0$ is known as "gapless superconductivity". It was originally found by Abrikosov and Gorkov in their analysis of an s-wave BCS superconductor with magnetic impurities[43]. In their case, gapless superconductivity exists in a finite parameter range before magnetic impurities destroy superconductivity. In general, gapless superconductivity emerges when the imaginary part of the fermionic self-energy at zero frequency remains finite, despite the fact that superconductivity gaps out low-energy excitations. Several researchers argued[44] in early days after BCS that any phonon-mediated s-wave superconductor is a gapless superconductor at a finite T because Im $\Sigma(\omega = 0)$ is finite due to scattering on thermally excited phonons. The same holds for electronically-mediated superconductivity in a clean metal. Still, at the lowest T, Im $\Sigma(\omega = 0)$ is strongly reduced, compared to its normal state value, due to the reduction of the phase space for low-energy scattering[45–48]. Numerical analysis of Eliashberg equations for several models of magnetically-induced d-wave superconductivity[7,16,37] and for strong

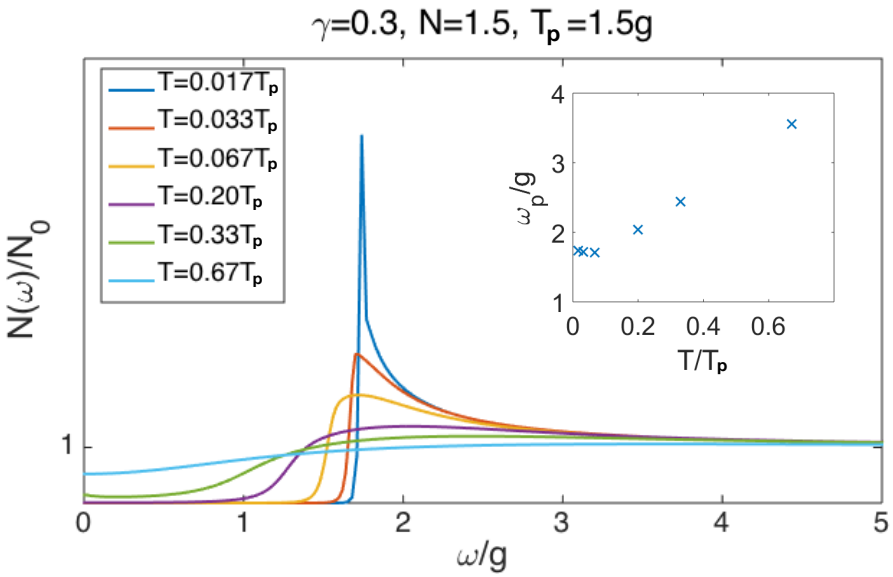

FIG. 4. A representative of our results for the DOS. We set $\gamma = 0.3$ and $N = 1.5$, which is smaller than N_{cr} for this γ. At low $T < T_{cross} \sim 0.1T_p$, the DOS has a peak at $\omega \approx \Delta(T)$, and the peak frequency decreases as temperature increases, i.e. the gap in the DOS closes. At $T > T_{cross}$ the DOS flattens up with increasing T (the gap fills in). In this T range the maximum in the DOS is located at $\omega_p \sim T$, which increases with increasing T.

coupling (small Debye frequency) limit of electron-phonon superconductivity[1–4] shows that $\Sigma''(0)$ rapidly increases above some $T < T_p$, and the maximum in the DOS shifts up from $\Delta(T)$ and remains at a finite frequency at T_p. This is consistent with our theory of two qualitatively different regimes of system behavior below and above T_{cross}.

The behavior of the spectral function is more involved because in $A(\omega)$ the thermal contribution does not cancel out. The expression for $A(\omega) = -(1/\pi)\,\mathrm{Im}[G(k_F, \omega)]$ at $\omega > 0$ is (see Eq.(70) below)

$$A(\omega) = \frac{1}{\pi}\,\mathrm{Im}\left[\frac{\omega + \Sigma(\omega)}{(\omega + \Sigma(\omega))^2 - \Phi(\omega)^2}\right] = \frac{1}{\pi}\,\mathrm{Im}\left[\frac{\omega + \Sigma^*(\omega)}{(\omega + \Sigma^*(\omega))^2 - \Phi^*(\omega)^2} L(\omega)\right] \tag{2}$$

$$L(\omega) = \frac{\sqrt{\Phi^*(\omega)^2 - (\omega + \Sigma^*(\omega))^2}}{P\,\mathrm{sgn}\,\mathrm{Im}\,\tilde{\Sigma}^* + \sqrt{\Phi^*(\omega)^2 - (\omega + \Sigma^*(\omega))^2}} \tag{3}$$

where, we remind, $\Phi^*(\omega)$ and $\Sigma^*(\omega)$ are the solutions of the modified Eliashberg equations without self-action terms. The frequency-independent $P = P(T)$ describes the thermal contribution to the self-energy. When $P > \sqrt{\Phi^*(\omega)^2 - (\omega + \Sigma^*(\omega))^2}$, $L(\omega) \approx$

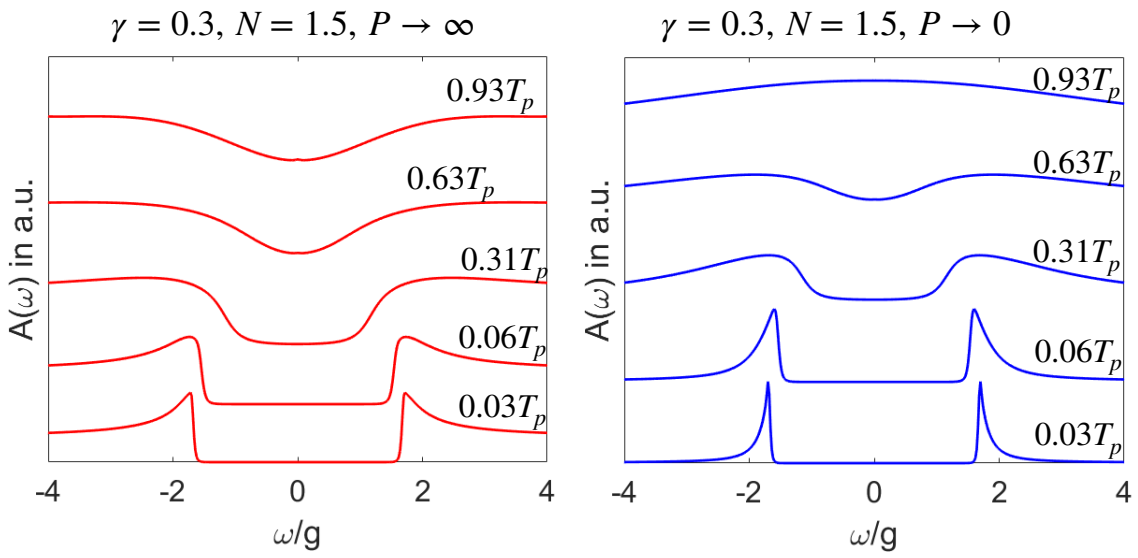

FIG. 5. A representative of our results for the spectral function $A(\omega)$ for $\gamma = 0.3$ and $N = 1.5$ ($N < N_{cr}$). Left panel is for the case when thermal contribution to $A(\omega)$ is strong, right panel is for the case when it is weak (in our notations, the cases $P \to \infty$ and $P \approx 0$, respectively). In both panels, $A(\omega)$ at low $T < T_{cross}$ has well pronounced peaks at $\omega = \pm\Delta(T)$. The peak frequency decreases with increasing T. At $T > T_{cross}$, the peaks disappear, and the spectral function shows a dip, when P is large, and a single peak at $\omega = 0$, when P is small.

$\sqrt{\Phi^*(\omega)^2 - (\omega + \Sigma^*(\omega))^2}/P$. In this case, $A(\omega) \propto N(\omega)$, i.e., the spectral function displays the same crossover from "gap closing" to "gap filling" as the DOS. In the opposite limit $P < \sqrt{\Phi^*(\omega)^2 - (\omega + \Sigma^*(\omega))^2}$, $L(\omega) \approx 1$. In this case, $A(\omega)$ at $T < T_{cross}$ shows two sharp peaks at $\omega = \pm\Delta(0)$. At temperatures above T_{cross}, the two peaks merge, and $A(\omega)$ develops a maximum at $\omega = 0$, resembling that of the normal state. A representative of our results for $A(\omega)$ is shown in Fig.5.

The transformation from "gap closing" to "gap filling" behavior in the DOS and the spectral function has been observed in several superconducting materials, most notably the $d-$wave cuprates[45,49–57] The spectral function in the cuprates shows the same behavior as the DOS in the antinodal regions, where the fermionic incoherence is the strongest, and the $d-$wave gap is the largest. In the regions near the Brillouin zone diagonals, the symmetrized spectral function has peaks at a finite frequency $\pm\Delta(0)$ at low temperatures, and a single maximum at $\omega = 0$ at higher temperatures. The angular range in which the system displays a

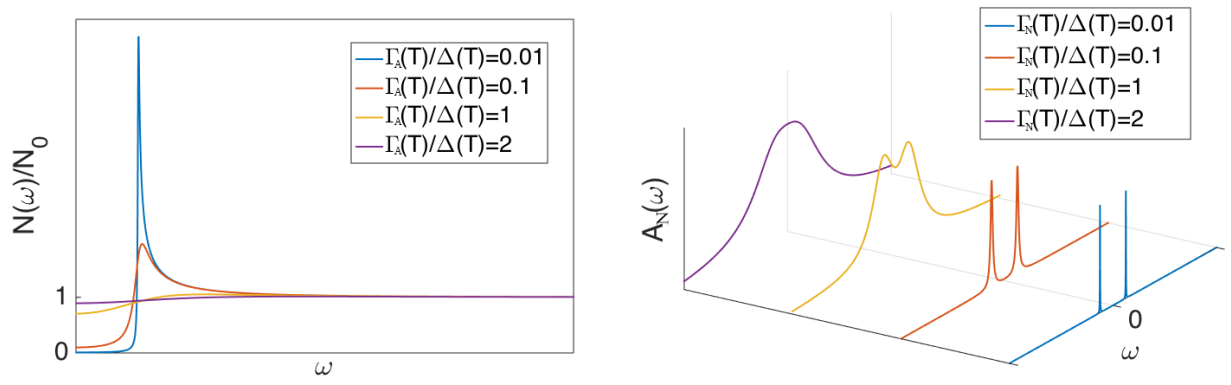

FIG. 6. The DOS $N(\omega)$ and the spectral function $A_N(\omega)$ in a dirty BCS superconductor, from Eq. (4) and Eq. (5).

single peak above a certain T has been termed a Fermi arc[45]. Our results, applied to $d-$wave case, reproduce and explain the observed behavior. We argue that for magnetically-mediated $d-$wave superconductor, the thermal piece in the self-energy $P = P_{k_F}$ in (3) is large in the antinodal region, hence $A(k_F, \omega) \propto N(\omega)$, while in the nodal region P_{k_F} is much weaker, hence $A(k_F, \omega)$ is given by Eq. (2) with $L(\omega) \approx 1$.

B. relation to phenomenological models

The crossover from "gap closing" to "gap filling" in the DOS and in $A(k_F, \omega)$ in the antinodal regions and the crossover from two peaks to a single peak in $A(k_F, \omega)$ in the nodal regions, have been phenomenologically described by assuming that the pairing vertex $\Phi(k_F, \omega)$ is independent of frequency and has the same form as in a weak coupling superconductor (not necessary $s-$wave), while the full self-energy $\Sigma(k_F, \omega) = i\Gamma_{k_F}(T)\,\mathrm{sgn}\,\omega$, where $\Gamma_{k_F}(T)$ is different in nodal (N) and antinodal (A) regions (Refs.[50,58–60]) Under this approximation, the DOS becomes (using $\Phi(k_F, T) = \Delta_{k_F}(T)$ to match the notations in earlier papers and assuming that $\Delta_{k_F}(T) \approx \Delta(T)$ weakly depends on $\mathbf{k}_F$ in the antinodal regions, which gives the largest contribution to the DOS)

$$N(\omega) = N_0\,\mathrm{Re}\left[\frac{1}{\sqrt{1-\left(\frac{\Delta(T)}{\omega+i\Gamma_A(T)}\right)^2}}\right] \tag{4}$$

where $\Gamma_A(T)$ is the damping in the antinodal region. At $\Gamma_A(T) = 0$, the DOS vanishes at $\omega < \Delta$ and is singular at $\omega = \Delta + 0$. A non-zero $\Gamma_A(T)$ makes $N(\omega)$ continuous and non-zero down to $\omega = 0$. Furthermore, the position of the peak in $N(\omega)$ shifts to a higher frequency from $\omega = \Delta(T)$ (see Fig.6) At vanishing $\Delta(T)$ the peak in $N(\omega) \approx N_0 \left(1 + \frac{1}{2}\Delta^2 \,\mathrm{Re}\left[\frac{1}{(\omega + i\Gamma_A)^2}\right]\right)$ remains at a finite $\omega = \sqrt{3}\Gamma_A$. In other words, the magnitude of the deviation of $N(\omega)$ from N_0 is set by Δ^2, while its frequency dependence is set by $\mathrm{Re}\,\frac{1}{(\omega + i\Gamma_A)^2}$ and does not depend on Δ. If one additionally sets phenomenologically $\Gamma_A(T) \propto T$, one obtains that the position of the maximum in the DOS increases linearly with T near $T = T_p$, when $\Gamma_A(T) > \Delta(T)$.

A similar phenomenolgical model, with the linear T dependence of the damping rate in the nodal region, $\Gamma_N(T) \propto T$, was used[60] to explain Fermi arcs. Indeed, approximating $\Phi(k_F, \omega)$ by $\Delta_N(T)$, with d-wave angular dependence, approximating $\Sigma(k_F, \omega)$ by $i\Gamma_N(T)\,\mathrm{sgn}\,\omega$, and using the first formula in (2), we obtain

$$\begin{aligned} A_N(\omega) &= -\frac{1}{\pi}\,\mathrm{Im}\left[\frac{\omega + i\Gamma_N(T)}{\left(\omega + i\Gamma_N(T)\right)^2 - \Delta_N^2(T)}\right] \\ &= \frac{1}{\pi}\frac{\omega^2 + \Delta_N^2(T) + \Gamma_N^2(T)}{\left(\omega^2 - \Delta_N^2(T) - \Gamma_N^2(T)\right)^2 + 4\omega^2\Gamma_N^2(T)} \end{aligned} \tag{5}$$

This spectral function has two separate peaks at positive and negative ω at $\Gamma_N(T) < \sqrt{3}\Delta_N(T)$, and a single maximum at $\omega = 0$ at $\Gamma_N(T) > \sqrt{3}\Delta_N(T)$ (Fig.6)

Phenomenological modeling of the spectral function in the antinodal region requires at least two parameters, as one has to reproduce the form proportional to the DOS. One phenomenological parameter is the analog of the thermal contribution $P(T)$ in Eq. (3), the other sets the form of $\Sigma^*(\omega) = i\Gamma_A^*(T)\,\mathrm{sgn}\,\omega$. The form of the spectral function in the antinodal region is reproduced when $P(T) \gg \Gamma_A^*(T)$.

Comparing our microscopic theory with the phenomenological ones, we note that we can extract from our results the effective damping rates in the nodal and antinodal regions, and these damping rates are indeed similar to the ones used in phenomenological models. Our formulas are more complex than just $\Sigma(\omega) = i\Gamma\,\mathrm{sgn}\,\omega$ and $\Phi(\omega) = \Delta$. Both Σ and Φ in our case are complex functions, with substantial frequency dependence. However, the key distinction between our theory and phenomenology is that we point out the specific reason for the linear in T dependence of the damping rate between T_{cross} and T_p, namely that the pairing in this T range is induced by fermions with $\omega_m = \pm\pi T$, due to the vanishing of $\Sigma^*(\pm\pi T)$.

The issue, which we do not address here, is the role of pairing fluctuations. We remind the reader that Eliashberg theory neglects phase and amplitude fluctuations of the pairing vertex and in this respect T_p, obtained by solving Eliashberg equations, should be treated as the onset temperature for the pairing, rather than the actual T_c for superconductivity. It is very likely that in some range below Eliashberg T_p, fluctuations destroy long-range superconducting order, and the actual $T_c < T_p$. This is corroborated by the analysis of the stiffness for phase fluctuations above T_{cross} (Ref.[39]). In between T_c and T_p, the system displays pseudogap behavior of preformed pairs. Our results for the DOS and the spectral function at $T > T_{cross}$ should survive at $T_c < T < T_p$ because they are the consequences of the fact that in this T range the feedback from the pairing on the fermionic self-energy is weak. Strong fluctuations of the pairing gap reduce this feedback even further. In other words, our theory describes gap filling and Fermi arcs both at $T \leq T_c$ and in the pseudogap region $T_c < T < T_p$. Still, to fully address the issue of gap fluctuations (both transverse and longitudinal), one needs to go beyond Eliashberg theory and analyze the full Luttinger-Ward functional[61].

The paper is organized as follows. In Sec. II we present the microscopic model of the pairing, mediated by a gapless boson with $\chi(\Omega_m) = (g/|\Omega_m|)^\gamma$ (the γ-model), and extend the model to $N > 1$. We present the set of coupled Eliashberg equations along Matsubara axis for the pairing vertex $\Phi(\omega_m)$ and the fermionic self-energy $\Sigma(\omega_m)$ and discuss how one can eliminate the self-action terms. In Sec. III we briefly review earlier results of the analysis of the linearized gap equation, the existence of the critical N_{cr} at $T = 0$, and the behavior of the onset temperature for the pairing $T_p(N)$. In Sec. IV we discuss system behavior at $N > N_{cr}$, first in Matsubara frequencies, in Sec. IV A, and then in real frequencies, in Sec. IV C. We present the analytical solution of the Eliashberg equations at large N and discuss the behavior of the pairing gap, the Free energy and the specific heat, the DOS, and the spectral function. In Sec. V we discuss system behavior at $N < N_{cr}$, again first in Matsubara frequencies, in Sec. V A, and then in real frequencies, in Sec.V B. In Sec. VI we summarize our results and compare them with the experimental data.

II. THE MODEL.

We consider a model of itinerant fermions at the onset of a long-range order in either spin or charge channel. At the critical point, a soft boson associated with the fluctuations of the emerging order parameter, becomes massless and mediates singular interaction between fermions. We follow earlier works[6,7,12–14,16,19,21,22,34,62] and assume that this interaction is attractive in at least one pairing channel and that bosons can be treated as slow modes compared to fermions, i.e., the Eliashberg approximation is valid. Within this approximation one can explicitly integrate over the momentum component perpendicular to the Fermi surface (for a given pairing symmetry) and reduce the pairing problem to a set of coupled integral equations for frequency dependent self-energy $\Sigma(\omega_m)$ and the pairing vertex $\Phi(\omega_m)$ for fermions on the Fermi surface. The interaction between fermions is mediated by a critical boson with $\chi(\Omega) = (g/|\Omega|)^\gamma$ (the γ-model, Refs.[6,7,12,22,34]). We made $\chi(\Omega)$ dimensionless by combining it with fermion-boson coupling constant g. The boson-mediated interaction simultaneously gives rise to the NFL form of the self-energy in the normal state and to pairing. Both effects develop at a scale of order g, which is the only parameter with the dimension of energy. The equations we analyze are

$$\begin{aligned}
\Phi(\omega_m) &= \pi T g^\gamma \sum_{m'} \frac{\Phi(\omega_{m'})}{\sqrt{\tilde{\Sigma}^2(\omega_{m'}) + \Phi^2(\omega_{m'})}} \; \frac{1}{|\omega_m - \omega_{m'}|^\gamma}, \\
\tilde{\Sigma}(\omega_m) &= \omega_m + g^\gamma \pi T \sum_{m'} \frac{\tilde{\Sigma}(\omega_m)}{\sqrt{\tilde{\Sigma}^2(\omega_{m'}) + \Phi^2(\omega_{m'})}} \; \frac{1}{|\omega_m - \omega_{m'}|^\gamma}
\end{aligned} \tag{6}$$

where here and below $\tilde{\Sigma}(\omega_m) = \omega_m + \Sigma(\omega_m)$. Note that we define $\Sigma(\omega_m)$ as a real function of frequency, i.e., without the overall factor of i. The self-energy along Matsubara axis, related by Kramers-Krong (KK) formula to $\Sigma''(\omega)$ along the real frequency axis, does contain i as the overall factor. The superconducting gap $\Delta(\omega_m)$ is defined as a real variable

$$\Delta(\omega_m) = \omega_m \frac{\Phi(\omega_m)}{\tilde{\Sigma}(\omega_m)} \tag{7}$$

The equation for $\Delta(\omega)$ is readily obtained from (6):

$$\Delta(\omega_m) = \pi T g^\gamma \sum_{m'} \frac{\Delta(\omega_{m'}) - \Delta(\omega_m)\frac{\omega_{m'}}{\omega_m}}{\sqrt{\omega_{m'}^2 + \Delta^2(\omega_{m'})}} \; \frac{1}{|\omega_m - \omega_{m'}|^\gamma}. \tag{8}$$

This equation contains a single function $\Delta(\omega)$, but for the price that $\Delta(\omega_m)$ appears on both sides of the equation, which makes (8) less convenient for the analysis than Eqs. (6).

Eq. (6) describes color superconductivity[9] ($\gamma = 0_+$, $\chi(\Omega_m) \propto \log|\omega_m|$), spin- and charge-mediated pairing in $D = 3 - \epsilon$ dimension[14,19,21] ($\gamma = O(\epsilon) \ll 1$), a 2D pairing [38] with interaction peaked at $2k_F$ ($\gamma = 1/4$), pairing at a 2D nematic/Ising-ferromagnetic QCP[5,23,63] ($\gamma = 1/3$), pairing at a 2D (π, π) SDW QCP[6,7,20,64] and an incommensurate CDW QCP[65,66] ($\gamma = 1/2$), a 2D pairing mediated by an undamped propagating boson ($\gamma = 1$), and the strong coupling limit of phonon-mediated superconductivity[1–4] ($\gamma = 2$). The pairing models with parameter-dependent γ have also been considered (Refs. 11 and 12). In this communication we consider the set of γ-models with $\gamma < 1$. The analysis for $\gamma > 1$ requires a separate consideration because of the divergence of the normal state self-energy at $T = 0$.

The full set of Eliashberg equations for electron-mediated pairing contains also the equation describing the feedback from the pairing on $\chi(\Omega)$, e.g., the emergence of a propagating mode (often called a resonance mode) in the dynamical spin susceptibility for $d-$wave pairing mediated by antiferromagnetic spin fluctuations [47,48]. To avoid additional complications, we do not include this feedback into our consideration. In general terms, the feedback from the pairing makes bosons less incoherent and can be modeled by assuming that the exponent γ moves towards larger value as T moves down from T_p.

The two equations in (6) describe the interplay between two competing tendencies – the tendency towards superconductivity, specified by Φ, and the tendency towards incoherent NFL behavior, specified by Σ. The competition between the two tendencies is encoded in the fact that Σ appears in the denominator of the equation for Φ and Φ appears in the denominator of the equation for Σ. Accordingly, a large, non-FL self-energy is an obstacle to Cooper pairing, while once Φ develops, it reduces the strength of the self-energy, i.e., moves a system back into a FL regime.

The r.h.s. of the equations for $\Phi(\omega_m)$ and $\Sigma(\omega_m)$ contain divergent contributions from the terms with $m' = m$, i.e., from $\chi(0)$. The divergence can be regularized by moving slightly away from a QCP, in which case $\chi(0)$ is large but finite. This term mimics the effect of non-magnetic impurities and by Anderson theorem should not affect T_p. To get rid of this thermal contribution in the equations for $\Phi(\omega)$ and $\Sigma(\omega)$, we follow Refs.[37,42] and use the same procedure as in the derivation of the Anderson theorem[67]. Namely, in each equation in (6) we pull out the term with $m' = m$ from the sumand move it to the l.h.s.. We then

introduce new variables $\Phi^*(\omega_m)$ and $\Sigma^*(\omega_m)$ as

$$\begin{aligned}\Phi^*(\omega_m) &= \Phi(\omega_m)\left(1 - Q(\omega_m)\right), \\ \tilde{\Sigma}^*(\omega_m) &= \tilde{\Sigma}(\omega_m)\left(1 - Q(\omega_m)\right)\end{aligned} \tag{9}$$

where

$$Q(\omega_m) = \frac{\pi T \chi(0)}{\sqrt{\tilde{\Sigma}^2(\omega_m) + \Phi^2(\omega_m)}} \tag{10}$$

The ratio $\Phi(\omega_m)/\tilde{\Sigma}(\omega_m) = \Phi^*(\omega_m)/\tilde{\Sigma}^*(\omega_m)$, hence $\Delta(\omega_m)$, defined in (7), is invariant under $\Phi(\omega_m) \to \Phi^*(\omega_m)$ and $\tilde{\Sigma}(\omega_m) \to \tilde{\Sigma}^*(\omega_m)$. Using (9), one can easily verify that the equations on $\Phi^*(\omega_m)$ and $\tilde{\Sigma}^*(\omega_m)$ are the same as in (6), but without the thermal contribution, i.e., the summation over m' now excludes the divergent term with $m' = m$. In the gap equation, the term with $m = m'$ vanishes because the vanishing of the numerator in the r.h.s. of (8). One can also solve (9) backwards and express $\Phi(\omega_m)$ and $\tilde{\Sigma}(\omega_m)$ via $\Phi^*(\omega_m)$ and $\tilde{\Sigma}^*(\omega_m)$ as

$$\begin{aligned}\Phi(\omega_m) &= \Phi^*(\omega_m)\left(1 + Q^*(\omega_m)\right), \\ \tilde{\Sigma}(\omega_m) &= \tilde{\Sigma}^*(\omega_m)\left(1 + Q^*(\omega_m)\right)\end{aligned} \tag{11}$$

where

$$Q^*(\omega_m)\frac{\pi T \chi(0)}{\sqrt{(\tilde{\Sigma}^*(\omega_m))^2 + (\Phi^*(\omega_m))^2}} \tag{12}$$

Like we said in the Introduction, our goal is to analyze the system behavior at $T_{cross} < T < T_p$, in particularly ω/T scaling in the DOS and the spectral function, which we associate with the special role of fermions with Matsubara frequencies $\omega_m = \pm\pi T$. To understand this behavior, it is instructive to extend the range where it holds by reducing the value of T_{cross}. We argue that this can be achieved by reducing the tendency towards pairing compared to that for the NFL normal state. To do this, we follow Refs.[21,68] and extend the model to matrix $SU(N)$. Under this extension, the interaction in the particle-hole channel remains intact, while the interaction in the particle-particle channel acquires an additional factor $1/N$. The outcome of the extension to $N > 1$ depends on whether it is done for the original Eliashberg equations, or for the modified ones, in which self-action terms are eliminated. In Refs.[21,68], the extension to $N > 1$ was done in the original Eliashberg equations. As a result, at $N > 1$ their gap equation at a QCP contains singular terms, which gave rise to qualitative changes in the system behavior between $N = 1$ and $N > 1$. We first eliminate the thermal contributions to $\Phi(\omega_m)$ and $\Sigma(\omega_m)$ only then extend the modified Eliashberg

equations for $\Phi^*(\omega_m)$ and $\Sigma^*(\omega_m)$ to $N \neq 1$, In this procedure, gap equation at $N > 1$ does not acquire singular terms. As our goal is to understand the system behavior at $N = 1$, we believe that our procedure is more adequate as in our case the extension to $N > 1$ reduces T_{cross} and makes it vanish at $N > N_{cr}$, but the structure of the gap equation and equations for the DOS and the spectral function remain the same as at $N = 1$.

The modified equations for $\Phi^*(\omega_m)$ and $\tilde{\Sigma}^*(\omega_m)$ become

$$\Phi^*(\omega_m) = \frac{\pi T}{N} g^\gamma \sum_{m' \neq n} \frac{\Phi^*(\omega_{m'})}{\sqrt{(\tilde{\Sigma}^*(\omega_{m'}))^2 + (\Phi^*(\omega_{m'}))^2}} \frac{1}{|\omega_m - \omega_{m'}|^\gamma},$$
$$\tilde{\Sigma}^*(\omega_m) = \omega_m + g^\gamma \pi T \sum_{m' \neq m} \frac{\tilde{\Sigma}^*(\omega_m)}{\sqrt{(\tilde{\Sigma}^*(\omega_{m'}))^2 + (\Phi^*(\omega_{m'}))^2}} \frac{1}{|\omega_m - \omega_{m'}|^\gamma}, \tag{13}$$

and the equation for $\Delta(\omega_m)$ becomes

$$\Delta(\omega_m) = \frac{\pi T}{N} g^\gamma \sum_{m' \neq m} \frac{\Delta(\omega_{m'}) - N\Delta(\omega_m)\frac{\omega_{m'}}{\omega_m}}{\sqrt{\omega_{m'}^2) + \Delta^2(\omega_{m'})}} \frac{1}{|\omega_m - \omega_{m'}|^\gamma}. \tag{14}$$

Below we will also need the expression for the Free energy F_{sc} of a superconductor, described by the Eliashberg theory. The formula for F_{sc} has been obtained in Refs.[61,69,70] for conventional $s-$wave superconductivity, mediated by an Einstein phonon (the case $\gamma = 2$, finite ω_D, and $N = 1$). Extending the results to $\gamma < 1$, QC regime, where the bosonic mass vanishes, and to $N \neq 1$, we obtain

$$F_{sc} = -N_0 \left(2\pi T \sum_m \frac{\omega_m^2}{\sqrt{\omega_m^2 + \Delta_m^2}} + \pi^2 T^2 g^\gamma \sum_{m \neq m'} \frac{\omega_m \omega_{m'} + \frac{1}{N}\Delta_m \Delta_{m'}}{\sqrt{\omega_m^2 + \Delta_m^2}\sqrt{\omega_{m'}^2 + \Delta_{m'}^2}} \frac{1}{|\omega_m - \omega_{m'}|^\gamma} \right) \tag{15}$$

where $\Delta_m = \Delta(\omega_m)$. The gap equation (14) is obtained from the condition $\delta F_{sc}/\delta \Delta_n = 0$ In the normal state the expression for the Free energy reduces to

$$F_n = -N_0 \left(2\pi T \sum_m |\omega_m| + \pi^2 T^2 g^\gamma \sum_{m \neq m'} \frac{\mathrm{sgn}\,\omega_m \,\mathrm{sgn}\,\omega_{m'}}{|\omega_m - \omega_{m'}|^\gamma} \right) \tag{16}$$

The difference between F_{sc} and F_n at $T = 0$ is the condensation energy of a superconductor. At a finite T,

$$\delta F = F_{sc} - F_n = -2\pi T N_0 \sum_m |\omega_m| \left(\frac{1}{\sqrt{1 + D_m^2}} - 1 \right)$$
$$-N_0 \pi^2 T^2 g^\gamma \sum_{m \neq m'} \frac{\mathrm{sgn}\,\omega_m \,\mathrm{sgn}\,\omega_{m'}}{|\omega_m - \omega_{m'}|^\gamma} \frac{1 + \frac{1}{N} D_m D_{m'} - \sqrt{1 + D_m^2}\sqrt{1 + D_{m'}^2}}{\sqrt{1 + D_m^2}\sqrt{1 + D_{m'}^2}} \tag{17}$$

where $D_n = D(\omega_n) = \Delta(\omega_n)/\omega_n$. Near $T = T_p$, one can expand δF in powers of Δ_m:

$$\begin{aligned}\delta F =& \pi T N_0 \sum_m |\omega_m| D_m^2 - N_0 \pi^2 T^2 g^\gamma \sum_{m\neq m'} \frac{\operatorname{sgn}\omega_m \operatorname{sgn}\omega_{m'}}{|\omega_m - \omega_{m'}|^\gamma} \left(\frac{1}{N} D_m D_{m'} - \frac{D_m^2 + D_{m'}^2}{2} \right) \\ &+ \frac{3}{4} \pi T N_0 \sum_m |\omega_m| D_m^4 - N_0 \pi^2 T^2 g^\gamma \sum_{m\neq m'} \frac{\operatorname{sgn}\omega_m \operatorname{sgn}\omega_{m'}}{|\omega_m - \omega_{m'}|^\gamma} \\ &\times \left(\frac{1}{4} D_m^2 D_{m'}^2 + \frac{3}{8} \left(D_m^4 + D_{m'}^4 \right) - \frac{1}{2N} D_m D_{m'} \left(D_m^2 + D_{m'}^2 \right) \right) \end{aligned} \tag{18}$$

III. THE LINEARIZED GAP EQUATION

To obtain T_p, it is sufficient to consider the linearized gap equation. It is obtained from (13) by setting Φ^* to be infinitesimally small. Then $\Phi^*(\omega_{m'})$ in the denominators of (13) can be ignored, and the self energy $\Sigma^*(\omega_m)$ can be approximated by its normal state form. The resulting equations are:

$$\begin{aligned}\Phi^*(\omega_m) &= \frac{g^\gamma}{N} \pi T \sum_{m'\neq m} \frac{\Phi^*(\omega_{m'})}{|\omega_{m'} + \Sigma^*(\omega_{m'})|} \frac{1}{|\omega_m - \omega_{m'}|^\gamma}, \\ \Sigma^*(\omega_m) &= g^\gamma \pi T \sum_{m'\neq m} \frac{\operatorname{sgn}(\omega_{m'})}{|\omega_m - \omega_{m'}|^\gamma}. \end{aligned} \tag{19}$$

By power counting, $\Sigma^*(\omega_m) \propto g^\gamma \omega_m^{1-\gamma}$. Substituting this into the equation for Φ in (19), we obtain that the pairing kernel $K_{m,m'} \equiv (g^\gamma/N)/(|\omega_{m'} + \Sigma^*(\omega_{m'})|)/|\omega_m - \omega_{m'}|^\gamma$ is marginal at $g \gg |\omega_{m'}| \gg |\omega_m|$, where $K_{m,m'} \propto 1/|\omega'_m|$, and decays as $K_{m,m'} \propto g^\gamma/|\omega_{m'}|^{1+\gamma}$ at $|\omega_{m'}| \gg g, \omega_m$. This implies that T_p, if it exists, should be generally of order g. The marginal form of the kernel is similar to that in the BCS case, and within the perturbation theory gives rise to the logarithmical growth of the pairing susceptibility. However, in distinction to BCS, the marginal form of $K_{m,m'}$ holds only if $|\omega_{m'}| > |\omega_m|$, i.e., at each order of perturbation, the logarithm is cut by the running frequency in the next cross-section in the Cooper ladder. As the consequence, the summation of the logarithms alone does not lead to the divergence of the pairing susceptibility[22]. In this situation, it would be natural to expect that the pairing is a threshold phenomenon, i.e., it occurs if the pairing vertex exceeds some finite value. The pairing strength in Eq. (19) is controlled by $1/N$, hence, by this logics, there should be a critical N_{cr}, separating superconducting state at $N < N_{cr}$ and non-superconducting NFL state at $N > N_{cr}$. The analysis of the pairing problem at $T = 0$

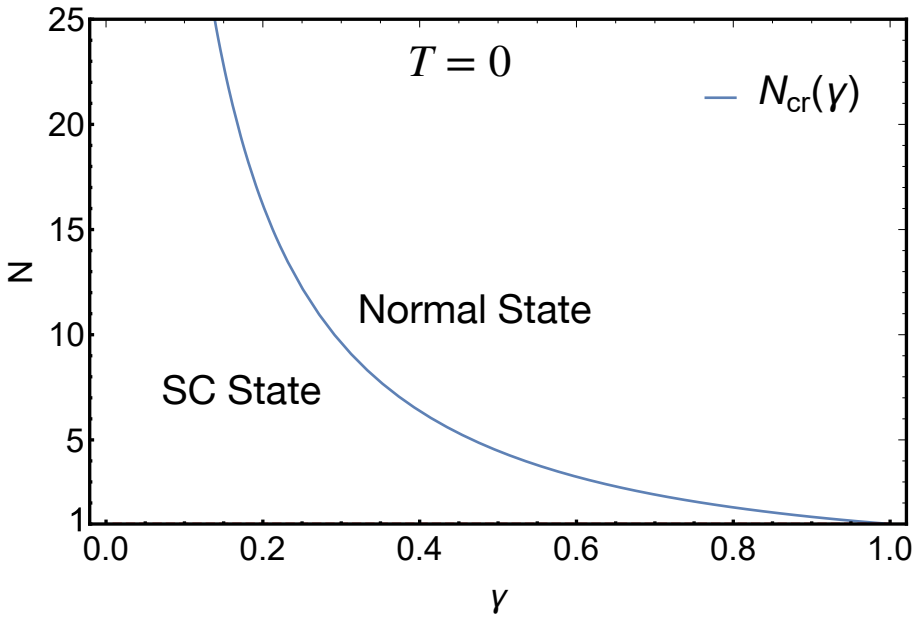

FIG. 7. The behavior of $N_{cr}(\gamma)$, given by Eq. (20). At $T = 0$, this critical N separates superconducting and normal states at $N < N_{cr}(\gamma)$ and $N > N_{cr}(\gamma)$, respectively.

yields exactly this behavior[21,22]: there exists

$$N_{cr} = (1-\gamma)\Gamma(\gamma/2)\left[\frac{\Gamma(\gamma/2)}{2\Gamma(\gamma)} + \frac{\Gamma(1-\gamma)}{\Gamma(1-\gamma/2)}\right], \tag{20}$$

separating superconducting and non-superconducting states ($\Gamma(...)$ is the Gamma function). We plot $N_{cr}(\gamma)$ in Fig.7. We see that $N_{cr} > 1$ for all $\gamma \leq 1$, which we consider here. The value of N_{cr} rapidly increases at small γ. This increase is just the consequence of the fact that in the limit $\gamma \to 0$, the pairing problem reduces to BCS theory without an upper cutoff for frequency integration. Once this cutoff is introduced, $N_{cr}(\gamma = 0)$ remains finite. We emphasize in this regard that for any finite γ, the pairing kernel at large running ω' decreases faster than $1/|\omega_{m'}|$ (as $K_{m,m'} \propto 1/|\omega_{m'}|^{1+\gamma}$), hence the gap equation is unltraviolet convergent even without frequency cutoff.

The existence of N_{cr} at $T = 0$ would normally imply that this is the termination point of the line $T_p(N)$. However, the numerical solution of (19) yields qualitatively different result: T_p is non-zero at any N, and the line $T_p(N)$ by-passes N_{cr} and approaches zero only at $N \to \infty$ (see Fig.8). The reason for this behavior has been named in Ref.[22]: the power counting argument that $\Sigma^*(\omega_m) \propto \omega_m^{1-\gamma}$ does not work for the first two Matsubara frequencies $\omega_m = \pm\pi T$. For these frequencies, Eq. (19) yields $\Sigma^*(\pm\pi T) = 0$ because

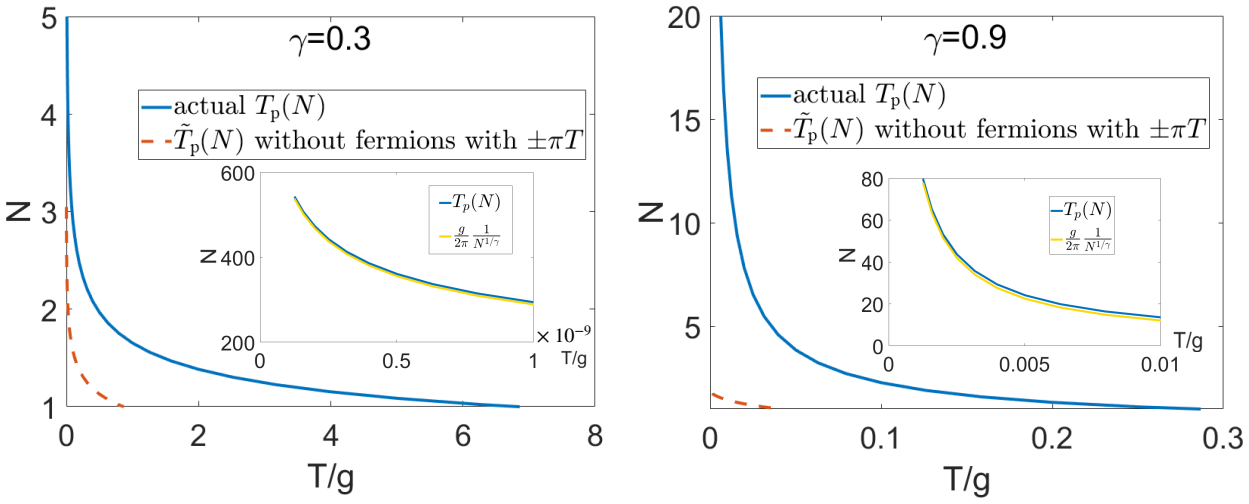

FIG. 8. The pairing instability temperature $T_p(N)$, obtained by solving the linearized gap equation (19) as an eigenvalue/eigengunvction problem for $M = 4000$ Matsubara frequencies, with N playing the role of an eigenvalue. Upper and lower panels are for $\gamma = 0.3$ and $\gamma = 0.9$, respectively. At large N, $T_p(N) \approx (g/2\pi)1/N^{1/\gamma}$. For comparison, we also show $\tilde{T}_p(N)$, which we obtained by solving the linearized gap equation without fermions with Matsubara frequencies $\pm\pi T$. The temperature $\tilde{T}_p(N)$ terminates at $T = 0$ at the critical $N = N_{cr}$.

contributions from positive and negative $\omega_{m'}$ exactly cancel out. To see the consequence of $\Sigma^*(\pm\pi T) = 0$, consider the equation for $\Phi(\omega_m)$ in the limit $N \gg 1$ and set external $\omega_m = \pi T(2m + 1)$ to πT (i.e., set $m = 0$). For $m' = O(1)$, but $m' \neq -1$, the product $\pi T K_{0,m'}$ is independent of T and is of order $1/N$. However, for $m' = -1$ ($\omega_{m'} = -\pi T$), $\pi T K_{0,-1} = (1/N)(g/(2\pi T))^\gamma$ becomes large at small enough T. A simple experimentation shows[22] that in this situation the gap equation reduces to

$$\Phi^*(\pi T) \approx \frac{1}{N}\left(\frac{g}{2\pi T}\right)^\gamma \Phi^*(-\pi T)$$
$$\Phi^*(\omega_m) = \frac{1}{N}\left(\frac{g}{2\pi T}\right)^\gamma \left(\frac{\Phi^*(\pi T)}{|\frac{1}{2} - \frac{\omega_{m'}}{2\pi T}|^\gamma} + \frac{\Phi^*(-\pi T)}{|\frac{1}{2} + \frac{\omega_{m'}}{2\pi T}|^\gamma}\right), \quad m \neq 0, -1 \tag{21}$$

We will be searching for even-frequency solutions of the gap equation: $\Phi^*(\omega_m) = \Phi^*(-\omega_m)$. Then the first equation in (21) sets $T_p = (g/2\pi)1/N^{1/\gamma}$, and the second shows that a non-zero $\Phi^*(\omega_m)$ is induced by $\Phi^*(\pm\pi T)$ and is suppressed by $N^{1/\gamma}$ for $T \to T_p$.

The functional form $T_p \propto 1/N^{1/\gamma}$ at large N has been verified numerically in Ref.[22] for a particular choice of $\gamma = 0.1$. In Fig.8 we show that the same behavior holds for $\gamma = 0.3$

and 0.9. To see that this behavior is indeed due to the vanishing of $\Sigma^*(\pm\pi T)$, we exclude $\omega_m = \pi T$ from the set of Matsubara frequencies and then solve again the linearized gap equation. The result is shown in Fig.8. We clearly see that $\tilde{T}_p$, obtained this way, tends to zero above some critical value of N, which numerically is close to $N_{cr}(\gamma)$ in Eq. (20). This implies that, without the first two Matsubara frequencies, the system would display a conventional behavior, with $\tilde{T}_p(N)$ line terminating at $N = N_{cr}$. That the actual $T_p(N)$ by-passes N_{cr} and vanishes only at $N = \infty$ is then entirely due to the vanishing of the self-energy for fermions with $\omega_m = \pm\pi T$. To check that only fermions with $\omega_m \pm \pi T$ special, we computed $\tilde{T}_{p,1}(N)$ by eliminating fermions with $\pm\pi T$ and $\pm 3\pi$T and obtained that $\tilde{T}_{p,1}(N)$ behaves similar to $\tilde{T}_p(N)$ and terminates at $N \approx N_{cr}$.

This result indicates that the system behavior may be qualitatively different at low $T < \tilde{T}_p(N)$, when all fermions contribute to the pairing, and at $\tilde{T}_p(N) < T < T_p$, when the pairing is induced by fermions with $\omega_m = \pm\pi T$. At $N > N_{cr}$, $\tilde{T}_p = 0$ and fermions with $\omega_m = \pm\pi T$ determine the system behavior for all $T < T_p$. At small γ, $N_{cr} \approx 4/\gamma \gg 1$, and the lines $T_p(N)$ and $\tilde{T}_p(N)$ remain close down to a very small $T \sim g(\gamma)^{1/\gamma} \ll g$. However, for $\gamma \leq 1$, the two lines are distinct already at $T \leq g$. We emphasize that at these γ, the sizable range $\tilde{T}_p(N) < T < T_p(N)$ exists even for the physical case of $N = 1$. The system properties in in this T range should be, at least qualitatively, the same as that at large N.

Below we study superconductivity, induced by fermions with $\omega_m = \pm\pi T$, in some detail by solving the non-linear gap equation at $T < T_p$. We first solve the gap equation in Matsubara frequencies and obtain the gap, the Free energy, and the specific heat, and then convert to real frequencies and obtain the gap function, the spectral function, and the DOS.

IV. NON-LINEAR GAP EQUATION, $N > N_{cr}$

We begin with the case $N > N_{cr}$ when $\tilde{T}_p = 0$, i.e. the pairing would be impossible if the self-energy did not vanish at $\omega_m = \pm\pi T$. The limit $N \gg 1$ can be treated analytically and we consider it in some detail below.

A. Non-linear gap equation in Matsubara frequencies.

The non-linear equation for the pairing vertex $\Phi^*(\omega_m)$ and the equation for the fermionic self-energy $\Sigma^*(\omega_m)$, which includes the feedback from the pairing, are given in (13). We recall that at large N, the pairing temperature $T_p(N)$ is obtained by solving the linearized equation for $\Phi^*(\omega_m)$ for fermions with only two Matsubara frequencies $\omega_m = \pm\pi T$; the pairing vertex $\Phi^*(\omega_m)$ for other ω_m is then expressed via $\Phi^*(\pi T) = \Phi^*(-\pi T)$. We assume and then verify that this holds also for $T < T_p$, i.e., that the non-linear gap equation can be approximated by restricting to $\omega_{m'} = \pm\pi T$ in the r.h.s. of Eq. (13). Re-labeling $\Phi^*(\pi T) = \Phi^*(-\pi T) = \Phi_0^*, \Sigma^*(\pi T) = -\Sigma^*(-\pi T) = \Sigma_0^*$, and $\tilde{\Sigma}_0^* = \pi T + \Sigma^*(\pi T)$, to shorten notations, we obtain from (13) the set of two coupled equations for Φ_0^* and $\tilde{\Sigma}_0^*$:

$$\Phi_0^* = \pi T \left(\frac{T_p}{T}\right)^\gamma \frac{\Phi_0^*}{\sqrt{(\Phi_0^*)^2 + (\tilde{\Sigma}_0^*)^2}}$$
$$\tilde{\Sigma}_0^* = \pi T \left[1 + N \left(\frac{T_p}{T}\right)^\gamma \left(1 - \frac{\tilde{\Sigma}_0^*}{\sqrt{(\Phi_0^*)^2 + (\tilde{\Sigma}_0^*)^2}}\right)\right] \tag{22}$$

The solution of (22) to leading order in $1/N$ is

$$\Phi_0^* = \pi T \left(\frac{2}{N}\right)^{1/2} \left(\frac{T_p}{T}\right)^\gamma \left(1 - \left(\frac{T}{T_p}\right)^\gamma\right)^{1/2}$$
$$\tilde{\Sigma}_0^* = \pi T \left(\frac{T_p}{T}\right)^\gamma, \quad or\ \Sigma_0^* = \pi T \left(\left(\frac{T_p}{T}\right)^\gamma - 1\right) \tag{23}$$

The superconducting gap $\Delta_0 \equiv \Delta(\pm\pi T) = \Phi_0^* \pi T / \tilde{\Sigma}_0^*$ is

$$\Delta_0 = \pi T \left(\frac{2}{N}\right)^{1/2} \left(1 - \left(\frac{T}{T_p}\right)^\gamma\right)^{1/2} \tag{24}$$

The gap Δ_0 vanishes both at $T = 0$ and at $T = T_p$. In between, it is finite, but for any T, $D_0 = \Delta_0/(\pi T)$ is small and at most of order $1/N^{1/2}$. In other words, the gap at $N \gg 1$ remains smaller than the temperature at all $T < T_p$.

Solving next the set of Eliashberg equations for other $\omega_m \neq \pm\pi T$ we obtain at large N

$$\Phi^*(\omega_m) \approx \Phi_0^* \left[\left(\frac{2\pi T}{|\omega_m - \pi T|}\right)^\gamma + \left(\frac{2\pi T}{|\omega_m + \pi T|}\right)^\gamma\right]$$
$$\Sigma^*(\omega_m) \approx 2N\tilde{\Sigma}_0^* H\left(\frac{|\omega_m| - \pi T|}{2\pi T}, \gamma\right) \mathrm{sgn}(m + 1/2) \tag{25}$$

where $H(a, b) = \sum_1^a n^{-b}$ is a Harmonic number. We plot $\Phi^*(\omega_m)$ and $\Sigma^*(\omega_m)$ in Fig.9. At

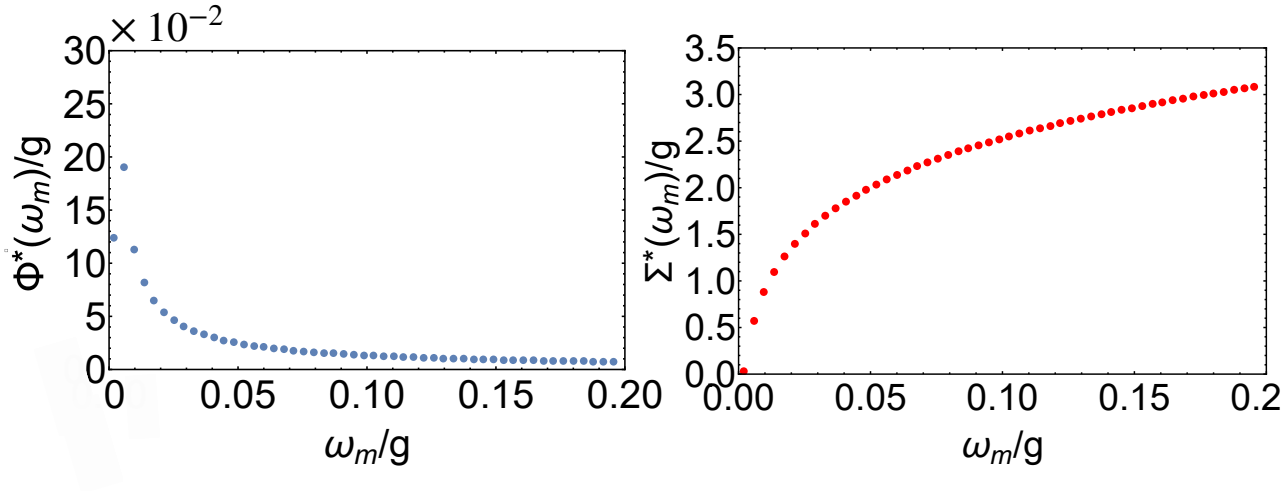

FIG. 9. The pairing vertex $\Phi^*(\omega_m)$ and the self-energy $\Sigma^*(\omega_m)$ from Eq. (25). For definiteness we set $\gamma = 0.9$, $N = 10$, and $T = 0.05T_p$.

large m (but still when $\Sigma^*(\omega_m) \gg \omega_m$)

$$\Phi^*(\omega_m) \approx \frac{2\Phi_0^*}{|m|^\gamma}, \quad \tilde{\Sigma}^*(\omega_m) \approx 2N \frac{|\tilde{\Sigma}_0^*|}{1-\gamma} |m|^{1-\gamma} \operatorname{sgn}(m) \tag{26}$$

Observe that the self-energy behaves as $\Sigma^*(\omega_m) \propto T^{1-\gamma}$, at all $\omega_m = O(T)$, including $\omega_m = \pm\pi T$. Still, the self-energy at $\pm\pi T$ is smaller in $1/N$ than $\Sigma^*(\omega_m)$ at other Matsubara frequencies. As the consequence, the pairing gap $\Delta(\omega_m)$ is parametrically larger at $\omega_m = \pm\pi T$ than at other frequencies. From (25) we have, at $|\omega_m| \neq \pi T$,

$$\Delta(\omega_m) = \frac{\Phi^*(\omega_m)}{\tilde{\Sigma}^*(\omega_m)} = \frac{1}{N} \frac{\Delta_0}{H(m,\gamma)} \left(\frac{1}{m^\gamma} + \frac{1}{(m+1)^\gamma} \right) \propto T \left(\frac{2}{N} \right)^{3/2} \left(1 - \left(\frac{T}{T_p} \right)^\gamma \right)^{1/2}. \tag{27}$$

We also see from see (27) that at any $T < T_p$, $\Delta(\omega_m)$ at any Matsubara frequency is parametrically smaller than T. Put it differently, $D(\omega_m) = \Delta(\omega_m)/\omega_m$ is small, of order $1/N^{3/2}$, at $m = O(1)$, and even smaller at larger m. We plot $\Delta(\omega_m)$ and $D(\omega_m)$ in Fig.10.

Taking $-iD_0$ as an estimate for small frequency limit of $D(\omega) \equiv \Delta(\omega)/\omega$ in real frequencies, we find that $D(\omega \to 0)$ tends to a finite imaginary value, i.e., at large N we have gapless superconductivity in the sense that $\Delta(\omega) \propto i\omega$ (See footnote[71]). Using then $N(\omega) = N_0 \operatorname{Re}[1/\sqrt{1 - D^2(\omega)}]$ for the DOS (N_0 is the normal state value), we find that the DOS at zero frequency $N(\omega = 0) = N_0/\sqrt{1 + D_0^2} \approx N_0 \left(1 - \frac{1}{2} D_0^2\right)$ is reduced below T_p, compared to the normal state value, but remains finite, as in a gapless superconductor.

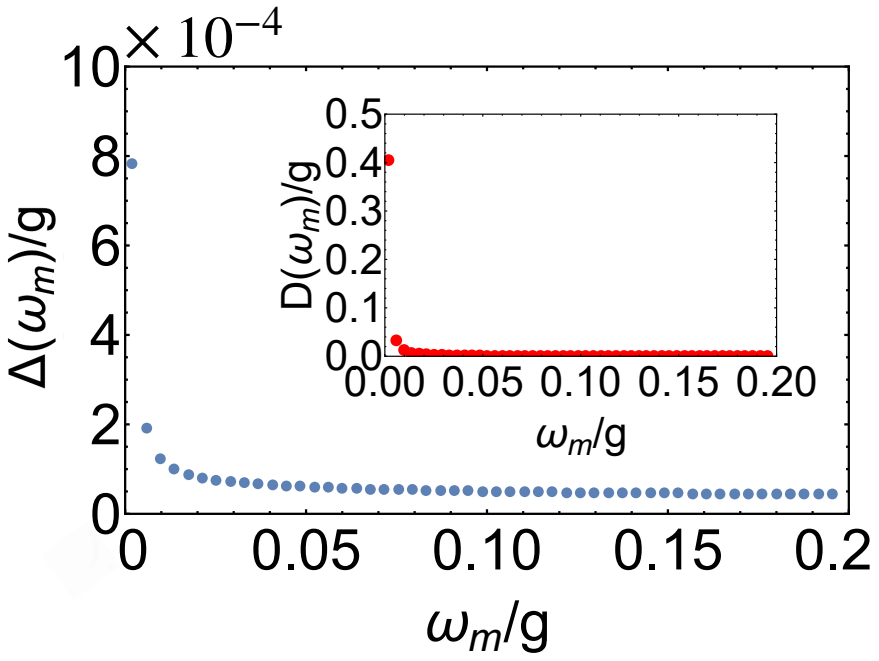

FIG. 10. The pairing gap $\Delta(\omega_m) = \Phi^*(\omega_m)\omega_m/\tilde{\Sigma}(\omega_m)$ and $D(\omega_m) = \Delta(\omega_m)/\omega_m$ for the same parameters as in Fig. 9. Observe that $\Delta(\pi T)$ and $D(\pi T)$ are much larger than at $3\pi T$, etc.

To verify this result and to get the full form of $N(\omega)$ we need to obtain $\Delta(\omega)$ as a function of a real frequency ω. This is what we will do in Sec. IV C. Before that, we use the result for $D(\omega_m)$ and obtain the Free energy $F_{sc}(T)$ and the specific heat $C(T)$ at $N > N_{cr}$.

1. *The Free energy and the specific heat*

The Free energy F_{sc} and $\Delta F = F_{sc} - F_n$ are given by Eqs. (15)-(18). At large N we keep only contributions which contain D_m, $D_{m'}$ with $m, m' = 0, -1$. Contributions from D_m with other m are smaller in $1/N$. Using that $\sum_m \frac{\text{sgn } m}{|\pi T \pm \omega_m|^\gamma} = 0$, we obtain from (18)

$$\delta F \approx -2\pi^2 T^2 N_0 \left(\frac{T_p}{T}\right)^\gamma \left[D_0^2 \left(1 - \left(\frac{T}{T_p}\right)^\gamma\right) - \frac{N D_0^4}{4}\right] \tag{28}$$

Varying δF by Δ_0, one reproduces Eq. (24). Substituting D_0 from (24) into (28), we obtain

$$\delta F \approx -\frac{2}{N}\pi^2 T^2 N_0 \left(\frac{T_p}{T}\right)^\gamma \left(1 - \left(\frac{T}{T_p}\right)^\gamma\right)^2 \tag{29}$$

The specific heat variation between the superconducting and the normal state, $\delta C_v = -T\partial^2 \delta F/\partial T^2$, is

$$\delta C_v = \frac{2}{N}\pi^2 T_p N_0 C_\gamma\left(\frac{T}{T_p}\right) \tag{30}$$

where the scaling function $C_\gamma(x)$ is

$$C_\gamma(x) = 2\gamma^2 x^{\gamma+1} - 2\gamma(3-\gamma)x(1-x^\gamma)$$
$$+(2-\gamma)(1-\gamma)x^{1-\gamma}(1-x^\gamma)^2 \tag{31}$$

At $T \to 0$, $C_\gamma(0) \to 0$, i.e., δC_v vanishes. At $T = T_p - 0$, $C_\gamma = 2\gamma^2$. This sets the magnitude of the specific heat jump at T_p:

$$\delta C_v = (4\gamma^2/N)\pi^2 T_p N_0. \tag{32}$$

The specific heat in the normal state is obtained from (16). The first term in (16) gives the conventional free-fermion contribution to the Free energy $F_{n,free}(T) = F_{n,free}(0) - N_0\pi^2 T^2/3$. The second term gives

$$F_{n,int}(T) = -N_0 N \pi^2 T^2 \left(\frac{T_p}{T}\right)^\gamma \sum_{m\neq m'} \frac{\mathrm{sgn}(m+1/2)\,\mathrm{sgn}(m'+1/2)}{|m-m'|^\gamma} \tag{33}$$

At $T \sim T_p$, this second term is larger by N than the free-fermion contribution. The calculation of the double sum in (33) requires care as one needs to extract the universal constant on top of formally ultra-violet divergent contribution to $F_{n,int}(T=0)$. To extract the universal constant, we note that the summation over $m - m'$ can be done explicitly. The result is

$$\sum_{m\neq m'} \frac{\mathrm{sgn}(m+1/2)\,\mathrm{sgn}(m'+1/2)}{|m-m'|^\gamma} = 4\sum_{m=0}^{\infty} H(m,\gamma), \tag{34}$$

where, we remind, $H(m,\gamma)$ is the Harmonic number. For the remaining summation we use the Euler-Maclaurin formula

$$\sum_{m=0}^{\infty} f(m+1/2) = \int_0^\infty f(x)dx + Q$$
$$Q = -\int_0^{1/2} f(x)dx + \frac{1}{2}f(1/2) - \sum_{n=2}^{\infty}\frac{B_n}{n!}\frac{d^{n-1}f}{dx^{n-1}}_{|\ x=1/2}, \tag{35}$$

where B_n are Bernoulli numbers. The first term in the first line in (35) contributes to $F_{n,int}(T=0)$, the second term determines the universal prefactor in the temperature-dependent piece in the Free energy. To apply this formula, we re-define the Harmonic

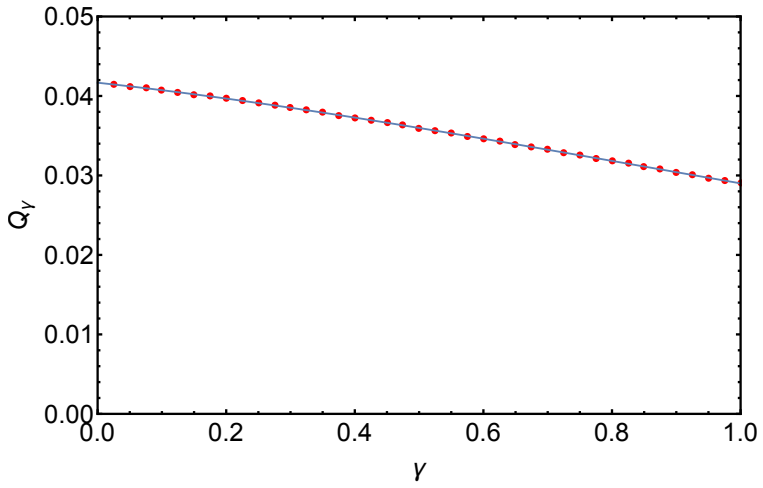

FIG. 11. The plots of the scaling functions Q_γ from Eq. (36).

number as $H(m,\gamma) \to H(m+1/2,\gamma) = \sum_1^{m+1/2-1/2} 1/p^\gamma$ and extend it to a function $H(x,\gamma)$ of a continuous variable x. Evaluating then the integral and the derivatives in the second line in (35) numerically, we obtain

$$\sum_{m=0}^{\infty} H(m,\gamma) = \int_0^\infty H(x,\gamma) + Q_\gamma. \tag{36}$$

We plot Q_γ in Fig.11.

Substituting this result into (33) and differentiating the Free energy over T, we obtain

$$C_{v,n} = N(4\pi^2 N_0 T_p)(2-\gamma)(1-\gamma)Q_\gamma \left(\frac{T}{T_p}\right)^{1-\gamma} \tag{37}$$

The ratio of the specific heat jump to its value at $T = T_p + 0$ is then

$$\frac{\delta C_v}{C_{v,n}} = \frac{1}{N^2}\frac{\gamma^2}{(2-\gamma)(1-\gamma)Q_\gamma} \tag{38}$$

We see that the relative jump of C_v at T_p is small by $1/N^2$. In Fig.12 we plot $C_v(T) = C_{v,n}(T) + \delta C_v(T)$ in the full temperature range below T_p. At sufficiently small T, both C_v and $C_{v,n}$ scale as $T^{1-\gamma}$.

B. Beyond leading order in $1/N$

We now go beyond the leading order in $1/N$. The goal here is to analyze how fermions with other ω_m affect the magnitudes of $\Phi^*(\pi T) = \Phi_0^*$ and $D(\pi T) = D_0$ at a small but finite

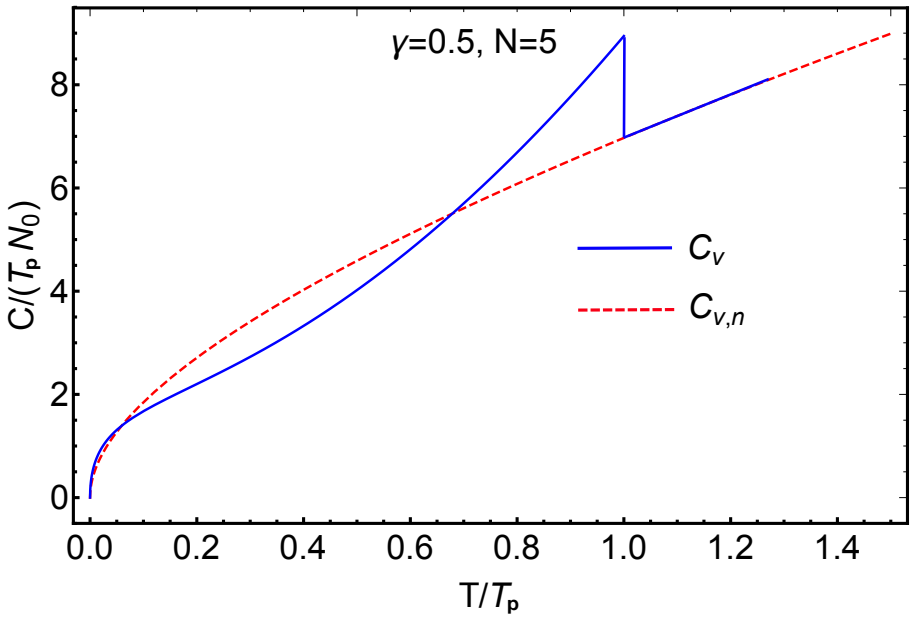

FIG. 12. The specific heat (in units of T_pN_0) vs T/T_p. The dashed line is the normal state result. We set $\gamma = 0.5$ and $N = 5$. Observe that the jump of $C(T)$ at T_p is small, and that at low T specific heat returns back to its normal state value.

temperature. We recall that at large N, $\Phi_0^* \approx (2/N)^{1/2}\pi T(T_p/T)^\gamma$ and $D_0 \approx (2/N)^{1/2}$. We show that both Φ_0 and D_0 increase as N get smaller.

For the analysis to next order in $1/N$ we use the fact that $D_0 \propto 1/N^{1/2}$, while for other Matsubara frequencies $D(\omega_m) \propto 1/N^{3/2}$ (see Eqs. (24) and (27)) Because D appears in even powers in the equation for the self-energy in (13), the inclusion of these $D(\omega_m)$ with $m \neq 0, -1$ would lead to corrections of at least of order $1/N^3$. To order $O(1/N)$ we then still have the same equation for $\tilde{\Sigma}_0^*$ as in (22). Expanding in this equation in two orders of $D_0^2 \propto 1/N$ and setting $T \ll T_p$, we obtain

$$\tilde{\Sigma}_0^* = N\pi T \left(\frac{T_p}{T}\right)^\gamma \left(\frac{D_0^2}{2} - \frac{3D_0^4}{8}\right) \tag{39}$$

The expansion to subleading order in $1/N$ in the equation for Φ_0^* requires more care, as the leading term (the one kept in the first equation in (22)) is of order $1/N^{1/2}$, while other terms in the r.h.s. of (13) are of order $D(\omega_m) \propto 1/N^{3/2}$, i.e., they contain only one additional

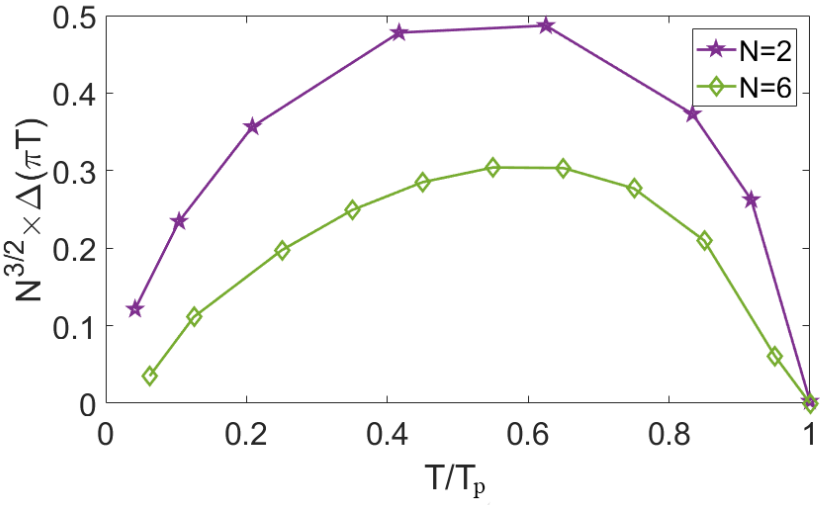

FIG. 13. The gap at the first Matsubara frequency $\Delta(\pi T) = \Delta_0$ as a function of temperature for $\gamma = 0.9$ and two different $N > N_{cr}$. The slope of $\Delta_0(T)$ at small T increases as N gets smaller.

power of $1/N$. Keeping these terms, we obtain from (13):

$$\Phi_0^* = N\pi T \left(\frac{T_p}{T}\right)^\gamma D_0 \left(1 - \frac{D_0^2}{2}\right) + \sum_{m=1}^{\infty} D(\omega_m) \left(\frac{1}{m^\gamma} + \frac{1}{(m+1)^\gamma}\right) \tag{40}$$

Substituting $D(\omega_m) = \Delta(\omega_m)/\omega_m$ from Eq. (27), we obtain

$$\Phi_0^* \left(1 - \frac{W_\gamma}{2N}\right) = N\pi T \left(\frac{T_p}{T}\right)^\gamma D_0 \left(1 - \frac{D_0^2}{2}\right) \tag{41}$$

where

$$W_\gamma = \sum_{m=1}^{\infty} \frac{1}{H(m,\gamma)} \left(\frac{1}{m^\gamma} + \frac{1}{(m+1)^\gamma}\right)^2 \tag{42}$$

We plot W_γ in the inset of Fig.14.

Solving (39) and (41) to order $1/N$ we obtain at low $T \ll T_p$

$$\begin{aligned} \Phi_0^* &= \left(\frac{2}{N}\right)^{1/2} \pi T \left(\frac{T_p}{T}\right)^\gamma \left(1 + \frac{3(W_\gamma - 1)}{4N}\right) \\ \tilde{\Sigma}_0^* &= \pi T \left(\frac{T_p}{T}\right)^\gamma \left(1 + \frac{W_\gamma - 2}{2N}\right) \\ D_0 &= \frac{\Delta_0}{\pi T} \left(\frac{2}{N}\right)^{1/2} \left(1 + \frac{W_\gamma + 1}{4N}\right) \end{aligned} \tag{43}$$

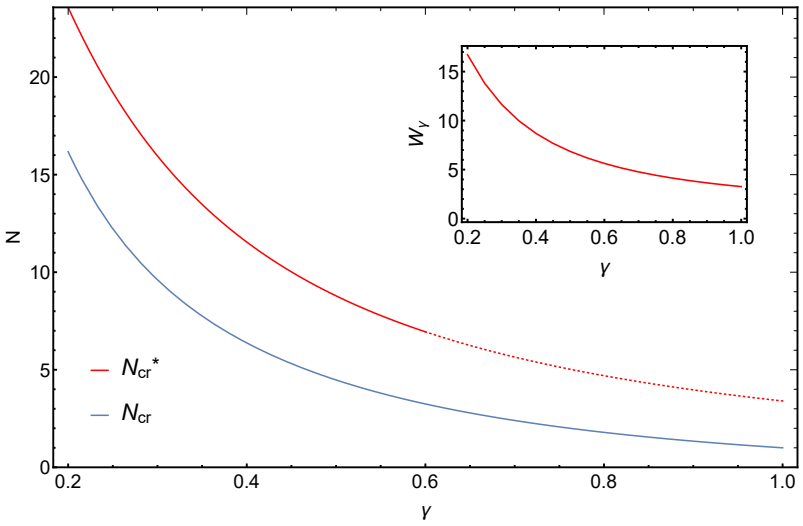

FIG. 14. The approximate $N^*_{cr}(\gamma) = 3(W_\gamma - 1)/2$ vs the actual $N_{cr}(\gamma)$. The inset shows W_γ given by Eq. (42).

The analysis at larger $T \leq T_p$ proceeds in the same way and we refrain from presenting the full formulas. In Fig. 13 we show $\Delta_0 = \Delta(\pi T)$ as a function of T/T_p for $\gamma = 0.9$ and two different values of $N > N_{cr}$ ($N_{cr} \sim 1.3$ for $\gamma = 0.9$). In both cases Δ_0 vanishes at $T = 0$, but the slope of $\Delta_0(T)$ at small T gets larger when N decreases.

The result for Φ_0^* to first order in $1/N$ can be cast into $\Phi_0^* \approx (2/(N - N^*_{cr}))^{1/2}\pi T \left(\frac{T_p}{T}\right)^\gamma$ where $N^*_{cr} = 3(W_\gamma - 1)/2$ is some γ-dependent constant. Taking this approximate formula as an indication of the evolution of Φ_0^* with decreasing N, we find $\Phi_0^* \propto T^{1-\gamma}/(N - N^*_{cr})^{1/2}$. At $N > N^*_{cr}(\gamma)$, Φ_0 vanishes at $T = 0$ (we recall that we consider $\gamma < 1$), but $N = N^*_{cr}(\gamma)$ the slope of $\Phi_0^*(T)/T^{1-\gamma}$ (and of Δ_0) diverges. This is consistent with the $T = 0$ analysis, which indicates that at $N < N_{cr}$, given by Eq. (20), the system has a superconducting order at $T = 0$. The $N^*_{cr}(\gamma) = 3(W_\gamma - 1)/2$ is an approximate function and predictably differs from the actual $N_{cr}(\gamma)$, given by Eq. (20). We plot both functions in Fig.14. Interestingly, $N^*_{cr}(\gamma)$ and $N_{cr}(\gamma)$ show quite similar variation with γ.

We emphasize that the increase of $\Phi_0^*(T \to 0)$ with decreasing N is due to the contribution from fermions with $|\omega_m| \neq \pi T$. We see that these fermions become progressively more involved in the pairing, as N get smaller.

We next consider the solutions for the pairing vertex and the self-energy in real frequencies. This will allow up to compute the spectral function $A(\omega)$ and the DOS $N(\omega)$.

C. Non-linear gap equation in real frequencies

The transformation of Elishberg equations from Matsubara to real frequencies has been discussed in several publications[1,3,4] for electron-phonon interaction. The computational procedure uses spectral decomposition method and analytical continuation. We extend this procedure to our case of electron-mediated pairing with the effective interaction $\chi(\Omega_m) = (g/|\Omega_m|)^\gamma$. The conversion to real frequencies requires special care for two reasons. First, if one simply replaces ω_m by $-i\omega$ in the bosonic propagator $\chi(\omega_{m'} - \omega_m) \to \chi(\omega_{m'} + i\omega)$, it will have a set of branch cuts in the complex ω plane, along $\omega = i\omega_m + b$, where b is real. One needs to add additional terms to the r.h.s. of the equations for retarded functions $\Phi^R(\omega)$ and $\Sigma^R(\omega)$ to cancel these singularities and restore analyticity. Second, we again need to eliminate singular contributions from the terms with zero bosonic Matsubara frequency. This can be done in the same way as in the calculations along the Matsubara axis. Namely, we introduce new functions $\Phi^{*,R}(\omega)$ and $\tilde{\Sigma}^{*,R}(\omega)$, related to $\Phi^R(\omega)$ and $\tilde{\Sigma}^R(\omega) = \omega + \Sigma^R(\omega)$ as

$$\Phi^{*,R}(\omega) = \Phi^R(\omega)\,(1 - Q(\omega))\,, \quad \tilde{\Sigma}^{*,R}(\omega) = \tilde{\Sigma}^R(\omega)\,(1 - Q(\omega))\,, \tag{44}$$

where $Q(\omega)$ is singular (see Eq. (48) below), but $\Phi^{*,R}(\omega)$ and $\tilde{\Sigma}^{*,R}(\omega)$ are free from singularities. The equations on $\Phi^{*,R}(\omega)$ and $\tilde{\Sigma}^{*,R}(\omega)$ are the same as on $\Phi^R(\omega)$ and $\tilde{\Sigma}^R(\omega)$, but with additional terms which cancel out divergent contribution from $\chi(0)$. The gap function $\Delta^R(\omega) = \omega\Phi^R(\omega)/\tilde{\Sigma}^R(\omega)$ is equally expressed in terms of $\Phi^{*,R}(\omega)$ and $\tilde{\Sigma}^{*,R}(\omega)$:

$$\Delta^R(\omega) = \omega\frac{\Phi^R(\omega)}{\tilde{\Sigma}^R(\omega)} = \omega\frac{\Phi^{*,R}(\omega)}{\tilde{\Sigma}^{*,R}(\omega)} \tag{45}$$

To simplify the formulas, below we skip the index R. All functions, which we obtain in real frequencies, are retarded functions.

Taking care of both the branch cuts and the divergent terms, we obtain the equations for $\Phi^*(\omega)$ an $\tilde{\Sigma}^*(\omega)$ in the form (see Appendix for details)

$$\Phi^*(\omega) = \frac{\pi T}{N}\sum_m \frac{\Phi^*(\omega_m)}{\sqrt{(\Phi^*(\omega_m))^2 + (\tilde{\Sigma}^*(\omega_m))^2}}\chi(\omega_m + i\omega)$$
$$+ \frac{1}{N}\int dx \left[S_\Phi(\omega - x)\chi^{''}(x)\left(n_F(x-\omega) + n_B(x)\right) - S_\Phi(\omega)\chi^{''}(x)\frac{T}{x}\right],$$
$$\tilde{\Sigma}^*(\omega) = \omega + i\pi T\sum_m \frac{\tilde{\Sigma}^*(\omega_m)}{\sqrt{(\Phi^*(\omega_m))^2 + (\tilde{\Sigma}^*(\omega_m))^2}}\chi(\omega_m + i\omega) \tag{46}$$
$$+ \int dx \left[S_\Sigma(\omega - x)\chi^{''}(x)\left(n_F(x-\omega) + n_B(x)\right) - S_\Sigma(\omega)\chi^{''}(x)\frac{T}{x}\right],$$

where

$$S_\Phi(\omega) = \frac{\Phi(\omega)}{\sqrt{\Phi^2(\omega) - \tilde{\Sigma}^2(\omega)}}, \quad S_\Sigma(\omega) = \frac{\tilde{\Sigma}(\omega)}{\sqrt{\Phi^2(\omega) - \tilde{\Sigma}^2(\omega)}} \tag{47}$$

and $\chi^{''}(x) = \mathrm{Im}\,\chi(x) = \mathrm{sgn}(x)\frac{g^\gamma}{|x|^\gamma}\sin\frac{\pi\gamma}{2}$. In (46), the solution of the Eliashberg equations in Matsubara frequencies, i.e., $\Phi^*(\omega_m)$ and $\tilde{\Sigma}^*(\omega_m)$ are considered as inputs. The first term in each of the two equations is obtained by just replacing ω_m by $-i\omega$, the second one cancels out non-analyticities, and last one cancels out the divergent contribution from $\chi(0)$. We re-iterate that we cancel out the divergence at $x = 0$ before extending the model to large N. The function $Q(\omega)$ in (44), which determines the relations between $\Phi^*(\omega)$ and $\tilde{\Sigma}^*(\omega)$ and $\Phi(\omega)$ and $\tilde{\Sigma}(\omega)$, is

$$Q(\omega) = \frac{P}{\sqrt{\Phi^2(\omega) - \tilde{\Sigma}^2(\omega)}} \tag{48}$$

where

$$P = \int dx\chi^{''}(x)\frac{T}{x} = \pi T\chi(0) \tag{49}$$

Equivalently, we can express $\Phi(\omega)$ and $\tilde{\Sigma}(\omega)$ via $\Phi^*(\omega)$ and $\tilde{\Sigma}^*(\omega)$ as

$$\Phi(\omega) = \Phi^*(\omega)\left(1 + Q^*(\omega)\right), \tilde{\Sigma}(\omega) = \tilde{\Sigma}^*(\omega)\left(1 + Q^*(\omega)\right), \tag{50}$$

where

$$Q^*(\omega) = \frac{P\,\mathrm{sgn}\,\mathrm{Im}\,\tilde{\Sigma}^*}{\sqrt{(\Phi^*)^2(\omega) - (\tilde{\Sigma}^*)^2(\omega)}} \tag{51}$$

In Eqs. (47-51) the square root is defined with a branch cut along negative real axis.

We now analyze the Eqs. (46). At $\omega = 0$ we have

$$\Phi^*(0) = \frac{\pi T}{N}\sum_m \frac{\Phi^*(\omega_m)}{\sqrt{(\Phi^*(\omega_m))^2 + (\tilde{\Sigma}^*(\omega_m))^2}}\chi(\omega_m) + \frac{1}{N}\int dx\chi^{''}(x)\left(\frac{S_\Phi(-x)}{\sinh x/T} - \frac{S_\Phi(0)}{x/T}\right)$$
$$\tilde{\Sigma}^*(0) = i\pi T\sum_m \frac{\tilde{\Sigma}^*(\omega_m)}{\sqrt{(\Phi^*(\omega_m))^2 + (\tilde{\Sigma}^*(\omega_m))^2}}\chi(\omega_m) + \int dx\chi^{''}(x)\left(\frac{S_\Sigma(-x)}{\sinh x/T} - \frac{S_\Sigma(0)}{x/T}\right) \tag{52}$$

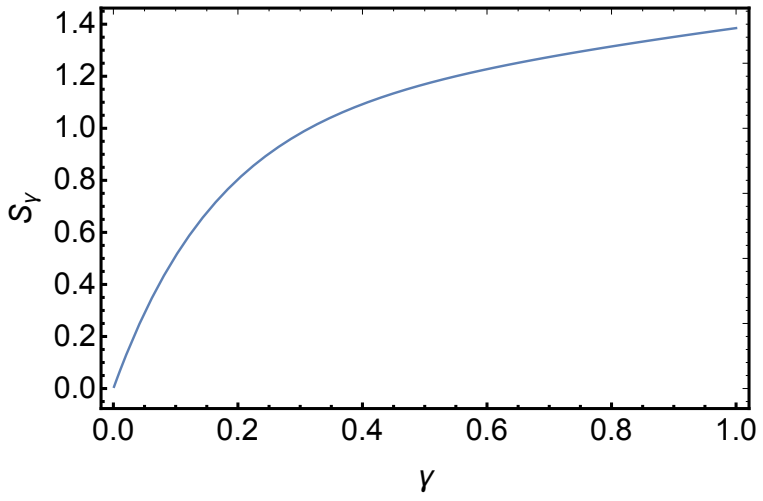

FIG. 15. The scaling function S_γ, defined in (54).

The first term in the formula for $\tilde{\Sigma}^*(0)$ vanishes by symmetry, after summing up the contributions from positive and negative ω_m.

We first consider large N. We assume and then verify that in this case $\tilde{\Sigma}^*$ is parametrically larger than Φ^* not only along the Matsubara axis but also along the real axis. To leading order in $1/N$ we then have for the self-energy, using $\tilde{\Sigma}(\omega)/\sqrt{-i\tilde{\Sigma}(\omega)} = i$, valid for a retarded $\tilde{\Sigma}(\omega)$,

$$\tilde{\Sigma}^*(0) = i \int dx \chi''(x) \left(\frac{1}{\sinh x/T} - \frac{T}{x} \right) = -i\pi T \left(\frac{g}{\pi T} \right)^\gamma S_\gamma, \tag{53}$$

where

$$S_\gamma = 2 \sin \pi\gamma/2 \int_0^\infty \frac{dx}{x^\gamma} \left(\frac{1}{\pi x} - \frac{1}{\sinh \pi x} \right). \tag{54}$$

We plot S_γ in Fig.15.

For $\Phi^*(0)$ we find from Eq. (52)

$$\Phi^*(0) \approx \frac{\pi T}{N} \sum_m \frac{\Phi^*(\omega_m)}{|\tilde{\Sigma}^*(\omega_m)|} \chi(\omega_m). \tag{55}$$

Using the fact that at large N the dominant contribution to the Matsubara sum comes from $m = 0, -1$ and substituting the expressions for $\Phi^*(\pm\pi T)$ and $\Sigma^*(\pm\pi T)$, we obtain

$$\Phi^*(0) = \left(\frac{2}{N} \right)^{3/2} \pi T \left(\frac{g}{\pi T} \right)^\gamma \left(1 - \left(\frac{T}{T_p} \right)^\gamma \right)^{1/2}. \tag{56}$$

Then $D_0 = \Phi^*(0)/\tilde{\Sigma}^*(0)$ is

$$D_0 = i \left(\frac{2}{N} \right)^{3/2} \frac{1}{S_\gamma} \left(1 - \left(\frac{T}{T_p} \right)^\gamma \right)^{1/2}, \tag{57}$$

and the DOS at zero frequency is

$$N(0) = N_0 \left(1 - \left(\frac{2}{N}\right)^3 \frac{\left(1 - \left(\frac{T}{T_p}\right)^\gamma\right)}{2S_\gamma^2}\right). \tag{58}$$

This agrees, up to a prefactor, with the estimate that we obtained in the analysis on the Matsubara axis, by just assuming that $D(\omega_m = \pi T)$ is comparable to $D(\omega = 0)$.

We emphasize that $N(0)$ differs from the normal state value N_0 at all $T < T_p$, including $T = 0$, where we expect superconductivity to disappear. We will show below that the limit $\omega \to 0$ and $T \to 0$ has to be taken with care, and at any non-zero ω the DOS indeed transforms into N_0 at $T \to 0$. Still, strictly at $\omega = 0$, $N(0) < N_0$. This is somewhat similar to the behavior of $N(\omega)$ in an ideal BCS superconductor, where $N(0) = 0$ for all T up to T_c, while $N(\omega \neq 0)$ approaches N_0 at $T \to T_c$.

We next move to finite ω. In the Eq. (46) for $\Phi(\omega)$, the second term ($(1/N)\int ...$) is of order $\Phi(\omega)/N$ and can be neglected at large N. Evaluating the first term by summing up the contributions from $m = 0, -1$, at which $\Phi^*(\omega_m)/|\tilde{\Sigma}^*(\omega_m)|$ is the largest, we obtain

$$\Phi^*(\omega) = \left(\frac{2}{N}\right)^{3/2} \pi T \left(\frac{g}{\pi T}\right)^\gamma \left(1 - \left(\frac{T}{T_p}\right)^\gamma\right)^{1/2} F_\Phi\left(\frac{\omega}{\pi T}\right), \tag{59}$$

where

$$F_\Phi(x) = \frac{1}{2}\left(\frac{1}{(1+ix)^\gamma} + \frac{1}{(1-ix)^\gamma}\right). \tag{60}$$

Note that $F_\Phi(x)$ is purely real and even in x, hence $\Phi^*(\omega)$ is real and even in ω.

Because $\Phi^*(\omega)$ is small in $1/N^{3/2}$, the self-energy at finite ω remains the same as in the normal state, up to $1/N^3$ corrections:

$$\Sigma^*(\omega) = \pi T \left(\frac{g}{\pi T}\right)^\gamma F_\Sigma\left(\frac{\omega}{\pi T}\right), \tag{61}$$

where

$$F_\Sigma(x) = i \sum_{m=0}^{\infty} \left(\frac{1}{(2m+1+ix)^\gamma} - \frac{1}{(2m+1-ix)^\gamma}\right)$$
$$-i \sin\frac{\pi\gamma}{2} \int_0^\infty \frac{dy}{y^\gamma}\left(\frac{2}{\pi y} - \coth\frac{\pi y}{2} + \frac{\sinh \pi y}{\cosh \pi y + \cosh \pi x}\right). \tag{62}$$

The first term in $F_\Sigma(x)$ is real, the second is imaginary. At large x (i.e., at $\omega \gg \pi T$), $F_\Sigma(x) \approx (x^{1-\gamma}/(1-\gamma))e^{i\pi\gamma/2}$. We plot the scaling functions $F_\Phi(x)$, $\mathrm{Re}[F_\Sigma(x)]$, and $\mathrm{Im}[F_\Sigma(x)]$ in Fig. 16.

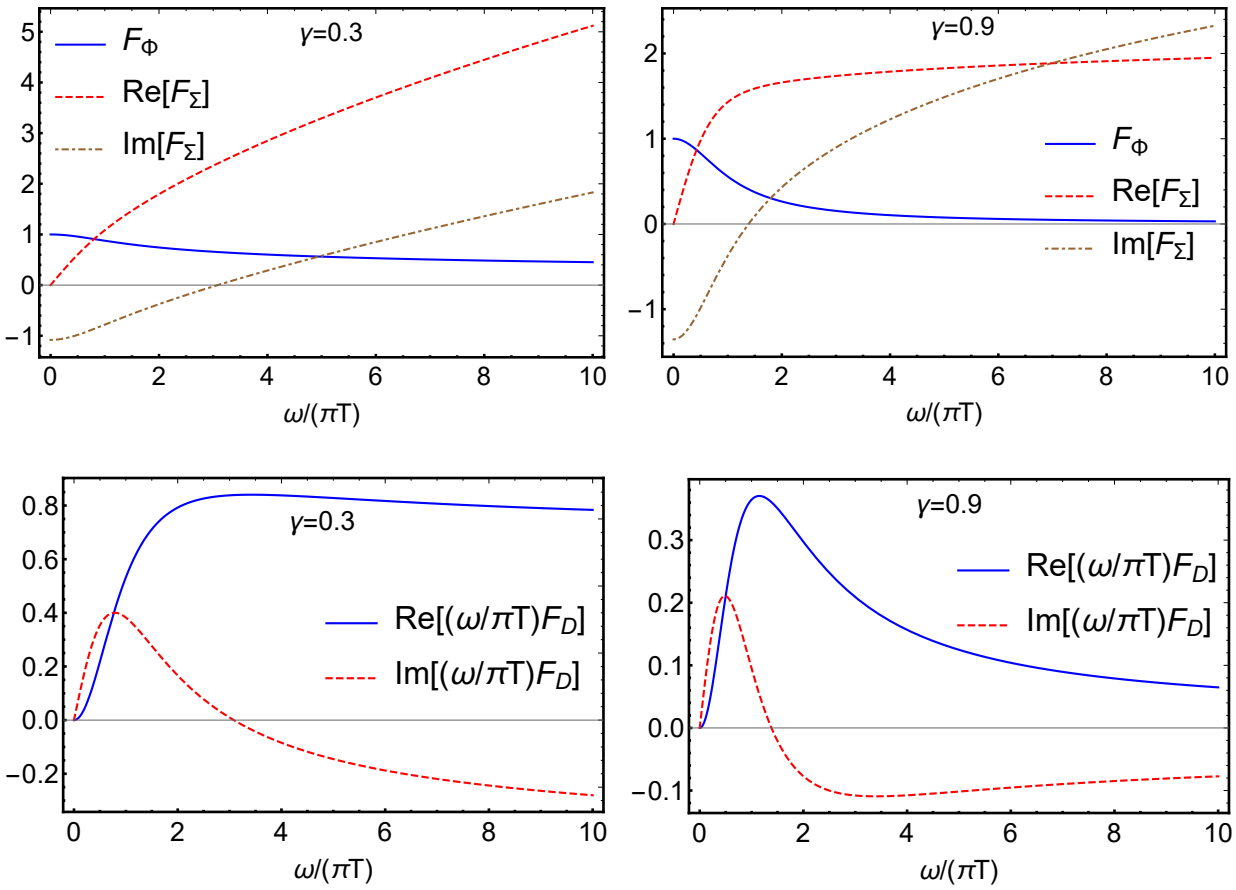

FIG. 16. The scaling functions $F_\Phi(\frac{\omega}{\pi T})$, $F_\Sigma(\frac{\omega}{\pi T})$ and $\frac{\omega}{\pi T}F_D(\frac{\omega}{\pi T}) = \frac{\omega}{\pi T}F_\Phi(\frac{\omega}{\pi T})/F_\Sigma(\frac{\omega}{\pi T})$ for the pairing vertex, the self-energy and the gap function respectively, see Eqs. (60), (62), and (65). We recall that $F_\Phi(\frac{\omega}{\pi T})$ and $F_\Sigma(\frac{\omega}{\pi T})$ are computed without the thermal contribution. The function $F_\Phi(x)$ is real, $F_\Sigma(x)$ and $F_D(x)$ are complex, i.e., the gap function $\Delta(x)$ is a complex function of frequency. The results are for $\gamma = 0.3$ and $\gamma = 0.9$. Observe that $\mathrm{Im}\, F_\Sigma(x)$ changes sign at some frequency. This sign change is necessary to satisfy KK relation on $\Sigma^*(\pi T) = 0$ (see Fig. 17).

We see that $\mathrm{Im}\left[F_\Sigma\left(\frac{\omega}{\pi T}\right)\right]$ changes sign as a function of frequency (hence, $\mathrm{Im}\,[\Sigma^*(\omega)]$ also changes sign). This sign change must happen because $\mathrm{Im}[\Sigma^*(\omega)]$ is related by Kramers-Kronig(KK) formula to $\Sigma^*(\pi T) = 0$:

$$2T\int_0^\infty d\omega \frac{\mathrm{Im}\,\Sigma^*(\omega)}{\omega^2 + (\pi T)^2} = \Sigma^*(\pi T) = 0. \tag{63}$$

The integral in the r.h.s. of (63) vanishes only if $\mathrm{Im}[\Sigma^*(\omega)]$ changes sign at least once. We verified numerically that the KK relation is indeed satisfied, see Fig.17. We remind in this

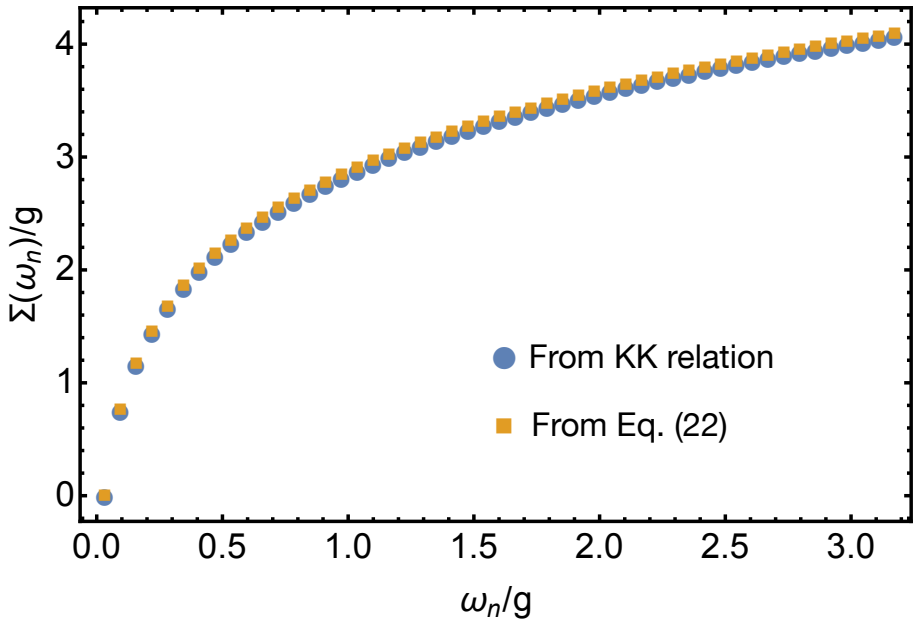

FIG. 17. The verification of the KK transformation. Yellow squares – the self-energy obtained directly along the Matsubara axis: $\Sigma^*(i\omega_n) = 2\pi T(g/2\pi T)^\gamma H(n,\gamma)$, Eq. (25). Blue circles – the self-energy $\Sigma^*(i\omega_n) = -i\pi T(g/\pi T)^\gamma F_\Sigma(\omega_n)$, where $F_\Sigma(i\omega_n) = (2i\omega_n/pi)\int_0^\infty dx\,\mathrm{Im}\,F_\Sigma(x)/(x^2+\omega_n^2)$ is obtained by KK transformation from $\mathrm{Im}\,F_\Sigma(x)$ along the real axis, see (62). The two expressions coincide. To better show this we manually split the two expressions for $\Sigma^*(i\omega_n)$ by multiplying the yellow curve by 1.01. Observe that $F_\Sigma(i\pi T) = 0$, i.e., the self-energy $\Sigma^*(i\omega_n)$, extracted from KK transformation, vanishes at the first Matsubara frequency. We set $\gamma = 0.9$ and $T = 0.01g$.

regard that Σ^* is the self-energy without the thermal contribution. The imaginary part of the full self-energy, $\mathrm{Im}[\Sigma(\omega)]$, indeed remains positive at all frequencies.

Substituting the results for $\Phi^*(\omega)$ and $\tilde{\Sigma}^*(\omega)$ into $\Delta(\omega) = \Phi^*(\omega)\omega/\tilde{\Sigma}^*(\omega)$ and $D(\omega) = \Delta(\omega)/\omega$, we obtain

$$\Delta(\omega) = \left(\frac{2}{N}\right)^{3/2}\left(1-\left(\frac{T}{T_p}\right)^\gamma\right)^{1/2}\omega F_D\left(\frac{\omega}{\pi T}\right),\ \ D(\omega) = \left(\frac{2}{N}\right)^{3/2}\left(1-\left(\frac{T}{T_p}\right)^\gamma\right)^{1/2} F_D\left(\frac{\omega}{\pi T}\right). \tag{64}$$

At $\omega \le g$, when $\tilde{\Sigma}^*(\omega) \approx \Sigma^*(\omega)$,

$$F_D(x) = \frac{F_\Phi\left(\frac{\omega}{\pi T}\right)}{F_\Sigma\left(\frac{\omega}{\pi T}\right)}. \tag{65}$$

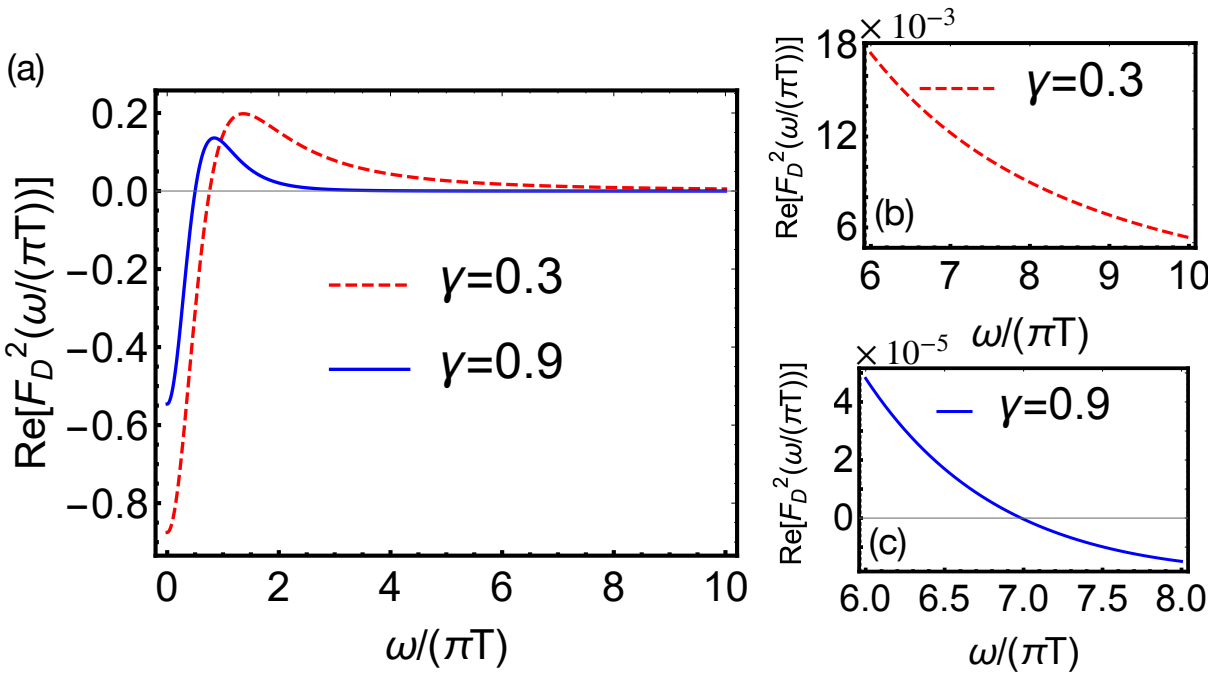

FIG. 18. (a) The real part of the scaling function $F_D^2(\frac{\omega}{\pi T})$, defined in Eq. (65), for $\gamma = 0.3$ and $\gamma = 0.9$. The $\mathrm{Re}[F_D^2(\frac{\omega}{\pi T})]$ determines the frequency dependence of the DOS at large N, Eq. (66). In the normal state $F_D = 0$. Observe that $\mathrm{Re}[F_D^2(\frac{\omega}{\pi T})]$ has a peak at $\omega \sim T$. (b) and (c) The magnified plots of $\mathrm{Re}[F_D^2(\frac{\omega}{\pi T})]$ at lager $\omega/(\pi T)$. For $\gamma = 0.3$, $\mathrm{Re}[F_D^2(\frac{\omega}{\pi T})]$ gradually decreases, for $\gamma = 0.9$ it changes sign at $\frac{\omega}{\pi T} \sim 7$.

The DOS is

$$N(\omega) = N_0\,\mathrm{Re}\left[\frac{1}{(1-D^2(\omega))^{1/2}}\right] \approx N_0\left(1+\frac{1}{2}\,\mathrm{Re}\left[D^2(\omega)\right]\right)$$
$$= N_0\left(1+\frac{1}{2}\left(\frac{2}{N}\right)^3\left(1-\left(\frac{T}{T_p}\right)^\gamma\right)\mathrm{Re}\left[F_D^2\left(\frac{\omega}{\pi T}\right)\right]\right). \tag{66}$$

We see that the magnitude of $N(\omega)/N_0 - 1 \approx \frac{1}{2}\,\mathrm{Re}\,D^2(\omega)$ is determined by the temperature-dependent factor in (64) and depends on T/T_p. However, the frequency dependence of $D(\omega)$ and of the DOS is determined by $F_D(\omega/(\pi T))$, which for any given γ is a universal function of ω/T and does not depend on T/T_p. This implies that the characteristic frequency, at which $N(\omega)$ deviates from N_0, is determined by the temperature rather than by the magnitude of the superconducting gap.

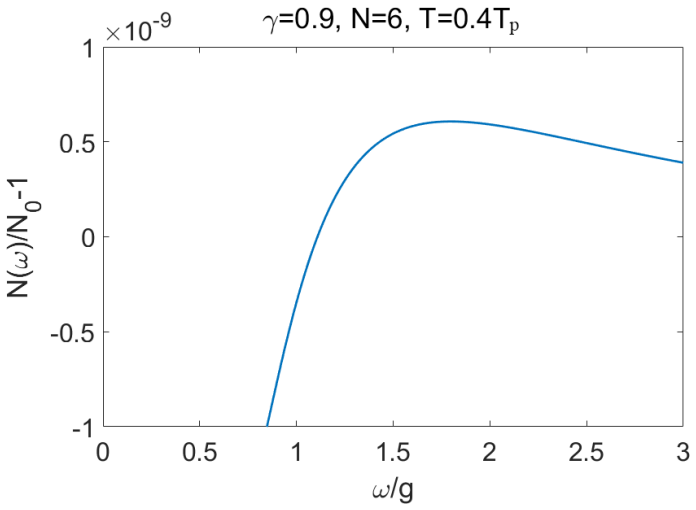

FIG. 19. DOS at large $\omega \sim g$ for $\gamma = 0.9$. We set $N = 6$ and $T = 0.4T_p$. At some $\omega \sim g$, $N(\omega) - N_0$ changes sign from negative to positive, and at even larger frequencies approaches zero from above.

Because $F_\Phi(x)$ is real,

$$\mathrm{Re}\, F_D^2(x) = F_\Phi^2(x) \frac{(\mathrm{Re}\, F_\Sigma(x))^2 - (\mathrm{Im}\, F_\Sigma(x))^2}{((\mathrm{Re}\, F_\Sigma(x))^2 + (\mathrm{Im}\, F_\Sigma(x))^2)^2}. \tag{67}$$

At small $x = \omega/\pi T$, $\mathrm{Re}\, F_\Sigma(x) \propto x^2$ and $\mathrm{Im}\, F_\Sigma(x)$ is finite. Then $\mathrm{Re}\, F_D^2(x)$ is negative. At x, where $\mathrm{Im}\, F_\Sigma(x)$ changes sign, $\mathrm{Re}\, F_\Sigma(x)$ is finite, hence for this x $\mathrm{Re}\, F_D^2(x)$ is positive. In between, $\mathrm{Re}\, F_D^2(x)$ necessary changes sign. This in turn implies that $N(\omega) < N_0$ at small x and $N(\omega) > N_0$ at larger x. Then $N(\omega)$ has a dip at $\omega = 0$ and a hump at a characteristic frequency set by temperature, rather than by the gap itself. This frequency *increases with increasing* T. This behavior is qualitatively different from that in a BCS superconductor, where the maximum in the DOS is located at $\omega = \Delta(T)$ and shifts to a lower frequency with increasing T because $\Delta(T)$ gets smaller. We plot $\mathrm{Re}\, F_D^2(x)$ in Fig.18 for two different values of the exponent γ. In both cases, the hump at $\omega \sim T$ is clearly visible. The position of the hump shifts to a lower frequency with increasing γ but remains at a finite ω even at $\gamma = 1$.

On a more careful look, we find that there is still a small difference in the behavior of the DOS at $\gamma < 1/2$ and $\gamma > 1/2$. Namely, at $\omega \gg T$, $\mathrm{Re}\, \Sigma^*(x) = \cos \pi\gamma/2(x^{1-\gamma}/(1-\gamma))$ and $\mathrm{Im}\, \Sigma^*(x) = \sin \pi\gamma/2(x^{1-\gamma}/(1-\gamma))$. As a result, $\mathrm{Re}\, F_D^2(x) \propto \cos \pi\gamma$ is positive at $\gamma < 1/2$ and negative at $\gamma > 1/2$. This implies that for $\gamma > 1/2$ $N(\omega)$ crosses N_0 twice at $\omega = O(T)$, because $(\mathrm{Im}\, F_\Sigma(x))^2$ is larger than $(\mathrm{Re}\, F_\Sigma(x))^2$ at both large and small x. The

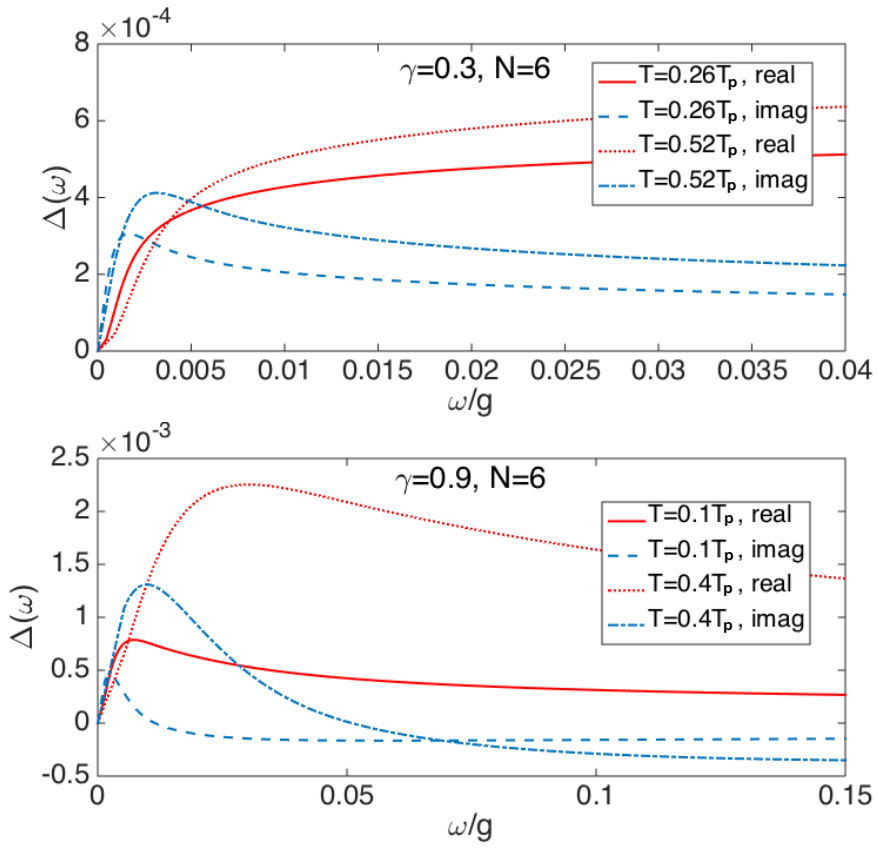

FIG. 20. $\Delta(\omega)$ for various $T > T_{cross}$. Upper panel: $\gamma = 0.3, N = 6$. Lower panel: $\gamma = 0.9, N = 6$. Red lines are for the real part $\Delta'(\omega)$ and blue lines are for the imaginary part $\Delta''(\omega)$. At small but non zero ω, both the real and imaginary parts are finite, in contrast to the BCS-like behavior where $\Delta''(\omega)$ is zero up to some $\omega_0 \approx \Delta'$ at low temperatures.

second crossing at $x \sim 7$ is seen in Fig. 16 for $\gamma = 0.9$. Digging further into this issue, we find that for $\gamma > 1/2$, $N(\omega)$ crosses N_0 one more time, now at $\omega \sim g \gg T$, when the bare ω term in $\tilde{\Sigma}^*(\omega)$ becomes relevant. To see this, we extend the analysis of the DOS to $\omega \sim g$. The calculation is straightforward and we only cite the result: the difference $N(\omega)/N_0 - 1$ at $\omega \sim g$ is proportional to $\cos\pi\gamma + (1-\gamma)^2(\omega/g)^{2\gamma} + 2(1-\gamma)(\omega/g)^{\gamma}\cos\pi\gamma/2$. Solving for $N(\omega) = N_0$, we find for $\gamma > 1/2$ the solution at $\omega = \omega_1 \sim g$. We show the behavior of $N(\omega)/N_0$ at large $\omega \sim g$ in Fig. 19.

In Figs.20 and 21 we show the results of the full numerical calculation of the temperature evaluation of the gap $\Delta(\omega)$ and the DOS $N(\omega)$ for two values of γ: $\gamma = 0.3$ and $\gamma = 0.9$ (one is larger than $1/2$, another is smaller). We set $N = 6$ in both cases (the numerical analysis

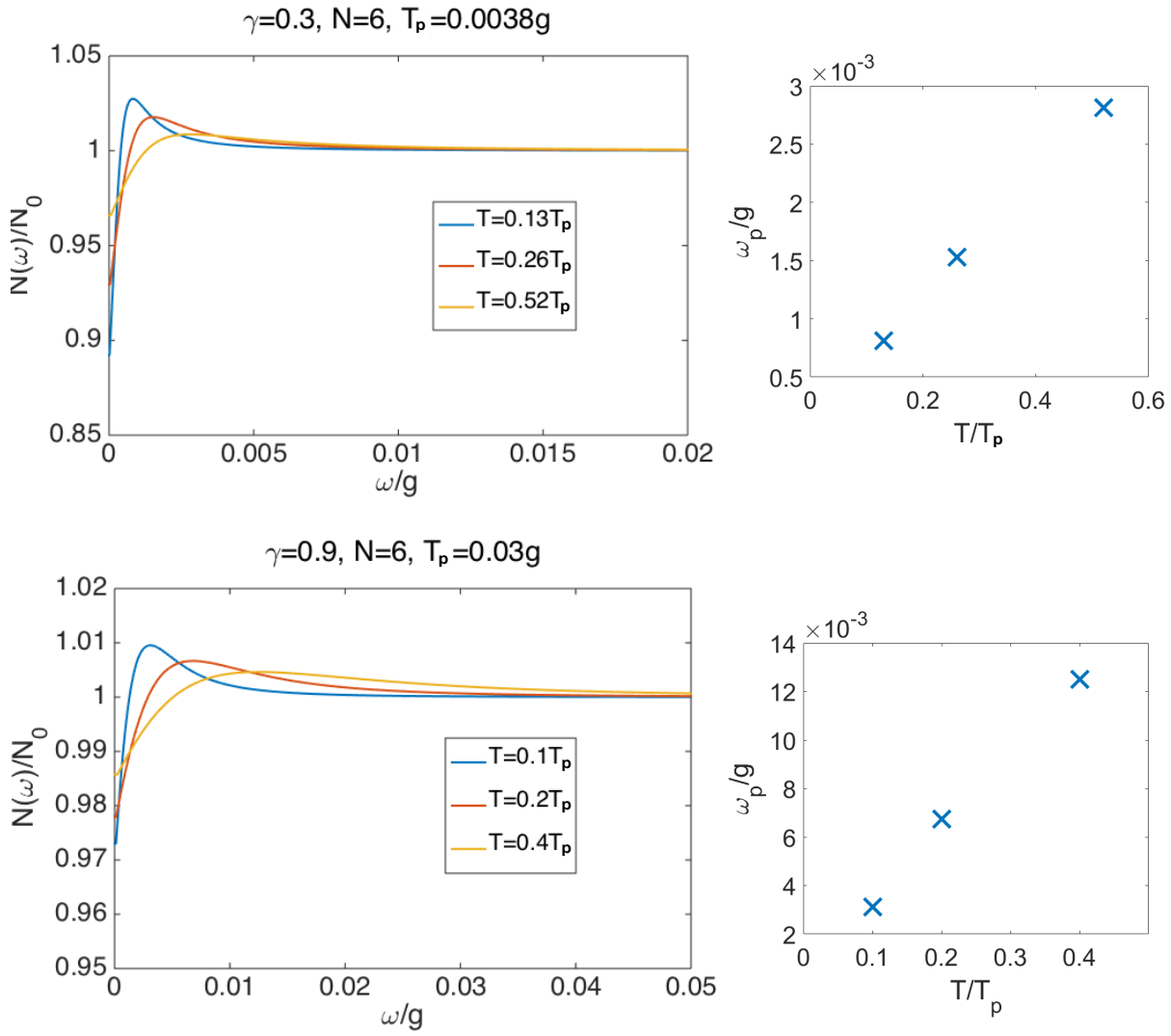

FIG. 21. The DOS $N(\omega)$ for various $T > T_{cross}$. Upper panel: $\gamma = 0.3, N = 6$. Lower panel: $\gamma = 0.9, N = 6$. Right panels: The temperature dependence of the characteristic frequency ω_p, defined as the peak position of the $N(\omega)$.

for larger N is too involved for $\gamma = 0.3$). For $\gamma = 0.9$, $N = 6$ is above $N_{cr} \sim 1.3$. For $\gamma = 0.3$, $N_{cr} \approx 9.6 > 6$. In this situation, the behavior similar to the one at $N > N_{cr}$ exists above the crossover temperature $T_{cross}(N)$ (see Sec. V), and we show the results only in this T range. The value of $T_{cross}(N = 6)$ for $\gamma = 0.3$ is only $0.01T_p$, so the range of $T > T_{cross}$ is rather wide.

We see from Fig.20 that the imaginary part of $\Delta(\omega)$ is finite even at very small ω,

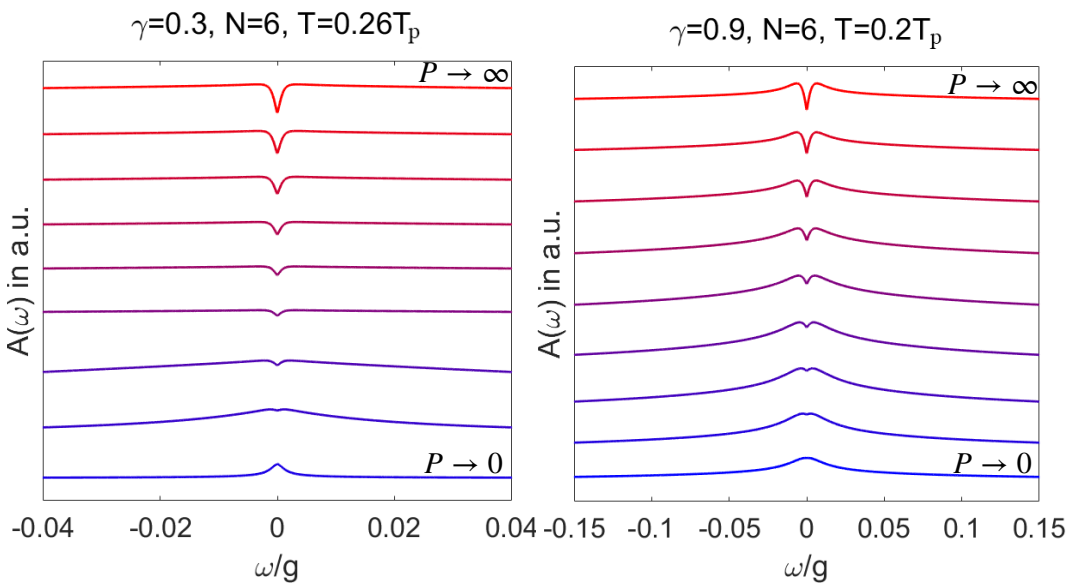

FIG. 22. The spectral function $A(\omega)$ at a fixed $T > T_{cross}$, plotted as a function of ω for various values of parameter P, which measures the strength of thermal contributions to the self-energy and the pairing vertex. At large P, $A(\omega)$ shows the same behavior as the DOS, with the dip at small ω. At small P, it shows instead the maximum at $\omega = 0$. The plots are for $\gamma = 0.3$ and $\gamma = 0.9$.

consistent with Eq. (64). For the DOS, we clearly see from Fig. 21 that there is a dip in $N(\omega)$ at small frequencies and the position of the maximum in $N(\omega)$ is set by the temperature.

A remark is in order here. The integrated DOS $\int d\omega N(\omega)$, with $N(\omega)$ as in Fig.21, does have some T dependence. This seems problematic, because the integrated DOS is proportional to the total number of particles, which is the conserved quantity. In fact, there is no contradiction. The reasoning is that the momentum integration in Eliashberg equations is performed assuming particle-hole symmetry, i.e., neglecting contributions from energies of order μ. There are additional contributions to the DOS from energies of order μ, both in the normal and the superconducting state. They are not equal, because μ changes between normal and superconducting states[72]. This additional contribution must be included to ensure particle conservation.

We next consider the spectral function $A(\omega) = -(1/\pi)\,\mathrm{Im}[G(k_F, \omega)]$. In terms of original $\Phi(\omega)$ and $\tilde{\Sigma}(\omega)$, we have

$$A(\omega) = -\frac{1}{\pi}\,\mathrm{Im}\left[\frac{\tilde{\Sigma}(\omega)}{\tilde{\Sigma}^2(\omega) - \Phi^2(\omega)}\right]. \tag{68}$$

Expressing $\tilde{\Sigma}(\omega)$ and $\Phi(\omega)$ via $\tilde{\Sigma}^*(\omega)$ and $\Phi^*(\omega)$ using Eq. (51), we find

$$A(\omega) = -\frac{1}{\pi} \mathrm{Im} \left[\frac{\tilde{\Sigma}^*(\omega)}{(\tilde{\Sigma}^*(\omega))^2 - (\Phi^*(\omega))^2} L(\omega) \right], \tag{69}$$

where

$$L(\omega) = \frac{1}{1+Q^*(\omega)} = \frac{\sqrt{\Phi^*(\omega)^2 - \tilde{\Sigma}^*(\omega)^2}}{P \,\mathrm{sgn}\,\mathrm{Im}\,\tilde{\Sigma}^* + \sqrt{\Phi^*(\omega)^2 - \tilde{\Sigma}^*(\omega)^2}}. \tag{70}$$

To leading order in $1/P$, $A(\omega) \propto \frac{1}{P} \mathrm{Re} \left[\frac{1}{\sqrt{1-\left(\Phi^*(\omega)/\tilde{\Sigma}^*(\omega)\right)^2}} \right] \propto N(\omega)/N_0$, i.e., the spectral function has the same dependence on ω as the DOS. Accordingly, at a finite T, $A(\omega)$ is non-zero for any frequency, and the position of the maximum in $A(\omega)$ scales with T and remains at a finite frequency at T_p (see Fig.22). If P is finite, either because the system is at some distance from a QCP, or we probe $A(\omega)$ for fermions connected by momenta different from the one at which static χ diverges (e.g., near-nodal fermions in the cuprates, if a pairing boson is an antiferromagnetic spin fluctuation), the behavior of $A(\omega)$ depends on the interplay between P and $\sqrt{\Phi^*(\omega)^2 - \tilde{\Sigma}^*(\omega)^2}$ at relevant ω. the other term in $L(\omega)$ in (70). If P is smaller, $L(\omega) \approx 1$, and

$$A(\omega) = -\frac{1}{\pi} \mathrm{Im} \left[\frac{\tilde{\Sigma}^*(\omega)}{(\tilde{\Sigma}^*(\omega))^2 - (\Phi^*(\omega))^2} \right]. \tag{71}$$

Substituting the expressions for $\Phi^*(\omega)$ and $\tilde{\Sigma}^*(\omega)$ we find that in this situation $A(\omega)$ is peaked at zero frequency, as if the system was in the normal state. We show this behavior in Fig.22.

The analysis beyond the leading order in $1/N$ proceeds in the same way as for Matsubara frequencies. As N gets smaller, the maximum in the DOS becomes more pronounced, and, at the same time, the DOS at zero frequency, $N(0)$ gets smaller. These modifications get larger as N decreases towards N_{cr} and eventually, at $N < N_{cr}$, the system behavior at the lowest T changes qualitatively. We discuss this in the next Section.

V. THE CASE $N < N_{cr}$

At smaller $N < N_{cr}$, the analytical solution is difficult to obtain because there is no obvious small parameter, so our discussion will be based on the numerical results.

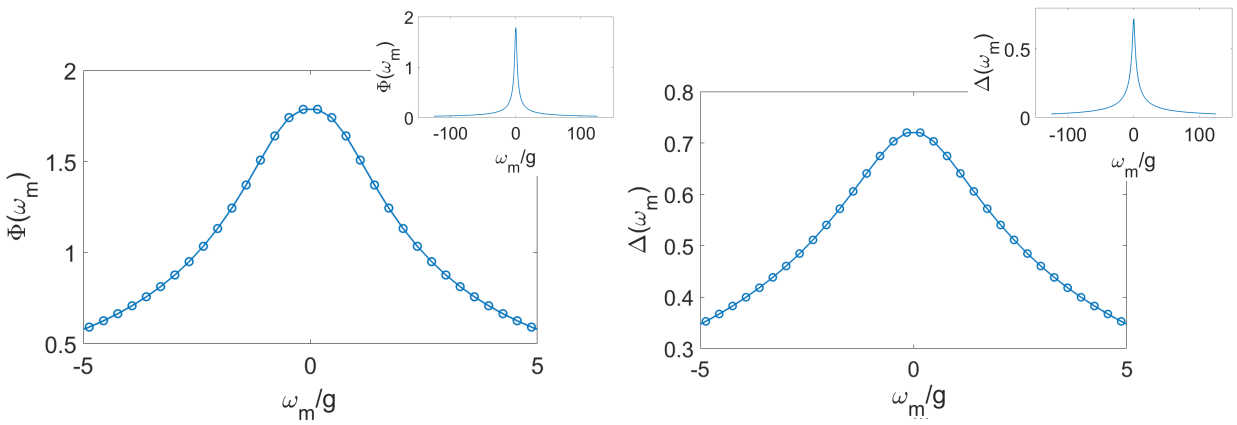

FIG. 23. The pairing vertex $\Phi(\omega_m)$ and the gap $\Delta(\omega_m)$ as functions of Matsubara frequency for $\gamma = 0.9$, $N = 1$, and $T = 0.18T_p < T_{cross}$. Observe that $\Delta(\omega_m)$ is a smooth function, i.e., $\Delta(\pm\pi T)$ is about the same as at $\pm 3\pi T$, etc.

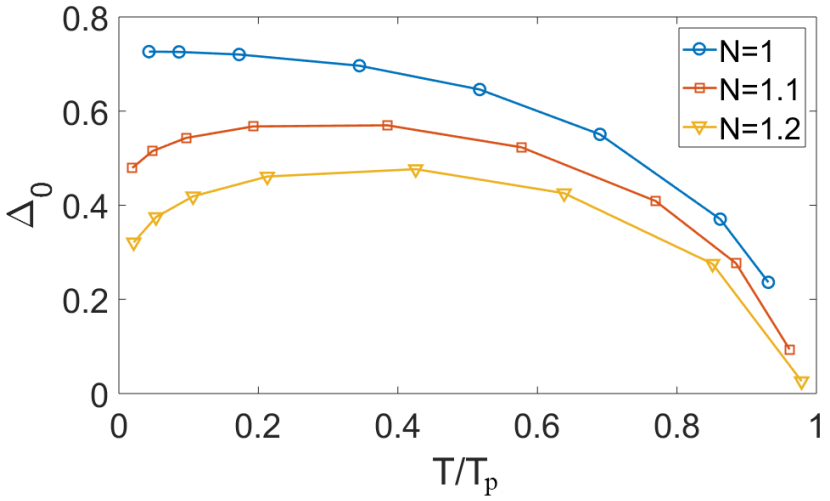

FIG. 24. The gap $\Delta(\pi T) = \Delta_0$ as a function of temperature for $\gamma = 0.9$ and three different $N < N_{cr} \approx 1.34$. The gap now tends to a finite value at $T = 0$. For N slightly below N_{cr}, $\Delta_0(T)$ is still non-monotonic, but for $N = 1$, Δ_0 monotonically increases with decreasing T.

A. Non-linear gap equation in Matsubara frequencies

In Fig.23 we show the results for $\Phi^*(\omega_m)$ and $\Delta(\omega_m)$ for $\gamma = 0.9$ and $N = 1$ (which is smaller than $N_{cr} \approx 1.3$) at the lowest temperatures. The results for $\gamma = 0.3$ and $N = 1$ are very similar. We see that now not only $\Phi^*(\omega_m)$, but also $\Delta(\omega_m)$ does not differ much

between $\omega_m = \pm\pi T$ and other Matsubara frequencies. This is quite different from $\Delta(\omega_m)$ at $N > N_{cr}$, see Fig.13. The smooth frequency dependence of $\Delta(\omega_m)$ in Fig. 23 implies that at $N < N_{cr}$ and low T fermions with Matsubara frequencies $\omega_m \neq \pm\pi T$ also contribute to the pairing. This is consistent with our earlier result that at $N < N_{cr}$ the transition temperature remains finite even we exclude fermions with $\omega_m = \pm\pi T$ from the Eliashberg equations (the corresponding temperature is $\tilde{T}_p(N)$ in Fig.8).

In Fig.24 we show $\Delta(\pi T) = \Delta_0$ as a function of T. We show the case $\gamma = 0.9$, but we verified that the T dependence of $\Delta(\pi T)$ is quite similar for other γ. We see that Δ_0 now tends to a finite value at $T = 0$. For N slightly below N_{cr}, the temperature dependence of Δ_0 is still non-monotonic, i.e., as T is reduced below T_p, Δ_0 first increases and then drops below a certain T, before reaching a finite value at $T \to 0$. At smaller N, the maximum in $\Delta_0(T)$ becomes shallow, and at $N = 1$, Δ_0 monotonically increases as T decreases.

Comparing the behavior of $\Delta_0(T)$ at $N > N_{cr}$ and $N < N_{cr}$, Figs. 13 and 24, we see that near T_p, the behavior in the two cases is the same, but at low T, $\Delta_0(T)$ at $N > N_{cr}$ continue decreasing, while $\Delta_0(T)$ at $N < N_{cr}$ saturates. The temperature, at which the two curve separate, marks the crossover, at $N < N_{cr}$, between the conventional superconducting behavior at low T and the behavior, similar to that at $N > N_{cr}$, at higher T. In the higher T region, the pairing can still be viewed as induced by fermions with Matsubara frequencies $\pm\pi T$. We label the crossover temperature as T_{cross}. It has the same dependence on N as $\tilde{T}_p(N)$ in Fig.8 (it also vanishes at $N = N_{cr}$), but numerically T_{croos} is larger than $\tilde{T}_p(N)$. We will see that the DOS and the spectral function undergo a crossover at $T \sim T_{cross}$.

B. Non-linear gap equation in real frequencies

We used the same computational procedure as at large N and obtained $\Phi^*(\omega)$, $\tilde{\Sigma}^*(\omega)$, and $\Delta(\omega)$ along the real frequency axis. We present the results in Fig.25. We clearly see the crossover in the system behavior around $T_{cross}(N)$. At $T < T_{cross}(N)$, the behavior of the gap function is conventional in the sense that Re $\Delta(\omega = 0)$ is finite and Im $\Delta(\omega)$ emerges only above a finite frequency, approximately equal to $\Delta(0)$. The self-energy $\Sigma^*(\omega)$ at $\omega < \Delta_0$ is strongly reduced compared to its value in the normal state. At $T > T_{cross}(N)$, Im $\Delta(\omega) \propto \omega$ at small frequencies, and Re $\Delta(\omega) \propto \omega^2$, i.e., the systems displays the same gapless superconductivity as at $N > N_{cr}$. In the same T range the self-energy $\Sigma^*(\omega)$ almost

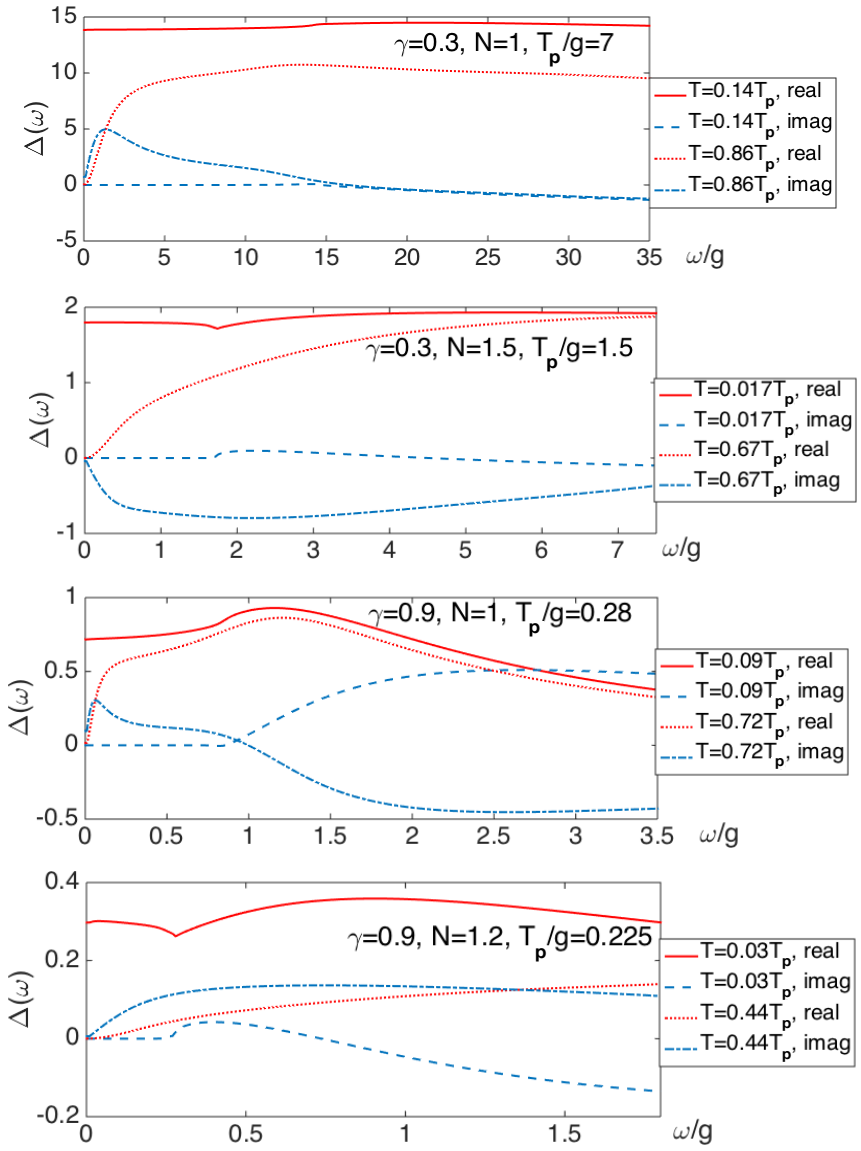

FIG. 25. Real and imaginary parts of the gap $\Delta(\omega)$ as functions of ω for various T. The results are for $\gamma = 0.3$ and $\gamma = 0.9$, in both cases for $N < N_{cr}$. Red and blue lines are for $\Delta'(\omega)$ and $\Delta''(\omega)$, respectively. The data clearly show a crossover at $T \sim T_{cross}$ from BCS-like behavior at smaller T to the behavior similar to that at $N > N_{cr}$, at larger T.

recovers the normal state value (see Fig.25).

In Fig.26 we show the behavior of the DOS $N(\omega)$. We see a qualitative change of the behavior between $T > T_{cross}(N)$ and $T < T_{cross}(N)$. At smaller T, $N(\omega)$ is similar to that in a BCS superconductor: it has a sharp peak at $\omega \approx \Delta(0)$ and nearly vanishes below the peak frequency. At T increases, but remains smaller than $T_{cross}(N)$, the position of the

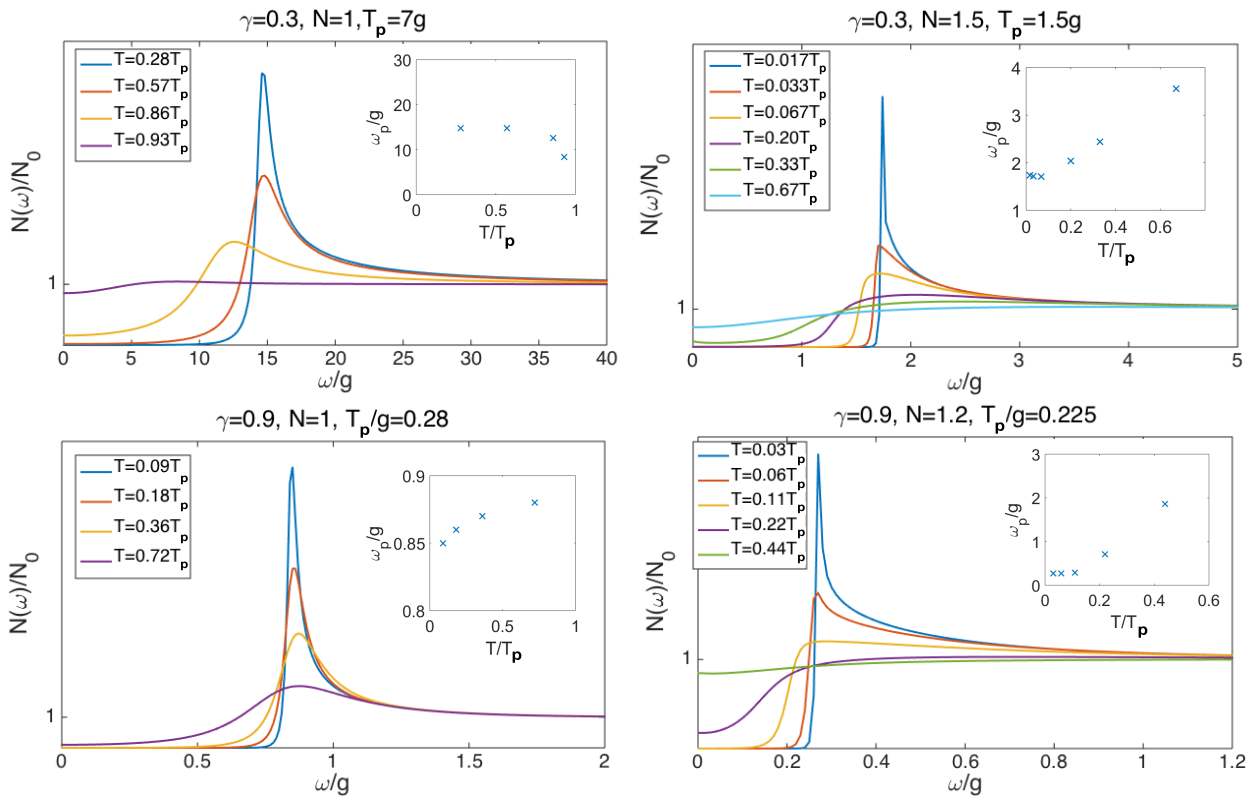

FIG. 26. DOS $N(\omega)$ as a function of frequency for $\gamma = 0.3$ and $\gamma = 0.9$ and several $N < N_{cr}(\gamma)$. At low $T < T_{cross}$, the DOS has a sharp peak at $\omega = \Delta(T)$ and nearly vanishes below the peak. At higher $T > T_{cross}$ the DOS has qualitatively the same functional form as for large N, and the peak position shifts to a higher frequency with increasing temperature. The insets: the peak position ω_p as function of T/T_p. The crossover at T_{cross} is clearly visible.

maximum in $N(\omega)$ shifts to a smaller frequency because $\Delta(0)$ decreases, i.e., the gap in the DOS "closes". However, at higher $T > T_{cross}(N)$, $N(\omega)$ becomes non-zero at all frequencies, and the position of its maximum shifts to a higher frequency as T increases, and remains finite at $T = T_p - 0$, i.e., the gap in the DOS "fills in". We plot the variation of the position of the maximum in $N(\omega)$ with T in the inserts of the plots of the DOS in Fig.26.

In Fig. 27 we present our results for the spectral function $A(\omega)$. It shows a similar crossover around T_{cross}. We recall that the form of the spectral function depends on the strength of the thermal contribution to the self-energy (the P term in Eq. (70)). In the limit when the thermal contribution is large, $A(\omega)$ displays the same behavior as $N(\omega)$. In the opposite limit when P is smaller, $L(\omega)$ in Eq. (70) is close to one, and $A(\omega)$ at $T < T_{cross}(N)$

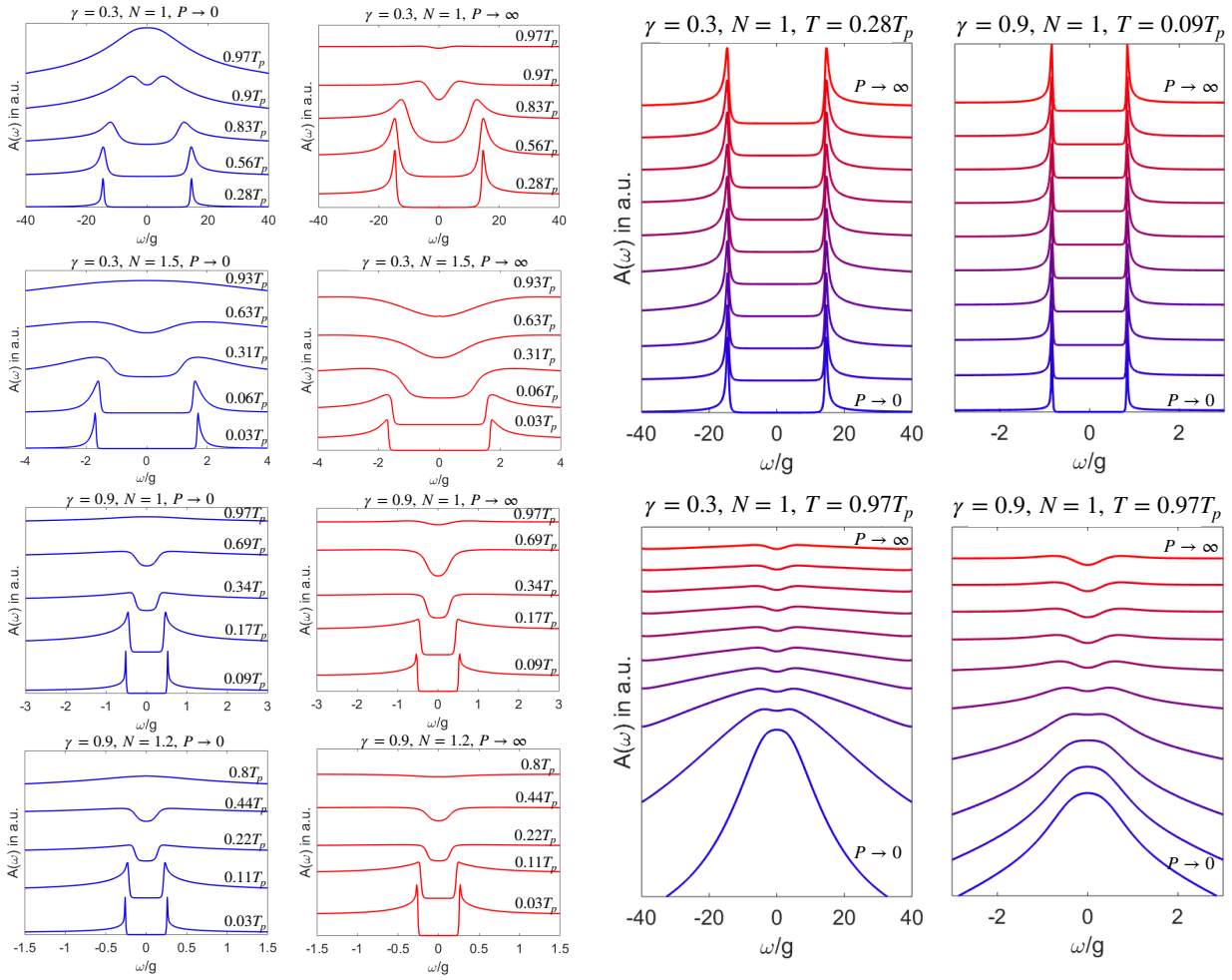

FIG. 27. The spectral function $A(\omega)$ for $\gamma = 0.3$ and $\gamma = 0.9$ and several $N < N_{cr}$. Left panels: $A(\omega)$ for a set of temperatures at either strong or weak thermal contribution (the limits $P = \infty$ and $P = 0$ in Eq. (70)). At small $T < T_{cross}$ the spectral function has sharp peaks at $\omega = \pm\Delta(T)$, like in a BCS superconductor. At $T > T_{cross}$, $A(\omega)$ shows the same behavior as the DOS in Fig. 26, when the thermal contribution is strong, and develops a single peak at $\omega = 0$ when the thermal contribution is weak. Right panels – $A(\omega)$ at a fixed T for different strengths of the thermal contribution. Upper panels – $T < T_{cross}$, lower panels – $T > T_{cross}$.

has two sharp peaks at frequencies close to $\pm\Delta(0)$, as expected in a BCS superconductor. At $T > T_{cross}(N)$, this behavior changes, and $A(\omega)$ has a single peak at $\omega = 0$. We show the variation of $A(\omega)$ between $T < T_{cross}(N)$ and $T > T_{cross}(N)$ in the right panels of Fig. 27, for both smaller and larger P. In the left panels, we show the evolution of $A(\omega)$ with increasing P at $T < T_{croos}(N)$ and at $T > T_{cross}(N)$.

VI. DISCUSSION

In this work, we analyzed the competition between the tendency towards fermionic incoherence and NFL and towards pairing near a quantum-critical point in a metal. We used the γ model of dynamical fermion-fermion interaction, mediated by a critical boson with susceptibility $\chi(\Omega_m) \propto (g/|\Omega_m|)^\gamma$. To understand the competition, we extended the model to $SU(N)$ global symmetry and used N as a parameter go gauge the relative strength of the interaction in the particle-particle and particle-hole channels. At large N, the interaction in the pairing channel is smaller by $1/N$ than the one that gives rise to a NFL in the normal state. Earlier work by some of us and others[22] found markedly different variation of system behavior with N at $T = 0$ and at a finite T. Namely, the calculations at $T = 0$ showed that superconductivity only develops if N is smaller than some γ-dependent N_{cr}, while at larger N the system remains in a NFL normal state. Computations of the onset temperature for the pairing $T_p(N)$, on the other hand, showed that the line $T_p(N)$ by-passes N_{cr} and $T_p(N)$ remains finite at any N, no matter how large N is (see Fig.2). The authors of[22] argued that this discrepancy is due to the fact that Eliashberg equations for spin-singlet pairing contain fermionic self-energy without thermal contribution, and this self-energy is large for all frequencies, except for $\omega_m = \pm\pi T$, at which it vanishes. The pairing interaction between fermions with πT and $-\pi T$ is then not countered by the self-energy. This pairing interaction scales as $1/(NT^\gamma)$ and opens up the gap $\Delta(\pm\pi T)$ at $T = T_p \propto 1/N^{1/\gamma}$. A non-zero $\Delta(\pm\pi T)$ then induces the pairing gap for fermions with other Matsubara frequencies.

In this paper we extended the analysis of the pairing problem to $T < T_p(N)$ and solved the non-linear gap equation. We analyzed the large N limit analytically and solved the gap equation at smaller N numerically. We first obtained $\Delta(\omega_m)$ along Matsubara axis and used it to compute the Free energy and the specific heat. We found that the specific heat jumps at T_p, but at large N the relative magnitude of the jump $\Delta C(T_p - 0)/C_n(T_p)$ is reduced by the factor $1/N^2$. The behavior of the specific heat below T_p is also rather unconventional, as $C(T)$ recovers its normal state form at $T \to 0$.

We then solved the gap equation along the real axis, using $\Delta(\omega_m)$ as input. We obtained $\Delta(\omega)$ and used it to compute the DOS $N(\omega)$ and the spectral function $A(\omega)$. In a weak coupling, BCS-type superconductor $A(\omega)$ and $N(\omega)$ are peaked at the gap value $\Delta(T)$, and the peak position shifts to a smaller ω as temperature increases towards T_p (the gap in $N(\omega)$

and $A(\omega)$ "closes" with increasing T).

We found that at $N > N_{cr}$, the behavior of $N(\omega)$ and $A(\omega)$ is very different. The DOS remains finite at all frequencies, including $\omega = 0$, and the position of the maximum in $N(\omega)$ increases linearly with T and remains finite at T_p. As T increases towards T_p, $N(\omega)$ at small ω increases and $N(\omega)$ at larger ω decreases, as if the gap in $N(\omega)$ "fills in" with increasing temperature. The form of the spectral function $A(\omega)$ depends on the strength of the thermal contribution to the self-energy. When this contribution is strong, $A(\omega)$ has the same frequency dependence as the DOS $N(\omega)$. When it is smaller, $A(\omega)$ has a a single peak at $\omega = 0$.

At $N < N_{cr}$, which includes the original case of $N = 1$, this behavior holds above a certain temperature $T_{cross}(N)$ (see Fig. 3). At $T < T_{cross}$, both $N(\omega)$ and $A(\omega)$ display a BCS-like behavior with peaks at $\omega = \Delta(T)$.

The issue, which we didn't discuss in this work, is whether gap fluctuations (transverse or longitudinal) destroy long-range superconducting order in some T range below $T_p(N)$. It is very likely that in some range below $T_p(N)$ long-range superconducting order gets destroyed, and the actual $T_c < T_p$. We analyze this issue in some detail in Ref.[39], where we argue that T_c is comparable to T_{cross}, i.e., the range $T_{cross} < T < T_p$ largely corresponds to pseudogap region. In the theory, which we presented here, the novel behavior at $T_{cross}(N) < T < T_p$ is due to the fact that in this T range the feedback from the pairing on the fermionic self-energy is weak. This does not critically depend on the existence of long-range superconducting order. In fact, if fluctuations destroy superconducting phase coherence, the feedback will be further reduced. In this respect, our results equally describe the system behavior in the pseudogap phase, more specifically, in the so-called weak pseudogap regime, where long-range superconducting order is destroyed by phase fluctuations, but the gap magnitude is still finite.

A. Application to the cuprates

The transformation from "gap closing" behavior at small T to "gap filling" behavior at $T \sim T_p$ has been observed in high-T_c cuprates, in the DOS[49] and ARPES measurements of the spectral function in the antinodal region[45,49–57]. Symmetrized data of MDC ARPES measurements along a particular direction of $\mathbf{k}$ in the near-nodal region showed the trans-

formation from two peaks at a finite frequency to a single peak at $\omega = 0$ (this is termed as the appearance of the Fermi arc). These results are consistent with our microscopic analysis for the DOS and also for the spectral function, if we assume that the thermal contribution is stronger in the antinodal region than in the near-nodal region. The strength of thermal contribution scales with the static bosonic susceptibility $\chi'(0)$. Static $\chi'(0)$ is larger for antinodal fermions in, e.g., spin-fluctuation models[7,16,18], where the interaction is peaked at momentum at or near (π, π).

To quantitatively apply our results to the cuprates, we need to extend our analysis to include the $d-$wave symmetry of the gap function. This is less relevant for the DOS and $A(\omega)$ in the antinodal region, as there the gap can be approximated by the constant, except for $N(\omega)$ at the smallest frequencies at $T < T_{cross}$, as the sharp peak in the DOS gets somewhat broadened after angular integration[73]. However, the $d-$wave angular dependence of the gap must be included into the analysis of the spectral function in the nodal region near Brillouin zone diagonals. To model the $d-$wave case, we added $\cos 2\theta$ factor to $\Phi^*(\omega)$ and solved the Eliashberg equations at a given T, and γ. We show the results in Fig. 28, where we plot the spectral function along the Fermi surface. For simplicity, in this calculation we set P to be angle-independent. Making P smaller for nodal fermions and larger for antinodal ones will widen the range of the behavior seen near the nodes.

We see from Fig. 28 that at $T < T_{cross}$, $A(\omega)$ has two weakly separated peaks in the nodal region and more strongly separated peaks in the antinodal region. This is the expected result for a d-wave superconductor at $T \ll T_c$. At high $T > T_{cross}$, the evolution of the spectral function is similar to the one in Fig.22. Namely, near the node $A(\omega)$ has a single maximum at $\omega = 0$, while in the antinodal region $A(\omega)$ has a dip at $\omega = 0$ and a shallow maximum, whose frequency scales with T. In between, the frequency dependence of $A(\omega)$ gradually evolves from a single peak at $\omega = 0$ to two maxima at finite ω and a dip at zero frequency.

This behavior reproduces the key features of ARPES data in Refs.[50–57]. The behavior of $N(\omega)$ is quite similar to that of $A(\omega)$ in the antinodal region. This is fully consistent with STM data[49].

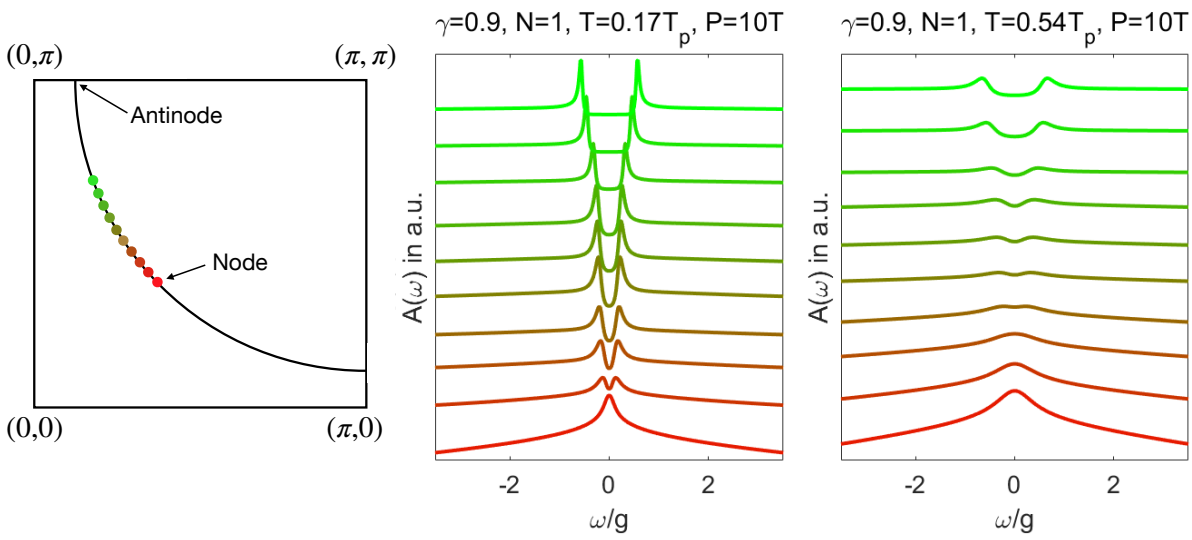

FIG. 28. The spectral function $A(\omega)$ along the Fermi surface. At $T < T_{cross}$ (the middle panel) $A(\omega)$ in the nodal region (Red) has two closely located peaks, which merge at the node. In the antinodal region (Green) the two peaks are well separated. At $T > T_{cross}$ (the right panel) $A(\omega)$ has a maximum in the nodal region, which corresponds the Fermi arc, but in the antinodal region $A(\omega)$ shows two separate maxima.

ACKNOWLEDGMENTS

We thank D. Dessau, A. Kanigel, A. Millis, N. Prokofiev, M. Randeria, S. Raghu, G. Torroba, and A. Yazdani for useful discussions. The work by Y. Wu and AVC was supported by the NSF DMR-1523036.

APPENDIX: ANALYTIC CONTINUATION FROM MATSUBARA AXIS TO REAL FREQUENCY AXIS

In this Appendix we show the derivation of Eq. (46) for the pairing vertex $\Phi^*(\omega)$ and the self-energy $\Sigma^*(\omega)$ along real frequency axis. We follow Ref.[3] and use spectral decomposition approach. Below we explicitly keep the factors i for Matsubara frequencies, e.g., define the interaction as $\chi(i\Omega_m) = \frac{g^\gamma}{|\Omega_m|^\gamma}$.

For a general complex z, we can define the retarded $\chi^R(z)$ as

$$\chi^R(z) = \left(\frac{-g^2}{z^2}\right)^{\gamma/2} \tag{72}$$

By definition, $\chi^R(z)$ is analytic in the upper half-plane of z and coincides with $\chi(i\Omega_m)$ at positive Ω_m.

Immediately above real frequency axis, at $z = \omega + i\delta$) we have from (72):

$$\begin{aligned} \mathrm{Re}\,\chi^R(\omega) &= \frac{g^\gamma}{|\omega|^\gamma}\cos\frac{\pi\gamma}{2} \\ \mathrm{Im}\,\chi^R(\omega) &= \frac{g^\gamma\,\mathrm{sgn}(\omega)}{|\omega|^\gamma}\sin\frac{\pi\gamma}{2}. \end{aligned} \tag{73}$$

The two functions are expressed via each other by Kramers-Kronig relations: $\mathrm{Re}\,\chi^R(\omega) = (2/\pi)\mathcal{P}\int_0^\infty dx\,\mathrm{Im}\,\chi^R(x)x/(x^2 - \omega^2)$; $\mathrm{Im}\,\chi^R(\omega) = -(2/\pi)\omega\mathcal{P}\int_0^\infty dx\,\mathrm{Im}\,\chi^R(x)/(x^2 - \omega^2)$. $\mathrm{Re}\,\chi^R(\omega)$ is even function of ω, and $\mathrm{Im}\,\chi^R(\omega)$ is odd in ω.

According to Cauchy theorem, a retarded $\chi^R(z)$ in the upper half-plane of z can be expressed via $\mathrm{Im}\,\chi^R(x)$ as

$$\chi^R(z) = \frac{1}{\pi}\int_{-\infty}^{\infty}\frac{\mathrm{Im}\,\chi^R(x)dx}{x - z}, \quad \mathrm{Im}\,z > 0. \tag{74}$$

In particular, at $\Omega_m > 0$,

$$\chi(i\Omega_m) = \frac{1}{\pi}\int_{-\infty}^{\infty}\frac{\mathrm{Im}\,\chi^R(x)dx}{x - i\Omega_m} = \frac{2}{\pi}\int_0^\infty\frac{\mathrm{Im}\,\chi^R(x)xdx}{x^2 + \Omega_m^2} \tag{75}$$

For negative Ω_m we need to introduce the retarded $\chi^A(z)$. It is related to $\mathrm{Im}\,\chi^R(x)$ by the same formula as (74), but z should be in the lower half-plane:

$$\chi^A(z) = \frac{1}{\pi}\int_{-\infty}^{\infty}\frac{\mathrm{Im}\,\chi^R(x)dx}{x - z}, \quad \mathrm{Im}\,z > 0 \tag{76}$$

We will need both $\chi^R(z)$ and $\chi^A(z)$ below for complex z. Along the Matsubara axis, $z = i\Omega_m$, we will just use the fact that $\chi(i\Omega_m)$ is an even function of Ω_m and extend (75) to negative Ω_m. We will use the same trick for the Green's function $G(i\omega_m\mathbf{k}_F)$ – we express it via $\mathrm{Im}\,G^R(x,\mathbf{k}_F)$ for $\omega_m > 0$ and use the fact that $G(i\omega_m\mathbf{k}_F)$ is odd in ω_m to extend the relation between $G(i\omega_m\mathbf{k}_F)$ and $\mathrm{Im}\,G^R(x,\mathbf{k}_F)$ to negative ω_m.

Now, the expressions for $\Phi(\omega_m)$ and $\tilde{\Sigma}(\omega_m)$, Eq. (6), contain the susceptibility $\chi(i\omega_m - i\omega_{m'})$, where ω_m is an external Matsubara frequency, which we want to convert to real axis. In distinction from $\chi(i\Omega_m)$, this susceptibility cannot be analytically continued from the

Matsubara axis by just replacing $i\omega_m$ by z, because $\chi(z - i\omega_{m'}) = (-g^2/(z - i\omega_{m'})^2)^{\gamma/2}$ has a set of branch cuts in the upper half-plane of z, at $z = i\omega_{m'} + z_0$, where z_0 is a real variable (Ref.[3]). Due to this complication, we have cannot simply replace $i\omega_m$ by real ω in $\chi(i\omega_m - i\omega_{m'})$ and have to implement the full spectral decomposition procedure. Namely, we depart from Eliashberg equations along Matsubara axis and use Cauchy theorem to express $G(i\omega_m, \boldsymbol{k})$ and $\chi(i\omega_m - i\omega_{m'})$ in terms of retarded $\mathrm{Im}\, G^R(x, \boldsymbol{k})$ and $\mathrm{Im}\, \chi^R(x)$ along real axis as

$$\begin{aligned} G(i\omega_m, \boldsymbol{k}) &= \int_{-\infty}^{\infty} \frac{dx}{\pi} \frac{\mathrm{Im}\, G^R(x, \boldsymbol{k})}{x - i\omega_m} \\ \chi(i\omega_m - i\omega_{m'}) &= \int_{-\infty}^{\infty} \frac{dy}{\pi} \frac{\mathrm{Im}\, \chi^R(y)}{y - i(\omega_m - \omega_{m'})} \end{aligned} \tag{77}$$

We then explicitly sum over $\omega_{m'}$ and integrate over $\mathbf{k}$ and obtain the expressions for $\tilde{\Sigma}(i\omega_m)$ and $\Phi(i\omega_m)$, in which the dependence on ω_m is only via $1/(i\omega_m - x - y)$. This form can be straightforwardly continued analytically from Matsubara to real frequency by just replacing $i\omega_m$ by $\omega + i0^+$.

For compactness, we do the calculations in Nambu formalism, in which one operates with the 2×2 matrix Green's function $\hat{G}(i\omega_m, \boldsymbol{k})$, in which $\Sigma(i\omega_m)$ and $\Phi(i\omega_m)$) as elements of the 2×2 matrix self-energy $\hat{\Sigma}(i\omega_m)$. The Eliashberg equation in Nambu formalism is

$$\hat{\Sigma}(i\omega_n) = -T \sum_m \int \frac{d^2k}{(2\pi)^2} \hat{\tau}_3 \hat{G}(i\omega_m, \boldsymbol{k}) \hat{\tau}_3 \chi(i\omega_n - i\omega_m), \tag{78}$$

where $\hat{\tau}_3$ is a Pauli matrix. $\hat{\Sigma} = \Sigma\hat{\tau}_0 - \Phi\hat{\tau}_1$, and the matrix $\hat{G}(i\omega_m, \boldsymbol{k}) = -(i\omega_m - \hat{\Sigma}(i\omega_m))^{-1}$. The diagonal and off-diagonal elements of $\hat{G}(i\omega_m, \boldsymbol{k})$ are normal and anomalous Green's functions in conventional notations.

Substituting the spectral representation (77) into (78) and performing the summation over ω_m, using $T\sum_{m=-\infty}^{\infty} \frac{1}{x - i\omega_m} \frac{1}{y - i\omega_n + i\omega_m} = \frac{n_F(x) + n_B(-y)}{i\omega_n - x - y}$, where n_F and n_B are Fermi and Bose distribution functions respectively, we obtain

$$\begin{aligned} \hat{\Sigma}(i\omega_n) &= -T \sum_m \int \frac{d^2k}{(2\pi)^2} \int \frac{dxdy}{\pi^2} \hat{\tau}_3 \frac{\mathrm{Im}\, \hat{G}^R(x, \boldsymbol{k})}{i\omega_m - x} \hat{\tau}_3 \frac{\mathrm{Im}\, \chi^R(y)}{i\omega_n - i\omega_m - y} \\ &= -\int \frac{d^2k}{(2\pi)^2} \int \frac{dxdy}{\pi^2} \hat{\tau}_3\, \mathrm{Im}\, \hat{G}^R(x, \boldsymbol{k}) \hat{\tau}_3\, \mathrm{Im}\, \chi^R(y) \frac{n_F(x) + n_B(-y)}{i\omega_n - x - y} \end{aligned} \tag{79}$$

Replacing $i\omega_n$ with $\omega + i0^+$, we obtain the retarded self-energy in real frequencies

$$\hat{\Sigma}^R(\omega) = -\int \frac{d^2k}{(2\pi)^2} \int \frac{dxdy}{\pi^2} \hat{\tau}_3 \frac{\mathrm{Im}\, \hat{G}^R(x, \boldsymbol{k})}{\omega - x - y + i0^+} \hat{\tau}_3\, \mathrm{Im}\, \chi^R(y)\, [n_F(x) + n_B(-y)] \tag{80}$$

Using the fact that for any two functions F and G we have $F\,\mathrm{Im}\,G = \mathrm{Im}(G\,\mathrm{Re}\,F) - i\,\mathrm{Re}(G\,\mathrm{Im}\,F)$, we express $\mathrm{Im}\,\hat{G}^R(x,\boldsymbol{k})/(\omega - x - y + i0^+)$ via the full $\hat{G}^R(x,\boldsymbol{k})$ as

$$\begin{aligned}
&\frac{2\,\mathrm{Im}\,\hat{G}^R(x,\boldsymbol{k})}{\omega - x - y + i0^+} = \mathrm{Im}\left[\hat{G}^R(x,\boldsymbol{k})\left(\frac{1}{\omega - x - y + i0^+} + \frac{1}{\omega - x - y - i0^+}\right)\right] \\
&-i\,\mathrm{Re}\left[\hat{G}^R(x,\boldsymbol{k})\left(\frac{1}{\omega - x - y + i0^+} - \frac{1}{\omega - x - y - i0^+}\right)\right] \\
&= \mathrm{Im}\left[\hat{G}^R(x,\boldsymbol{k})\left(\frac{1}{\omega - x - y + i0^+} + \frac{1}{\omega - x - y - i0^+}\right)\right] + 2\pi i\delta(\omega - x - y)\,\mathrm{Re}\,i\hat{G}^R(x,\boldsymbol{k}).
\end{aligned}$$

We substitute this form into (80) and integrate over x by closing the integration contour over the upper half-plane of complex x. Because $\hat{G}^R(x,\boldsymbol{k})$ is analytic in the upper half plane, the poles come from $1/(\omega - x - y + i0^+)$, at $x = y - \omega + i0^+$ with residue 1 and from $n_F(x)$, at $x = i(2n+1)\pi T$, $n \geq 0$, with residues $-T$. Using the residue theorem, we find

$$\begin{aligned}
&\hat{\Sigma}^R(\omega) = -\frac{1}{2}\int\frac{d^2k}{(2\pi)^2}\int\frac{dy}{\pi}\,\mathrm{Im}\,\chi^R(y) \\
&\times\,\mathrm{Im}\left[\int\frac{dx}{\pi}\left(n_F(x) + n_B(-y)\right)\hat{\tau}_3\hat{G}^R(x,\boldsymbol{k})\hat{\tau}_3\left(\frac{1}{\omega - x - y + i0^+} + \frac{1}{\omega - x - y - i0^+}\right)\right] \\
&- i\int\frac{d^2k}{(2\pi)^2}\int\frac{dy}{\pi}\,\mathrm{Im}\,\chi^R(y)\left(n_F(\omega - y) + n_B(-y)\right)\mathrm{Re}\left[i\hat{\tau}_3\hat{G}^R(\omega - y,\boldsymbol{k})\hat{\tau}_3\right] \\
=&\int\frac{d^2k}{(2\pi)^2}\int\frac{dy}{\pi}\,\mathrm{Im}\,\chi^R(y)T\sum_{\omega_n>0}\mathrm{Im}\left[i\hat{\tau}_3\hat{G}^R(i\omega_n,\boldsymbol{k})\hat{\tau}_3\frac{2}{\omega - i\omega_n - y}\right] \\
&+\int\frac{d^2k}{(2\pi)^2}\int\frac{dy}{\pi}\,\mathrm{Im}\,\chi^R(y)\left(n_F(\omega - y) + n_B(-y)\right)\times\left[\mathrm{Im}(i\hat{\tau}_3 G^R(\omega - y,\boldsymbol{k})\hat{\tau}_3) - i\,\mathrm{Re}(i\hat{\tau}_3 G^R(\omega - y,\boldsymbol{k})\hat{\tau}_3)\right] \\
=&2T\sum_{\omega_n>0}\int\frac{d^2k}{(2\pi)^2}\,\mathrm{Im}\left[i\hat{\tau}_3\hat{G}^R(i\omega_n,\boldsymbol{k})\hat{\tau}_3\int\frac{dy}{\pi}\frac{\mathrm{Im}\,\chi^R(y)}{\omega - i\omega_n - y}\right] \\
&-\int\frac{d^2k}{(2\pi)^2}\int\frac{dy}{\pi}\hat{\tau}_3\hat{G}^R(\omega - y,\boldsymbol{k})\hat{\tau}_3\,\mathrm{Im}\,\chi^R(y)\left(n_F(y - \omega) + n_B(y)\right), \qquad (81)
\end{aligned}$$

where we also used $n_F(\omega - y) + n_B(-y) = -\left[n_F(y - \omega) + n_B(y)\right]$.

According to (76), $(1/\pi)\int dy\,\mathrm{Im}\,\chi(y)/(\omega - i\omega_n - y) = -\chi^A(\omega - i\omega_n)$, because complex $z = \omega - i\omega_n$ is in the lower half-plane of complex z. For practical purposes, however, we just have

$$\chi^A(\omega - i\omega_n) \equiv \chi(\omega - i\omega_n) = \left(\frac{g^2}{(\omega - i\omega_n)^2}\right)^{\gamma/2} \qquad (82)$$

Using this, we finally obtain

$$\begin{aligned}
\hat{\Sigma}^R(\omega) = -2T\sum_{\omega_n>0}\int\frac{d^2k}{(2\pi)^2}\,\mathrm{Im}[i\hat{\tau}_3\hat{G}^R(i\omega_n,\boldsymbol{k})\hat{\tau}_3\chi(\omega - i\omega_n)] \\
-\int\frac{d^2k}{(2\pi)^2}\int\frac{dy}{\pi}\,\mathrm{Im}[\chi^R(y)]\hat{\tau}_3\hat{G}^R(\omega - y,\boldsymbol{k})\hat{\tau}_3\left(n_F(y - \omega) + n_B(y)\right).
\end{aligned} \qquad (83)$$

Let's now spit this matrix equation into the equations for the pairing vertex $\Phi^R(\omega)$ and conventional (non-anomalous) self-energy $\Sigma^R(\omega)$ by expressing $\hat{\Sigma}^R(\omega)$ as

$$\hat{\Sigma}^R(\omega) = \Sigma^R(\omega)\hat{\tau}_0 - \Phi^R(\omega)\hat{\tau}_1 \tag{84}$$

and expressing $\hat{\tau}_3 G(\omega, \boldsymbol{k})\hat{\tau}_3$ as

$$\hat{\tau}_3 G^R(\omega, \boldsymbol{k})\hat{\tau}_3 = \frac{-(\omega + \Sigma^R(\omega))\hat{\tau}_0 - \xi_{\boldsymbol{k}}\hat{\tau}_3 + \Phi^R(\omega)\hat{\tau}_1}{\xi_{\boldsymbol{k}}^2 + \Phi^R(\omega)^2 - (\omega + \Sigma^R(\omega))^2}. \tag{85}$$

where $\xi_{\boldsymbol{k}}$ is the fermionic dispersion. This procedure requires some care because, strictly speaking, the Dyson equation holds for time-ordered Green's functions, but not for retarded Green's functions. Eq. (85) is valid assuming that we can analytically continue the Dyson equation for time-ordered Green's functions

$$\hat{\tau}_3 G(\omega, \boldsymbol{k})\hat{\tau}_3 = \frac{-(\omega + \Sigma(\omega))\hat{\tau}_0 - \xi_{\boldsymbol{k}}\hat{\tau}_3 + \Phi(\omega)\hat{\tau}_1}{\xi_{\boldsymbol{k}}^2 + \Phi(\omega)^2 - (\omega + \Sigma(\omega))^2}$$

into the upper half-plane. This holds if $(z + \Sigma^R(z))^2 - \Phi^R(z)^2$ does not become real and positive anywhere in the upper half plane of complex z, so there are no extra poles, induced by the denominator. In our case, we are safe because already in the normal state the largest term in $\Sigma^R(z)$ is the imaginary thermal contribution $+i\pi T\chi(0)$ with the same sign as $\mathrm{sgn}[\mathrm{Im}\, z]$.

Expressing next $\int d^2k/(2\pi)^2 = N_0 \int d\xi_{\boldsymbol{k}}$, where N_0 is the DOS in the normal state, and integrating over $\xi_{\boldsymbol{k}}$, we obtain from (85)

$$\int \frac{d^2k}{(2\pi)^2}\hat{\tau}_3 G^R(\omega, \boldsymbol{k})\hat{\tau}_3 = N_0 \int_{-\infty}^{\infty} d\xi_{\boldsymbol{k}}\hat{\tau}_3 G^R(\omega, \boldsymbol{k})\hat{\tau}_3 = \pi N_0 \frac{-\tilde{\Sigma}^R(\omega)\hat{\tau}_0 + \Phi^R(\omega)\hat{\tau}_1}{\sqrt{(\Phi^R(\omega))^2 - (\tilde{\Sigma}^R(\omega))^2}}, \tag{86}$$

where $\tilde{\Sigma}^R(\omega) = \omega + \Sigma^R(\omega)$. Substituting this into the r.h.s. of (83), absorbing the density of states N_0 into χ, splitting $\hat{\Sigma}^R(\omega)$ into normal and anomalous components, and using the fact that $-i\tilde{\Sigma}^R(i\omega_n)$ and $\Phi^R(i\omega_n)$ are real, we obtain

$$\begin{aligned}
\tilde{\Sigma}^R(\omega) &= \omega - \pi T \sum_{\omega_m > 0} \frac{-i\tilde{\Sigma}(i\omega_m)}{\sqrt{(\Phi(i\omega_m))^2 + (-i\tilde{\Sigma}(i\omega_m))^2}} \left(\chi(\omega + i\omega_m) - \chi(\omega - i\omega_m)\right) \\
&\quad + \int dy \left[S_\Sigma(\omega - y)\, \mathrm{Im}\, \chi^R(y)\, (n_F(y - \omega) + n_B(y))\right] \\
\Phi^R(\omega) &= \pi T \sum_{\omega_m > 0} \frac{\Phi(i\omega_m)}{\sqrt{(\Phi(i\omega_m))^2 + (-i\tilde{\Sigma}(\omega_m))^2}} \left(\chi(\omega + i\omega_m) + \chi(\omega - i\omega_m)\right) \\
&\quad + \int dy \left[S_\Phi(\omega - y)\, \mathrm{Im}\, \chi^R(y)\, (n_F(y - \omega) + n_B(y))\right]
\end{aligned} \tag{87}$$

where

$$S_\Phi(\omega) = \frac{\Phi^R(\omega)}{\sqrt{(\Phi^R(\omega))^2 - (\tilde{\Sigma}^R(\omega))^2}}$$
$$S_\Sigma(\omega) = \frac{\tilde{\Sigma}^R(\omega)}{\sqrt{(\Phi^R(\omega))^2 - (\tilde{\Sigma}^R(\omega))^2}} \tag{88}$$

At a finite T and small y, $n_B(y) \approx T/y$. Then $\mathrm{Im}\,\chi^R(y) n_B(y)$ scales as $T/|y|^{1+\gamma}$, and the integrals over dy in the expressions for $\tilde{\Sigma}(\omega)$ and $\Phi(\omega)$ in (87) diverge. The divergent contribution can be eliminated by introducing new $\Phi^{*,R}(\omega)$ and $\tilde{\Sigma}^{*,R}(\omega)$, related to $\Phi^R(\omega)$ and $\tilde{\Sigma}^R(\omega)$ by

$$\tilde{\Sigma}^{*,R}(\omega) = \tilde{\Sigma}^R(\omega)(1 - Q(\omega)), \quad \Phi^{*,R}(\omega) = \Phi^R(\omega)(1 - Q(\omega)), \tag{89}$$

where

$$Q(\omega) = \frac{P}{\sqrt{(\Phi^R(\omega))^2 - (\tilde{\Sigma}^R(\omega))}}, \quad P = \int_{-\infty}^{\infty} dy\, \mathrm{Im}\,\chi(y) \frac{T}{y} = \pi T \chi(0) \tag{90}$$

One can easily verify that the equations for $\Phi^{*,R}(\omega)$ and $\tilde{\Sigma}^{*,R}(\omega)$ are the same as for $\Phi^R(\omega)$ and $\tilde{\Sigma}^R(\omega)$, but without the divergent pieces:

$$\begin{aligned}
\tilde{\Sigma}^{*,R}(\omega) &= \omega + i\pi T \sum_{\omega_m > 0} \frac{\tilde{\Sigma}(\omega_m)}{\sqrt{(\Phi(\omega_m))^2 + (\tilde{\Sigma}(\omega_m))^2}} \left(\chi(\omega_m + i\omega) - \chi(\omega_m - i\omega)\right) \\
&+ \int dy\, \mathrm{Im}\,\chi^R(y) \left[S_\Sigma(\omega - y) \left(n_F(y - \omega) + n_B(y)\right) - S_\Sigma(\omega) \frac{T}{y} \right] \\
\Phi^{*,R}(\omega) &= \pi T \sum_{\omega_m > 0} \frac{\Phi(\omega_m)}{\sqrt{(\Phi(\omega_m))^2 + (\tilde{\Sigma}(\omega_m))^2}} \left(\chi(\omega_m + i\omega) + \chi(\omega_m - i\omega)\right) \\
&+ \int dy\, \mathrm{Im}\,\chi^R(y) \left[S_\Phi(\omega - y) \left(n_F(y - \omega) + n_B(y)\right) - S_\Phi(\omega) \frac{T}{y} \right]
\end{aligned} \tag{91}$$

The ratio $\Phi^{*,R}(\omega)/\tilde{\Sigma}^{*,R}(\omega)$ is the same as $\Phi^R(\omega)/\tilde{\Sigma}^R(\omega)$, i.e., the gap function $\Delta^R(\omega) = \omega\Phi^R(\omega)/\tilde{\Sigma}^R(\omega)$ can be equally expressed via non-singular $\Phi^{*,R}(\omega)$ and $\tilde{\Sigma}^{*,R}(\omega)$. Furthermore, a little experimentation shows that $S_\Phi(\omega)$ and $S_\Sigma(\omega)$, given by (88), can be equally expressed via $\Phi^{*,R}(\omega)$ and $\tilde{\Sigma}^{*,R}(\omega)$, as

$$S_\Phi(\omega) = \frac{\Phi^{*,R}(\omega)}{\sqrt{(\Phi^{*,R}(\omega))^2 - (\tilde{\Sigma}^{*,R}(\omega))^2}} \mathrm{sgn}\,\mathrm{Im}\,\tilde{\Sigma}^{*,R}(\omega)$$
$$S_\Sigma(\omega) = \frac{\tilde{\Sigma}^{*,R}(\omega)}{\sqrt{(\Phi^{*,R}(\omega))^2 - (\tilde{\Sigma}^{*,R}(\omega))^2}} \mathrm{sgn}\,\mathrm{Im}\,\tilde{\Sigma}^{*,R}(\omega). \tag{92}$$

Equations (91) are free from divergencies and can be readily extended to $N \neq 1$, as we did in the main text. Note that the sign of $\mathrm{Im}\,\tilde{\Sigma}^{*,R}(\omega)$ is not fixed by causality and can change between different ω, in distinction to $\mathrm{Im}\,\tilde{\Sigma}^{R}(\omega)$, which has to be positive.

Note by passing that $\Phi^R(\omega)$ and $\tilde{\Sigma}^R(\omega)$ can be expressed via $\Phi^{*,R}(\omega)$ and $\tilde{\Sigma}^{*,R}(\omega)$ in a manner similar to Eq. (89):

$$\Phi^R(\omega) = \Phi^{*,R}(\omega)\left(1 + Q^*(\omega)\right), \tilde{\Sigma}^R(\omega) = \tilde{\Sigma}^{*,R}(\omega)\left(1 + Q^*(\omega)\right), \tag{93}$$

where

$$Q^*(\omega) = \frac{\pi T \chi(0) \mathrm{sgn}\,\mathrm{Im}\,\tilde{\Sigma}^{*,R}(\omega)}{\sqrt{(\Phi^{*,R})^2(\omega) - (\tilde{\Sigma}^{*,R})^2(\omega)}} \tag{94}$$

Eqs. (91) have been solved numerically by iterations. For practical purposes, we found that in some cases the convergence is faster if we do calculations in two steps: first evaluate intermediate $\Phi^{**,R}$ and $\tilde{\Sigma}^{**,R}$, related to Φ^R and $\tilde{\Sigma}^R$ by the same formulas as in (89), but with $P = \int_{-\delta}^{\delta} dy\, \mathrm{Im}\,\chi^R(y)\frac{T}{y}$, where δ is some finite number, and then compute $\Phi^{*,R}$ and $\Sigma^{*,R}$ by adding the rest of the integral in P. The best convergence is achieved by adjusting the value of δ. In the calculations for a finite P, we computed $\Phi^R(\omega)$ and $\tilde{\Sigma}^R(\omega)$ directly, without introducing $\Phi^{*,R}(\omega)$ and $\tilde{\Sigma}^{*,R}(\omega)$.

---

[1] R. Combescot, Phys. Rev. B **51**, 11625 (1995).

[2] Bergmann, G. and Rainer, D. Z. Physik (1973) 263: 59. P. B. Allen and D. Rainer, Nature **349**, 396 EP (1991); P. B. Allen and R. C. Dynes, Phys. Rev. B **12**, 905 (1975).

[3] F. Marsiglio, M. Schossmann, and J. P. Carbotte, Phys. Rev. B **37**, 4965 (1988); F. Marsiglio and J. P. Carbotte, Phys. Rev. B **43**, 5355 (1991), for more recent results see F. Marsiglio and J.P. Carbotte, "Electron-Phonon Superconductivity", in "The Physics of Conventional and Unconventional Superconductors", Bennemann and Ketterson eds., Springer-Verlag, (2006) and references therein.

[4] A. Karakozov, E. Maksimov, and A. Mikhailovsky, Solid State Communications **79**, 329 (1991).

[5] N. E. Bonesteel, I. A. McDonald, and C. Nayak, Phys. Rev. Lett. **77**, 3009 (1996).

[6] A. Abanov, A. V. Chubukov, and A. M. Finkel'stein, EPL (Europhysics Letters) **54**, 488 (2001).

[7] A. Abanov, A. V. Chubukov, and J. Schmalian, Advances in Physics **52**, 119 (2003); A. Abanov and A. V. Chubukov, Phys. Rev. Lett. **83**, 1652 (1999).

[8] A. Abanov, A. V. Chubukov, and S. J., Journal of Electron spectroscopy and related phenomena **117**, 129 (2001).

[9] D. T. Son, Phys. Rev. D **59**, 094019 (1999); A. V. Chubukov and J. Schmalian, Phys. Rev. B **72**, 174520 (2005).

[10] S.-S. Lee, Phys. Rev. B **80**, 165102 (2009); D. Dalidovich and S.-S. Lee, Phys. Rev. B **88**, 245106 (2013).

[11] S. Sachdev, M. A. Metlitski, Y. Qi, and C. Xu, Phys. Rev. B **80**, 155129 (2009); E. G. Moon and S. Sachdev, Phys. Rev. B **80**, 035117 (2009).

[12] E.-G. Moon and A. Chubukov, Journal of Low Temperature Physics **161**, 263 (2010).

[13] M. A. Metlitski and S. Sachdev, Phys. Rev. B **82**, 075127 (2010); Phys. Rev. B **82**, 075128 (2010).

[14] D. F. Mross, J. McGreevy, H. Liu, and T. Senthil, Phys. Rev. B **82**, 045121 (2010).

[15] R. Mahajan, D. M. Ramirez, S. Kachru, and S. Raghu, Phys. Rev. B **88**, 115116 (2013); A. L. Fitzpatrick, S. Kachru, J. Kaplan, and S. Raghu, Phys. Rev. B **88**, 125116 (2013); Phys. Rev. B **89**, 165114 (2014); G. Torroba and H. Wang, Phys. Rev. B **90**, 165144 (2014); A. L. Fitzpatrick, G. Torroba, and H. Wang, Phys. Rev. B **91**, 195135 (2015), and references therein.

[16] P. Monthoux, D. Pines, and G. G. Lonzarich, Nature **450**, 1177 (2007).

[17] M.R. Norman in "Novel Superconductors", Bennemann and Ketterson eds., Oxford University Press (2014), and references therein.

[18] D. J. Scalapino, Rev. Mod. Phys. **84**, 1383 (2012); S. Lederer, Y. Schattner, E. Berg, and S. A. Kivelson, Proceedings of the National Academy of Sciences **114**, 4905 (2017); L. Fratino, P. SÃĭmon, G. Sordi, and A.-M. S. Tremblay, Scientific Reports **6**, 22715 (2016); S. Maiti and A. V. Chubukov in "Novel Superconductors", Bennemann and Ketterson eds., Oxford University Press (2014), and references therein.

[19] M. A. Metlitski, D. F. Mross, S. Sachdev, and T. Senthil, Phys. Rev. B **91**, 115111 (2015); K. B. Efetov, H. Meier, and C. Pepin, Nature Physics **9**, 442 (2013).

[20] Y. Wang and A. V. Chubukov, Phys. Rev. Lett. **110**, 127001 (2013); A. V. Chubukov and P. Wölfle, Phys. Rev. B **89**, 045108 (2014).

[21] S. Raghu, G. Torroba, and H. Wang, Phys. Rev. B **92**, 205104 (2015).

[22] Y. Wang, A. Abanov, B. L. Altshuler, E. A. Yuzbashyan, and A. V. Chubukov, Phys. Rev. Lett. **117**, 157001 (2016).

[23] S. Lederer, Y. Schattner, E. Berg, and S. A. Kivelson, Phys. Rev. Lett. **114**, 097001 (2015).

[24] A. M. Tsvelik, Phys. Rev. B **95**, 201112 (2017); K.-Y. Yang, T. M. Rice, and F.-C. Zhang, Phys. Rev. B **73**, 174501 (2006).

[25] M. Vojta and S. Sachdev, Phys. Rev. Lett. **83**, 3916 (1999).

[26] E. Fradkin, S. A. Kivelson, M. J. Lawler, J. P. Eisenstein, and A. P. Mackenzie, Annual Review of Condensed Matter Physics **1**, 153 (2010).

[27] J. M. Bok, J. J. Bae, H.-Y. Choi, C. M. Varma, W. Zhang, J. He, Y. Zhang, L. Yu, and X. J. Zhou, Science Advances **2** (2016), 10.1126/sciadv.1501329.

[28] T. Shibauchi, A. Carrington, and Y. Matsuda, Annual Review of Condensed Matter Physics **5**, 113 (2014).

[29] D. Vilardi, C. Taranto, and W. Metzner, arXiv:1810.02290 and references therein (2018); J. Sýkora, T. Holder, and W. Metzner, Phys. Rev. B **97**, 155159 (2018).

[30] M. H. Gerlach, Y. Schattner, E. Berg, and S. Trebst, Phys. Rev. B **95**, 035124 (2017); Y. Schattner, S. Lederer, S. A. Kivelson, and E. Berg, Phys. Rev. X **6**, 031028 (2016); X. Wang, Y. Schattner, E. Berg, and R. M. Fernandes, Phys. Rev. B **95**, 174520 (2017).

[31] K. Haule and G. Kotliar, Phys. Rev. B **76**, 104509 (2007); W. Xu, G. Kotliar, and A. M. Tsvelik, Phys. Rev. B **95**, 121113 (2017); G. Sordi, P. Simon, K. Haule, and A.-M. S. Tremblay, Phys. Rev. Lett. **108**, 216401 (2012).

[32] A. Georges, L. d. Medici, and J. Mravlje, Annu. Rev. Condens. Matter Phys. **4**, 137 (2013); W. Wu, M. Ferrero, A. Georges, and E. Kozik, Phys. Rev. B **96**, 041105 (2017).

[33] D. V. Khveshchenko and W. F. Shively, Phys. Rev. B **73**, 115104 (2006).

[34] T.-H. Lee, A. Chubukov, H. Miao, and G. Kotliar, arXiv **1805**, 10280 (2018); Y.-M. Wu, A. Abanov, and A. V. Chubukov, Phys. Rev. B **99**, 014502 (2019).

[35] J. Rech, C. Pépin, and A. V. Chubukov, Phys. Rev. B **74**, 195126 (2006).

[36] There is a large body of literature on QCP with $q = 0$. For recent works, see; S. Sur and S.-S. Lee, Phys. Rev. B **91**, 125136 (2015); M. Punk, Phys. Rev. B **91**, 115131 (2015), and references therein.

[37] A. Abanov, A. V. Chubukov, and M. R. Norman, Phys. Rev. B **78**, 220507 (2008).

[38] B. L. Altshuler, L. B. Ioffe, and A. J. Millis, Phys. Rev. B **52**, 5563 (1995); D. Bergeron, D. Chowdhury, M. Punk, S. Sachdev, and A.-M. S. Tremblay, Phys. Rev. B **86**, 155123 (2012); Y. Wang and A. Chubukov, Phys. Rev. B **88**, 024516 (2013).

[39] Ar. Abanov, Y-M Wu,Y. Wang and A. V. Chubukov, arXiv:1812.07634.

[40] P. Anderson, Journal of Physics and Chemistry of Solids **11**, 26 (1959).

[41] A. A. Abrikosov and L. P. Gor'kov, JETP **9**, 220 (1959).

[42] A. J. Millis, S. Sachdev, and C. M. Varma, Phys. Rev. B **37**, 4975 (1988).

[43] A. A. Abrikosov and L. P. Gor'kov, JETP **12**, 227 (1961).

[44] K. Maki, Physics Physique Fizika **1**, 21 (1964); P. Fulde and K. Maki, Phys. Rev. Lett. **15**, 675 (1965); Y. WADA, Rev. Mod. Phys. **36**, 253 (1964); D. J. Scalapino, Y. Wada, and J. C. Swihart, Phys. Rev. Lett. **14**, 102 (1965).

[45] J.C. Campuzano, M.R. Norman, and M. Randeria "Photoemission in the high-T_c supercondutors", in "Novel Superconductors", v.2, K.H. Bennemann and J.B. Ketterson eds, Springer 2008.

[46] J. Fink, A. Koitzsch, J. Geck, V. Zabolotnyy, M. Knupfer, B. Büchner, A. Chubukov, and H. Berger, Phys. Rev. B **74**, 165102 (2006).

[47] A. Abanov and A. V. Chubukov, Phys. Rev. Lett. **83**, 1652 (1999).

[48] M. Eschrig, Advances in Physics **55**, 47 (2006).

[49] O. Fischer, M. Kugler, I. Maggio-Aprile, C. Berthod, and C. Renner, Rev. Mod. Phys. **79**, 353 (2007).

[50] T. J. Reber, N. C. Plumb, Z. Sun, Y. Cao, Q. Wang, K. McElroy, H. Iwasawa, M. Arita, J. S. Wen, Z. J. Xu, G. Gu, Y. Yoshida, H. Eisaki, Y. Aiura, and D. S. Dessau, Nature Physics **8**, 606 EP (2012); T. J. Reber, N. C. Plumb, Y. Cao, Z. Sun, Q. Wang, K. McElroy, H. Iwasawa, M. Arita, J. S. Wen, Z. J. Xu, G. Gu, Y. Yoshida, H. Eisaki, Y. Aiura, and D. S. Dessau, Phys. Rev. B **87**, 060506 (2013); (), haoxiang Li, Xiaoqing Zhou, Stephen Parham, Theodore J. Reber, Helmuth Berger, Gerald B. Arnold, and Daniel S. Dessau, Nature Communications, vol. 9, 26 (2018); (), haoxiang Li, Xiaoqing Zhou, Stephen Parham, Kyle N. Gordon, R. D. Zhong, J. Schneeloch, G. D. Gu, Y. Huang, H. Berger, G. B. Arnold, D. S. Dessau, arXiv:1809.02194.

[51] T. Kondo, A. D. Palczewski, Y. Hamaya, T. Takeuchi, J. S. Wen, Z. J. Xu, G. Gu, and A. Kaminski, Phys. Rev. Lett. **111**, 157003 (2013); T. Kondo, A. F. Santander-Syro, O. Copie, C. Liu, M. E. Tillman, E. D. Mun, J. Schmalian, S. L. Bud'ko, M. A. Tanatar, P. C. Canfield, and A. Kaminski, Phys. Rev. Lett. **101**, 147003 (2008).

[52] A. Kanigel, M. R. Norman, M. Randeria, U. Chatterjee, S. Souma, A. Kaminski, H. M. Fretwell, S. Rosenkranz, M. Shi, T. Sato, T. Takahashi, Z. Z. Li, H. Raffy, K. Kadowaki, D. Hinks,

L. Ozyuzer, and J. C. Campuzano, Nature Physics **2**, 447 EP (2006); A. Kanigel, U. Chatterjee, M. Randeria, M. R. Norman, S. Souma, M. Shi, Z. Z. Li, H. Raffy, and J. C. Campuzano, Phys. Rev. Lett. **99**, 157001 (2007); H. Ding, J. C. Campuzano, A. F. Bellman, T. Yokoya, M. R. Norman, M. Randeria, T. Takahashi, H. Katayama-Yoshida, T. Mochiku, K. Kadowaki, and G. Jennings, Phys. Rev. Lett. **74**, 2784 (1995).

[53] A. Damascelli, Z. Hussain, and Z.-X. Shen, Rev. Mod. Phys. **75**, 473 (2003); M. Hashimoto, I. M. Vishik, R.-H. He, T. P. Devereaux, and Z.-X. Shen, Nature Physics **10**, 483 EP (2014), review Article.

[54] P. D. Johnson, T. Valla, A. V. Fedorov, Z. Yusof, B. O. Wells, Q. Li, A. R. Moodenbaugh, G. D. Gu, N. Koshizuka, C. Kendziora, S. Jian, and D. G. Hinks, Phys. Rev. Lett. **87**, 177007 (2001).

[55] A. A. Kordyuk and S. V. Borisenko, Low Temperature Physics **32**, 298 (2006); A. A. Kordyuk, Low Temperature Physics **41**, 319 (2015).

[56] Y. He, Y. Yin, M. Zech, A. Soumyanarayanan, M. M. Yee, T. Williams, M. C. Boyer, K. Chatterjee, W. D. Wise, I. Zeljkovic, T. Kondo, T. Takeuchi, H. Ikuta, P. Mistark, R. S. Markiewicz, A. Bansil, S. Sachdev, E. W. Hudson, and J. E. Hoffman, Science **344**, 608 (2014).

[57] Y. Peng, J. Meng, D. Mou, J. He, L. Zhao, Y. Wu, G. Liu, X. Dong, S. He, J. Zhang, X. Wang, Q. Peng, Z. Wang, S. Zhang, F. Yang, C. Chen, Z. Xu, T. K. Lee, and X. J. Zhou, Nature Communications **4**, 2459 EP (2013), article.

[58] A. V. Balatsky, I. Vekhter, and J.-X. Zhu, Rev. Mod. Phys. **78**, 373 (2006); M. L. Kulić and O. V. Dolgov, Phys. Rev. B **60**, 13062 (1999); A. F. Kemper, D. G. S. P. Doluweera, T. A. Maier, M. Jarrell, P. J. Hirschfeld, and H.-P. Cheng, Phys. Rev. B **79**, 104502 (2009).

[59] M. R. Norman, H. Ding, M. Randeria, J. C. Campuzano, T. Yokoya, T. Takeuchi, T. Takahashi, T. Mochiku, K. Kadowaki, P. Guptasarma, and D. G. Hinks, Nature **392**, 157 EP (1998); M. R. Norman, M. Randeria, H. Ding, and J. C. Campuzano, Phys. Rev. B **57**, R11093 (1998); M. Franz and A. J. Millis, Phys. Rev. B **58**, 14572 (1998); A. Paramekanti and E. Zhao, Phys. Rev. B **75**, 140507 (2007); E. Berg and E. Altman, Phys. Rev. Lett. **99**, 247001 (2007), and references therein.

[60] A. V. Chubukov, M. R. Norman, A. J. Millis, and E. Abrahams, Phys. Rev. B **76**, 180501 (2007).

[61] J. M. Luttinger and J. C. Ward, Phys. Rev. **118**, 1417 (1960).

[62] R. Haslinger and A. V. Chubukov, Phys. Rev. B **68**, 214508 (2003).

[63] Z. Wang, W. Mao, and K. Bedell, Phys. Rev. Lett. **87**, 257001 (2001); R. Roussev and A. J. Millis, Phys. Rev. B **63**, 140504 (2001); A. V. Chubukov, A. M. Finkel'stein, R. Haslinger, and D. K. Morr, Phys. Rev. Lett. **90**, 077002 (2003).

[64] A. J. Millis, Phys. Rev. B **45**, 13047 (1992).

[65] C. Castellani, C. Di Castro, and M. Grilli, Phys. Rev. Lett. **75**, 4650 (1995); A. Perali, C. Castellani, C. Di Castro, and M. Grilli, Phys. Rev. B **54**, 16216 (1996); S. Andergassen, S. Caprara, C. Di Castro, and M. Grilli, Phys. Rev. Lett. **87**, 056401 (2001).

[66] D. Chowdhury and S. Sachdev, Phys. Rev. B **90**, 134516 (2014); Phys. Rev. B **90**, 245136 (2014); Y. Wang and A. V. Chubukov, Phys. Rev. B **92**, 125108 (2015).

[67] A. A. Abrikosov, L. P. Gorkov, and I. E. Dzyaloshinski, *Methods of Quantum Feld Theory in Statistical Physics*, 2nd edition, (Pergamon Oxford, 1965).

[68] H. Wang, Y. Wang, and G. Torroba, Phys. Rev. B **97**, 054502 (2018).

[69] J. Bardeen and M. Stephen, Phys. Rev. **136**, A1485 (1964).

[70] G. M. Eliashberg, JETP **11**, 696 (1960).

[71] Note that $\Delta(\omega) \propto i\omega$ should not be confused with odd-frequency pairing. This $\Delta(\omega)$ is a retarded function, for which Re $\Delta(\omega)$ ius even in frequency, and Im $\Delta(\omega)$ is odd.

[72] A. V. Chubukov, I. Eremin, and D. V. Efremov, Phys. Rev. B **93**, 174516 (2016).

[73] Ar. Abanov, A.V. Chubukov, and J. Schmalian, Journal of Electron Spectroscopy and Related Phenomena, v117, p129 (2001).